BROADBAND VENTILATED ACOUSTIC METAMATERIAL DESIGN WITH COUPLED SPACE-COILED RESONATORS

by

Ahmet Karakoyun

B.S., Mechanical Engineering, Boğaziçi University, 2017

Submitted to the Institute for Graduate Studies in
Science and Engineering in partial fulfillment of
the requirements for the degree of
Master of Science

Graduate Program in Mechanical Engineering
Boğaziçi University

2023

ACKNOWLEDGEMENTS

Foremost, I would like to express my deepest gratitude to my thesis advisor Prof. Çetin Yılmaz for his great patience, help and understanding during my thesis writing period. I would like to thank him for his endless support in guiding me to write my thesis in a perfect manner.

Moreover, I would like to thank Prof. Mehmet Burçin Ünlü and Assoc. Prof. Polat Şendur for giving their valuable time to evaluate my thesis.

Finally, I would like to express my special appreciation to my beloved family. My wife, Rüveyda Karakoyun, has given significant technical support in addition to emotional support. I owe a great thank to her. I would like to thank my mother, Güllü Karakoyun, and my father, Abdulkadir Karakoyun. They have brought me up to this day. During my entire life, they have provided me perfect opportunities for my education. I am also grateful to my sisters, Yağmur Karakoyun and Eylül Nisa Karakoyun, for their support and encouragement.

ABSTRACT

BROADBAND VENTILATED ACOUSTIC METAMATERIAL DESIGN WITH COUPLED SPACE-COILED RESONATORS

In this thesis, broadband ventilated acoustic metamaterial design with coupled space-coiled resonators is studied. The main aim is to determine acoustic metamaterial designs, which provide high level of sound attenuation in a wide frequency range and results in minimum air pressure loss during airflow. The number and dimensions of the resonators are optimized for this aim. In order to accomplish coupling with more than two resonators, i.e., channels, an analytical model of the design having one resonator is obtained by using the transfer matrix method. Consequently, transmission loss characteristics are compared with the finite element model for verification. After verification for one resonator, the analytical model of the design having two resonators is obtained by using parallel connection of transfer matrices. Once the derivation regarding parallel connection of transfer matrices is done, a new methodology for the analytical model of the design having more than two resonators is proposed. By using this methodology, optimization is conducted by changing the number and/or the dimensions of the coupled resonators to accomplish sound isolation in the widest frequency range for a given transmission loss constraint. After determining the proper number and dimensions of the resonators, the finite element model of the proposed design is constructed. By using genetic algorithm, the analytical resonator lengths are updated to determine the lengths in the finite element model. Parametric studies are conducted to show the dependence of isolation bandwidth on target transmission loss and channel dimensions. It is shown that for low transmission loss targets such as 10 dB, a two channel design can provide both large isolation bandwidth and low pressure loss. On the other hand, for high transmission loss targets such as 50 dB or 60 dB, a three or four channel design can provide both wider isolation bandwidth and lower pressure loss than a two channel design.

ÖZET

UZAYDA KIVRILMIŞ BAĞLAŞIK REZONATÖRLERLE GENİŞ BANTLI HAVALANDIRMALI AKUSTİK METAMALZEME TASARIMI

Bu tezde, uzayda kıvrılmış bağlaşık rezonatörlerle geniş bantlı havalandırmalı akustik metamalzeme tasarımı incelenmiştir. Temel amaç geniş bir frekans aralığında yüksek düzeyde ses azalması sağlayan ve hava akışı sırasında minimum hava basıncı kaybı ile sonuçlanan akustik metamalzeme tasarımları belirlemektir. Rezonatörlerin sayısı ve boyutları bu amaç için optimize edilmiştir. İkiden fazla rezonatörü (kanalı) birleştirmek için tek rezonatörlü tasarımın analitik modeli transfer matris yöntemi kullanılarak oluşturulmuştur. Akabinde doğrulama için iletim kaybı özellikleri sonlu elemanlar modeli ile karşılaştırılır. Bir rezonatör için doğrulamadan sonra, transfer matrislerinin paralel bağlanması kullanılarak iki rezonatörlü tasarımın analitik modeli elde edilmiştir. Transfer matrislerinin paralel bağlantısına yönelik türetme yapıldıktan sonra, ikiden fazla rezonatöre sahip tasarımın analitik modeli için yeni bir yöntem önerilmiştir. Bu yöntem kullanılarak, belirli bir iletim kaybı kısıtlaması için en geniş frekans aralığında ses yalıtımı gerçekleştirmek amacıyla bağlaşık rezonatörlerin sayısı ve/veya boyutları değiştirilerek eniyileme yapılmıştır. Rezonatörlerin uygun sayısı ve boyutları belirlendikten sonra, önerilen tasarımın sonlu eleman modeli oluşturulmuştur. Genetik algoritma kullanılarak, sonlu elemanlar modelindeki uzunlukları belirlemek için analitik rezonatör uzunlukları güncellenmiştir. Yalıtım aralığının hedef iletim kaybı ve kanal boyutlarına bağlılığını göstermek için parametrik çalışmalar yapılmıştır. 10 dB gibi düşük iletim kaybı hedefleri için, iki kanallı tasarımın hem geniş yalıtım aralığı hem de düşük basınç kaybı sağlayabildiği gösterilmiştir. Öte yandan, 50 dB veya 60 dB gibi yüksek iletim kaybı hedefleri için üç veya dört kanallı tasarım iki kanallı tasarımdan daha geniş yalıtım aralığı ve daha düşük basınç kaybı sağlayabilmektedir.

TABLE OF CONTENTS

LIST OF FIGURES

LIST OF TABLES

LIST OF SYMBOLS

c	The wave speed
d_o	The width of the overall design domain
d_1	The slit width of the first resonator
d_2	The slit width of the second resonator
d_3	The slit width of the third resonator
d_4	The slit width of the fourth resonator
d_{n+1}	The slit width of the (n+1)th resonator
f	Frequency
k	The wave number
k_e	The loss coefficient
l_1	The total length of the first resonator
l_2	The total length of the second resonator
l_3	The total length of the third resonator
l_4	The total length of the fourth resonator
l_{n+1}	The total length of the (n+1)th resonator
l_{end}	End correction term at each end
m_1	The slit ratio of the first resonator
m_2	The slit ratio of the second resonator
m_3	The slit ratio of the third resonator
m_{n+1}	The slit ratio of the (n+1)th resonator
P	The acoustic pressure
P_1	Inlet air pressure of a design
P_2	Outlet air pressure of a design
P_i	The inlet acoustic pressure of the resonator
P_{i1}	The inlet acoustic pressure of the first resonator
P_{i2}	The inlet acoustic pressure of the second resonator
P_o	The outlet acoustic pressure of the resonator
P_{o1}	The outlet acoustic pressure of the first resonator
P_{o2}	The outlet acoustic pressure of the second resonator

$shape_{coiled}$	The shape of corners for the space-coiled channel
t_{op}	The out-of-plane thickness of the design
T_1	Transfer matrix of the first resonator
T_2	Transfer matrix for the second resonator
T_3	Transfer matrix for a third resonator
T_{n+1}	Transfer matrix for parallel combination of (n+1)th resonator
T_{p2}	The parallel transfer matrix of two coupled resonators
T_{p3}	The parallel transfer matrix of three coupled resonators
T_{pn}	Transfer matrix for parallel combination of n resonators
$T_{p(n+1)}$	Transfer matrix for parallel combination of (n+1) resonators
TL_1	Transmission loss for one resonator
TL_3	Transmission loss of the acoustic metamaterial involving three resonators
TL_{n+1}	Transmission loss of the acoustic metamaterial involving (n+1) resonators
TL_{p2}	Transmission loss of the acoustic metamaterial involving two coupled resonators
U_i	The inlet acoustic velocity of the resonator
U_o	The outlet acoustic velocity of the resonator
v_i	The inlet speed of air
λ	Wavelength
ρ	The air density

LIST OF ACRONYMS/ABBREVIATONS

AIT	Acoustically Induced Transparency
EIT	Electromagnetically Induced Transparency
FEM	Finite Element Method
FP	Fabry-Perot
LRSC	Locally Resonant Sonic Crystal
TL	Transmission Loss

1. INTRODUCTION

1.1. Broadband Ventilated Acoustic Metamaterial Design

In this thesis, broadband ventilated acoustic metamaterial design with coupled space-coiled resonators is studied. This area has been enlightened with the development of phononic crystals [1-3]. The aim of the thesis is to find an acoustic metamaterial design, which provides high level of attenuation in a wide frequency range and produces minimum pressure loss for effective ventilation. Basically, the goal is to block sound waves but allow air flow. The thickness of the acoustic metamaterial will be much less than the wavelength of the sound in the targeted frequency range. In order to achieve this aim, the number and/or the dimensions of coupled space-coiled resonators will be optimized. In this section, several definitions regarding the thesis are made.

The first usage of the term metamaterial was in 1999 by Rodger Walser of the University of Texas. According to their usage, metamaterials were a periodic cellular structure which did not exist in nature [4]. In the study of Iannace et al., an acoustic barrier designed with metamaterial was inspected in terms of sound cancellation. Their design involved distinct changing rows of cylindrical bars, spacing each bar with an empty space for the sake of making regular geometries [5]. The term subwavelength is used to denote the thickness of structure that is less than the wavelength of the sound in the targeted frequency range. A subwavelength grating is a grating period which is much smaller than the wavelength of the sound employed [6]. An incident angle is the angle formed by a ray or wave incident on a surface and a line perpendicular to the surface at the point of incidence. Normal incidence represents an incident angle of 0°. Oblique incidence represents an incident angle different from 0° [7]. Band gaps are the frequency ranges where there is no wave propagation [8]. Sound control is one of the most proven applications of band gaps [9]. Fabry-Perot cavities are widespread phenomena in the field of optics, especially for lasers where the amplification includes light rays confinement in resonant cavities [10]. Standard acoustic resonators are straight channels in which if the two ends are open, the first resonance occurs at half the wavelength and if one end is closed and the other is open, the first resonance occurs at quarter wavelength. In a space-coiled resonator, the resonator is a curved

channel in which the thickness of the resonator is much smaller than an equivalent straight channel resonator. When more than one resonator is used together in a design, resonator coupling can occur which provides sound opacity in a more effective way [11]. Moreover, in phononic crystals, the unit cell dimension is on the order of the acoustic wavelength whereas in acoustic metamaterials the unit cell dimension is much smaller than the acoustic wavelength. Locally Resonant Sonic Crystal (LRSC), which is explained in the Literature Review section, is a significant example of resonant acoustic metamaterials [12].

The term end correction has been investigated in the literature by different researchers. At low frequencies, one dimensional analytical approach can be utilized for prediction of the acoustic attenuation behavior of silencers [13]. In the study of Torregrosa et al., it was revealed that in order to get approximately true prediction of the acoustic behavior of extended duct and perforated duct mufflers, the appropriate end correction had to be introduced into one dimensional analytical models [14]. In the study of Kang and Ji, it was explored that chamber geometry such as chamber length, diameter ratio and duct extension had significant effects on the end correction. They contributed an approximate explanation for determination of the end correction [15]. In the study of Chaitanya and Munjal, the effect of wall thicknesses of the inlet and outlet ducts on the end correction was examined in addition to the chamber geometry properties. They revealed that the wall thicknesses of the inlet and outlet ducts have crucial effect on the end correction. They provided an approximate expression for determination of the end correction by taking into account wall thicknesses of the inlet and outlet ducts and the chamber geometry properties including chamber length, diameter ratio and duct extension [16]. Hence, there are various studies in the literature regarding end correction. In this thesis, analytical and numerical models will be compared by using appropriate end correction terms.

In the thesis, broadband low frequency sound screening will be investigated considering locally resonant acoustic metamaterials. The effect of coupling in space-coiled resonators will be utilized for sound opacity. Consequently, the design will be optimized such that the acoustic metamaterial achieves high attenuation level in a wide frequency range and results in minimum air pressure loss when subject to air flow. The modelling and optimization of the design will be done both analytically by using MATLAB and numerically by using ANSYS. Coupling of several resonators will be considered to increase

the sound isolation bandwidth. Moreover, design strategies will be provided to decrease pressure loss in case of airflow.

1.2. Literature Review

Phononic crystals utilize fundamental features of waves, such as diffusion or Bragg scattering phenomena. The aim of using phononic crystals is to generate band gaps, which can be defined as the frequency bands in which there exist no wave propagation [8]. There are several applications of band gaps. Sound control is one of them. The frequency range for the human ear is approximately from 20 Hz to 20 kHz. For low frequencies, wavelengths can be several meters in air. As the unit cell size of sonic crystals is on the order to the wavelength, handling low frequency excitations is very hard and not very feasible in terms of size constraints. A suitable example for middle frequencies is the sculpture Organo of Eusebio Sempere [9]. The significant development related to phononic crystals in the fields of elastic or acoustic waves has led to new perspectives about figuring out and controlling wave propagation [1-3].

Different studies including resonators have recently revealed how to handle the limitations regarding these large dimensions and make proper applications [17,18]. An example study includes metal spheres coated with an elastic material, and which identical local resonators are generated resulting in band gaps at frequencies less than that of a classical Bragg-based sonic crystal of equal dimensions. This study is the case of the Locally Resonant Sonic Crystal (LRSC) done by Liu et al. in 2000 [12]. A more recent study includes an elastic membrane with a central mass that acts as a local resonator [19]. This is actually a panel version of LRSC. An approximately total reflection occurs around the resonance for this metamaterial. Moreover, it is realized with the recent studies that using space-coiling in acoustic metamaterials leads to some significant features in terms of obtaining good effective properties in compact size [20]. There are many studies that are conducted towards the advancement of both resonant [21] and non-resonant [22-25] acoustic metamaterials including space-coiling.

The resonant acoustic metamaterials including space-coiling were utilized to enlarge sensor capacities of detection by producing a sound pressure level gain. This utilization

succeeds to reach the Enhanced Acoustic Transmission for wavelength 15 times larger than the periodicity [26]. In this regard, space-coiling provides an important alternative for their capacity to reach larger wavelengths. On the other hand, the relative bandwidth of this type of attenuation is narrow compared to the case of general resonant phenomena. In fact, these resonances are classical for relatively simple systems in the point that they perform symmetric Lorentzian line shapes [27,28]. However, resonances with asymmetrical line shapes, which are called as Fano resonances, have also been pointed out [29]. Indeed, it is explained by Ugo Fano that they are generated from the constructive and destructive interference of a narrow discrete resonance with a broad spectral line or continuum [30,31]. Through this explanation, various studies have provided a better knowledge about Fano resonances in different areas of physics such as electromagnetism and plasmonics [32]. Moreover, several studies based on this explanation have enlightened the area of acoustics [33,34] with the help of the acoustic analogue of Electromagnetically Induced Transparency (EIT) [35]. It has been recently found that the opaque counterpart of Acoustically Induced Transparency (AIT) was also succeeded by using an array of Fabry-Perot (FP) resonators in the ultrasonic regime. These resonators were also coupled to each other unless the coupling was performed laterally by the fluid-solid interaction [36]. It has been proven that this type of coupling was significantly efficient at normal incidence. However, this coupling was more restricted at oblique incidence. In fact, apertures also exhibit as a diffraction grating while constituting a periodic array [37]. In this sense, it was revealed that the primary limitation of an omnidirectional screening related to this type of resonator was concerned about diffraction [38].

Traditional acoustic absorbers cause significant problems in real applications in low frequency bandwidth since they generally have a design with a thickness comparable to the working wavelength. In the study of Yong Li and Badreddine M. Assouar, an acoustic metasurface having a deep subwavelength thickness down to a feature size of approximately $\lambda/223$ was designed such that it could achieve the total absorption of acoustic wave in a deeply low frequency bandwidth. Their design was a metasurface which includes a perforated plate and a coiled coplanar air chamber [39]. The traditional methods regarding acoustic metamaterials are based on constructing dispersive materials or structures with local resonators. In the study of Zhu et al., an acoustic metasurface having a helical shape was proposed such that it could apply dispersion-free sound cancellation. Thanks to adjusting the

helicity of design, their proposed helical acoustic metamaterial provided a non-dispersive effective refractive index [40]. In the study of Sanjay Kumar and Heow Pueh Lee, it was stated that acoustic metamaterials which provided low-frequency sound absorption had been utilized for the areas of architectural acoustics and traffic noise reduction. Their review paper revealed the existing challenges and progresses in this field [41]. Recently, in the study of Magnani et al., a design methodology regarding sound attenuation was proposed for acoustic metamaterials involving acoustic coiled-up quarter-wave resonators which have a limited space. Their purpose was to enlarge the capacity of potential applications even in the low-frequency region. For this purpose, they designed different configurations of quarter-wave resonators with different dimensions coupled in parallel or in series [42].

Traditional acoustic metamaterials which are designed for the purpose of sound absorption prevent air transition. However, there are some situations in which noise reduction and airflow occur simultaneously. For instance, natural ventilation, which can be defined as a key structure of green buildings, inescapably leads residents to hear the concomitant sprawling noise. To find a sound insulator metamaterial permeating airflow, the widespread method is to design a window which allows a winding airflow path with insulative linings or perforated partitions. In reality, a more winding lined path provides a more sufficient noise reduction. However, this situation results in a larger pressure drop, which means a poorer ventilation effect. Therefore, there has always been a trade-off between the effectiveness of ventilation and noise reduction [43]. In the study of Ghaffarivardavagh et al., it was demonstrated that a transversely placed bilayer medium with many degrees of contrast in the layers' acoustic features provided an asymmetric sound transmission like in the case of Fano-like interference. Their design was a deep-subwavelength acoustic metasurface unit cell which included approximately 60% open area for air transition while it enabled selective sound absorption [44]. In the study of Sun et al., an acoustic ventilation barrier having a planar-profile and subwavelength thickness (nearly $\lambda/8$) was designed such that it prevented sound in a broad bandwidth. Their design was a metasurface which includes a central hollow orifice and two surrounding helical pathways with varying pitch. Thanks to a hollowed-out hornlike helical metasurface, they proposed a metamaterial which provided broadband sound reduction and large airflow transition simultaneously [43]. In the study of Sanjay Kumar and Heow Pueh Lee, the subject regarding the acoustic metamaterials' performance about the simultaneous utility of sound

absorption and air ventilation was explained with existing methodologies. Their review paper discussed various kinds of acoustic metamaterials including space-coiled, labyrinthine, locally resonant, and Fano resonant [45]. Recently, in the study of Dong et al., an ultrabroadband ventilation barrier with hybridization of dissipation and interference was designed such that it prevented sound in an ultrabroad bandwidth. They contributed a methodology regarding noise control in flowing-fluid-filled conditions [46]. In the study of Fusaro et al, natural ventilation and noise control of windows were discussed simultaneously. They proposed an acoustic metamaterial design for windows such that it allowed noise control independent from the natural ventilation duration and vice versa [47]. In the study of Dong et al., a full-sized acoustic ventilation barrier having a lightweight metasurface with internal helical sound paths was designed such that it had high transmission losses at low frequencies. Thanks to identical meta-units including a central hole surrounded by an open helical structure, their design allowed air transition for ventilation and worked in a broadband diffuse field [48]. More recently, in the study of Liu et al., a design methodology regarding sound absorption and ventilation at low frequencies was proposed for a type of broadband muffler. Their design consisted of a bypass coiling tunnel which was connected to a central open hole. Through this property, they obtained a large bandgap at low frequencies while serving as ventilation purposes [49].

1.3. Motivation and Research Objective

In this thesis, optimization of two dimensional space-coiled resonator to design an acoustic metamaterial is studied. The aim of the thesis is to find an acoustic metamaterial design, which provides high level of sound attenuation for a wide frequency range and produces minimum pressure loss for effective ventilation. For this aim, the number and/or dimensions of coupled space-coiled resonators will be optimized. In the meantime, air flow across the acoustic metamaterial will be analyzed to minimize pressure loss. The motivation of the thesis and the contributions to the literature can be summarized as follows:

- There are studies in the literature in which the coupled acoustic response of two open ended channels (resonators) are analyzed. In these studies, there is a short straight channel and a space-coiled long channel. In this thesis, acoustic metamaterial designs will be proposed that involve coupling of more than two channels. The goal is to

obtain high attenuation level over a broader frequency range compared to the designs in the literature.

- In the literature, there exist some studies related to parallel assembly of transfer matrices based on admittance sum method. In this thesis, a new derivation will be given for parallel connection of transfer matrices.

- An analytical model of the problem for the design having one channel is formed in order to make coupling with more than two resonators. The model is based on transfer matrix method and constructed in MATLAB. After forming of the analytical model via MATLAB, the finite element model is formed in ANSYS. The transmission loss characteristics of the analytical model in MATLAB and finite element model in ANSYS are compared for model verification. To match the analytical and finite element results, end correction terms are found.

- The analytical model is used to get coupling two channels in the same design domain. Parallel connection of the transfer matrices is used for this purpose. Once the analytical model is formed via MATLAB, it is compared with the finite element method via ANSYS. After matching operation is done, the model is verified. This model based on parallel connection of transfer matrices can be used for designing an acoustic metamaterial which has two channels.

- The analytical model is used to get coupling more than two channels in the same design domain in order to provide high level of sound attenuation for a wide frequency range. Firstly, adding one more channel to the design having two channels is explained. After this, the general methodology to allow coupling of multiple channels systematically is proposed. By using this proposed methodology, optimization of the design is done with MATLAB by changing the number and/or the dimensions of space-coiled channels to provide isolation in the widest frequency range for a targeted transmission loss constraint. The resulting design is formed in ANSYS. This methodology can be used for designing an acoustic metamaterial which has more than two channels.

- In the literature, acoustic metamaterial designs are generally analyzed in terms of their sound isolation characteristics. In this thesis, these designs are analyzed in terms of pressure loss characteristics in addition to their acoustic analyses. The relations between frequency bandwidth, transmission loss and air pressure loss are investigated. These relations can be used for the selection of the proper acoustic metamaterial design in terms of the predefined criteria for frequency bandwidth, transmission loss and air pressure loss.

2. PROBLEM STATEMENT

In the thesis, the problem is to find the transmission properties of an acoustic metamaterial including space-coiled cavities and operating at low frequency compared to their thickness. In the study of Elayouch et al., both numerical and experimental investigation is made regarding the transmission properties of an acoustic metamaterial constituted with Fabry-Perot cavities [11]. When two modes of neighboring cavities interfere, an asymmetric Fano lineshape of transmission can occur. In their proposed design, this is succeeded by using Fabry-Perot cavities, which have distinct quality factors, and by placing them side by side. They experimentally revealed that a wide frequency band of sound opacity can be achieved with the proposed acoustic metamaterial with proper subwavelength thickness. Moreover, they numerically showed that the behavior of this low frequency sound screening avoids the frequency of diffraction occurrence. This phenomenon has previously proved to be the primary restriction of the omnidirectional capabilities of locally resonant perforated plates. They finally achieve more than 30 dB attenuation at low frequencies, through a metamaterial thickness fifteen times smaller than the wavelength ($\lambda/15$) [11]. The structure of the experimental design is given in Figure 2.1.

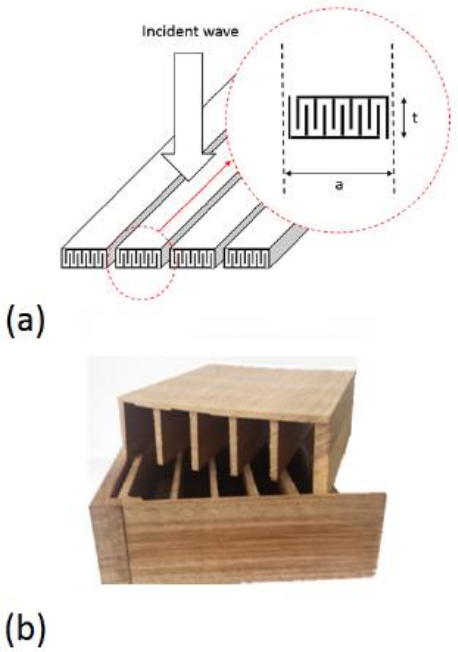

Figure 2.1. (a) Schematics of the design. (b) Photograph of the design [11].

As it can be seen from Figure 2.1(a), schematics of the design are constituted with periodically perforated plate. Moreover, this figure contains a zoom of a unit cell constituting the array, and made of two Fabry-Perot cavities, one of which is space-coiled. The acoustic metamaterial shown in the photograph in Figure 2.1(b) is fabricated from wood. The transmission loss characteristics of the plate perforated with periodically distributed Fabry-Perot cavities, which are obtained by finite element method [11], are given in Figure 2.2.

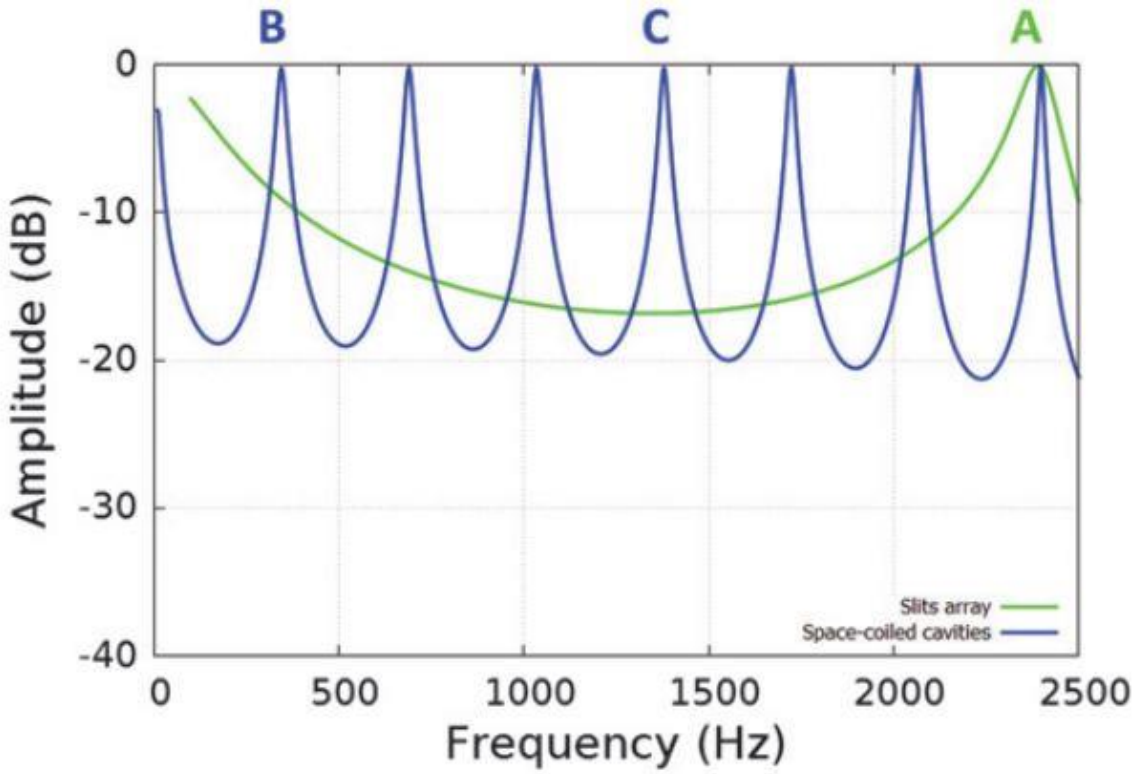

Figure 2.2. The green line represents the acoustic response of a slits array. The blue line represents an array of space-coiled cavities [11].

As it can be seen from the green line in Figure 2.2, a resonance occurs at the frequency of $f_A = 2390$ Hz for the case of a plate periodically constituted of straight slits, wherein each of the slits refers a Fabry-Perot resonant cavity. From the blue line in Figure 2.2, it can be concluded that a series of Fabry-Perot resonances from starting $f_B = 345$ Hz occurs for the case of space-coiled Fabry-Perot cavities [11].

The final case of the transmission loss characteristics, which is given in Figure 2.3, belongs to the acoustic metamaterial constituted by two resonant cavities. The first cavity is a straight aperture whereas the second cavity is a space-coiled one, as shown in Figure 2.1(a) and 2.1(b). Therefore, the acoustic metamaterial contains two Fabry-Perot cavities, which have different resonance frequencies. Moreover, the inputs and outputs of the cavities are placed side by side in order to enhance the interaction between them [11].

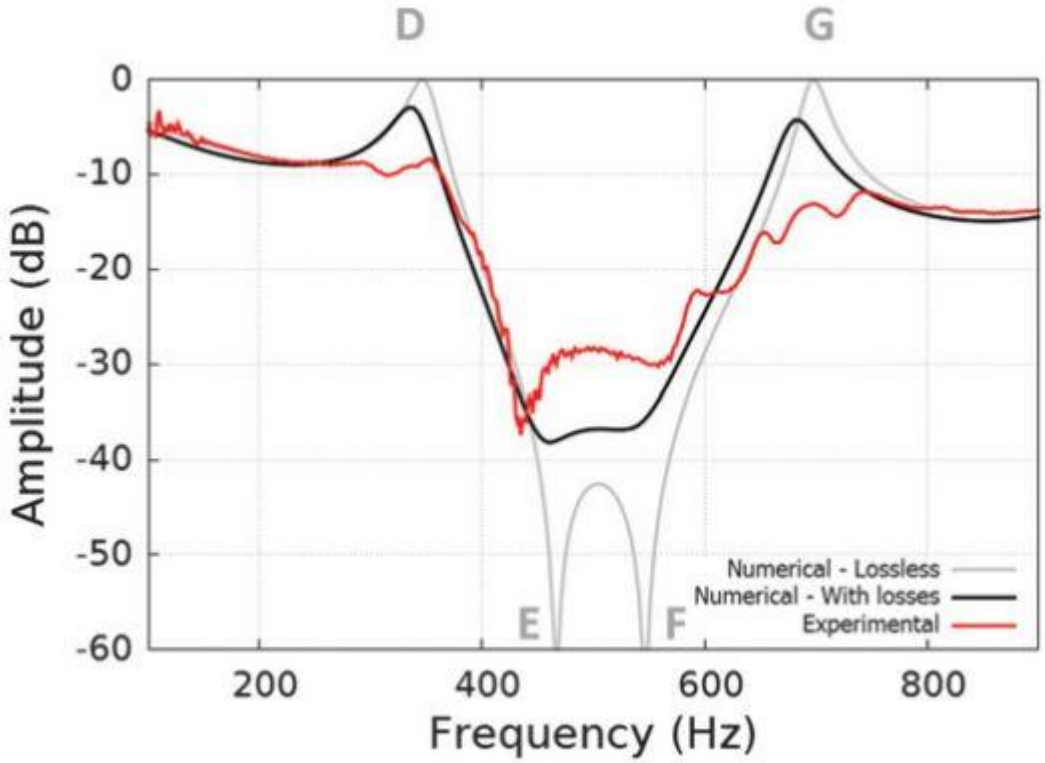

Figure 2.3. The transmission loss characteristics of the acoustic metamaterial. The grey and the black curves represent the finite element results without and with losses, respectively. The red curve represents the experimental results using a Kundt's tube [11].

As it can be seen from the grey line in Figure 2.3, a series of Fabry-Perot resonances (D and G) and antiresonances (E and F) occur. This phenomenon results in an attenuation band, which is centered at 500 Hz, with a transmission loss more than 35 dB of attenuation over a relative band of 30% [11].

The term air pressure loss is used to denote the pressure difference between the inlet and the outlet of the acoustic metamaterial. It can be calculated for the design, which involves two-ports as inlet and outlet, as follows [50]

$$P_1 = P_2 + k_e \frac{1}{2} \rho v_i^2 \, . \tag{2.1}$$

In this equation, P_1 and P_2 are the inlet and outlet pressures, respectively. k_e represents the loss coefficient. ρ is the fluid density. v_i is the inlet speed of the fluid. According to this equation, it can be concluded that the pressure loss is proportional to the square of inlet speed [50].

In the thesis, the coupled resonator design in the study of Elayouch et al. will be improved. The aim is to design an acoustic metamaterial, which provides more attenuation over a wider frequency range while keeping the subwavelength size. In the study of Elayouch et al., two coupled resonators are utilized, one of which is a space-coiled resonator [11]. In the current study, many space-coiled resonators are aimed to be used in the design and their dimensions will be optimized to achieve coupling among all the resonators in the desired frequency range. Moreover, a general methodology will be proposed on achieving multiple coupling in a targeted frequency range. Finally, air pressure loss response will be investigated.

3. BENCHMARKING

In the beginning, the three different designs for acoustic metamaterials are constructed by using ANSYS in order to benchmark our analysis with the results in the study of Elayouch et al. [11]. The pressure fields and the resulting transmission loss of the first design are given in Figure 3.1. In the analyses, speed of sound is 343 m/s and the density of air is 1.2 kg/m^3.

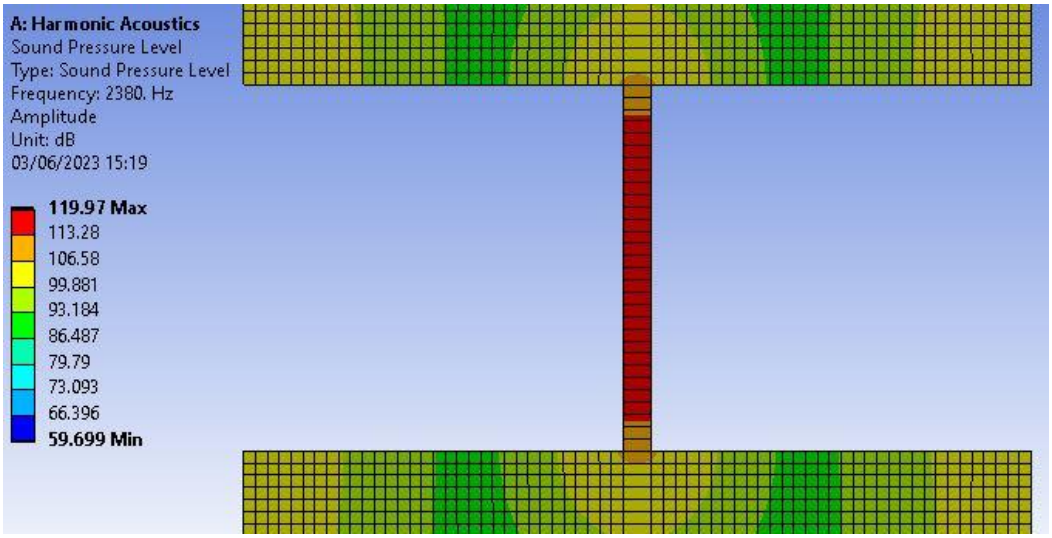

(a)

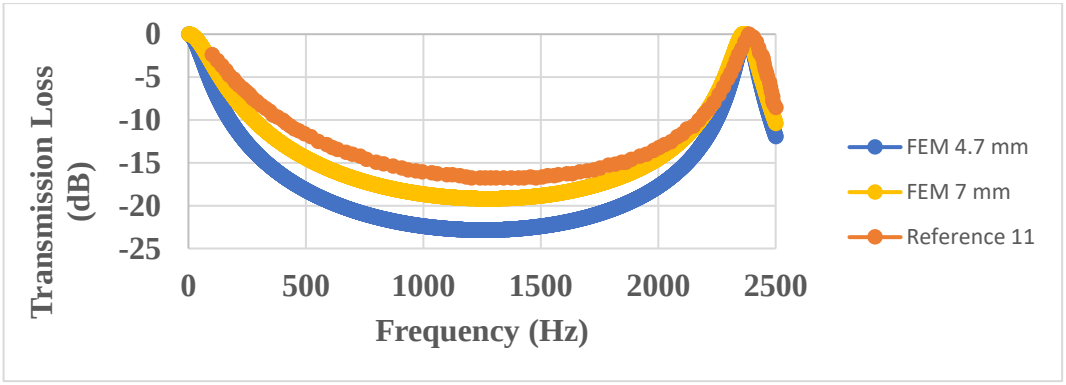

(b)

Figure 3.1. (a) Sound pressure level at the resonance frequency, (b) The resulting transmission loss graphs of the straight channel with length 60 mm for the widths of 4.7 mm and 7 mm via FEM, and reference article [11]. The width of the overall design domain is 129 mm.

As it can be seen from Figure 3.1, the first design is constituted with one straight channel with a length of 60 mm. Two different widths (4.7 mm and 7 mm) are considered in the analyses. The length of the channel determines the frequency peaks in the transmission loss graph and they are the same as the values in reference article [11]. It can also be seen that FEM result with 7 mm width gives a better match with reference article in terms of the maximum dB value [11]. However, this straight channel will be coupled with a space-coiled channel and the coupled response will be compared with reference article [11]. It will be shown that 4.7 mm width gives a better fit for the coupled response.

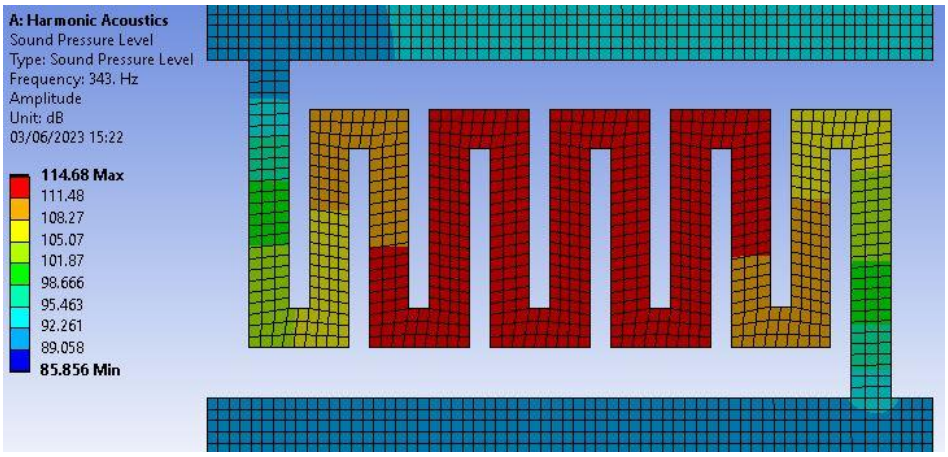

(a)

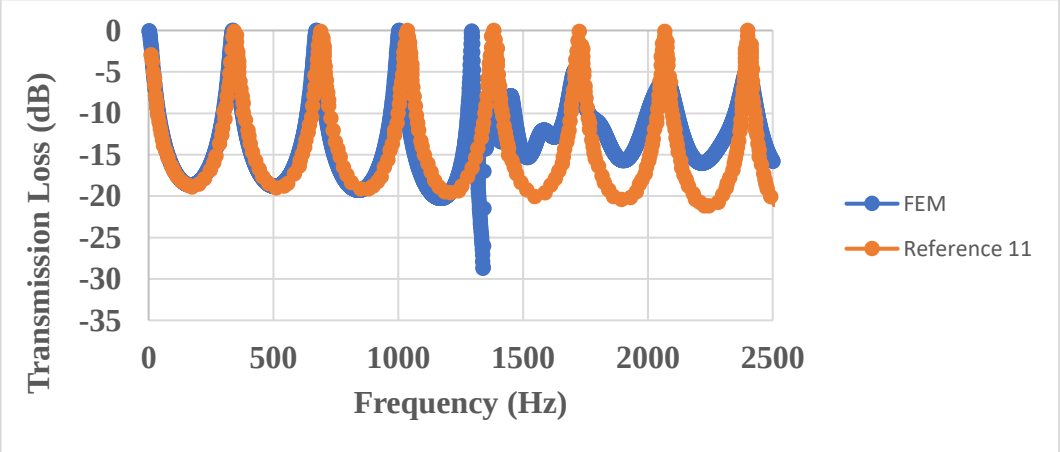

(b)

Figure 3.2. (a) Sound pressure level at the first resonance frequency, (b) The resulting transmission loss graphs of the space-coiled channel with length 500 mm and width 7 mm via FEM, and reference article [11]. The width of the overall design domain is 129 mm.

As it can be seen from Figure 3.2, the second design involves a space-coiled channel with a total length 500 mm that has 7 mm width. The resulting transmission loss graph is similar with the one in Figure 2.2 for only frequencies less than 1000 Hz.

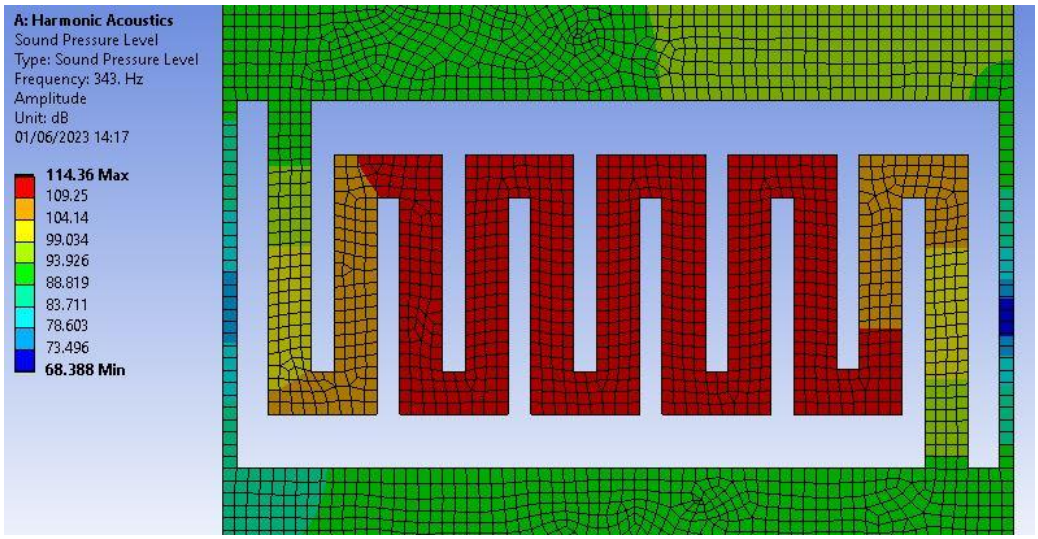

(a)

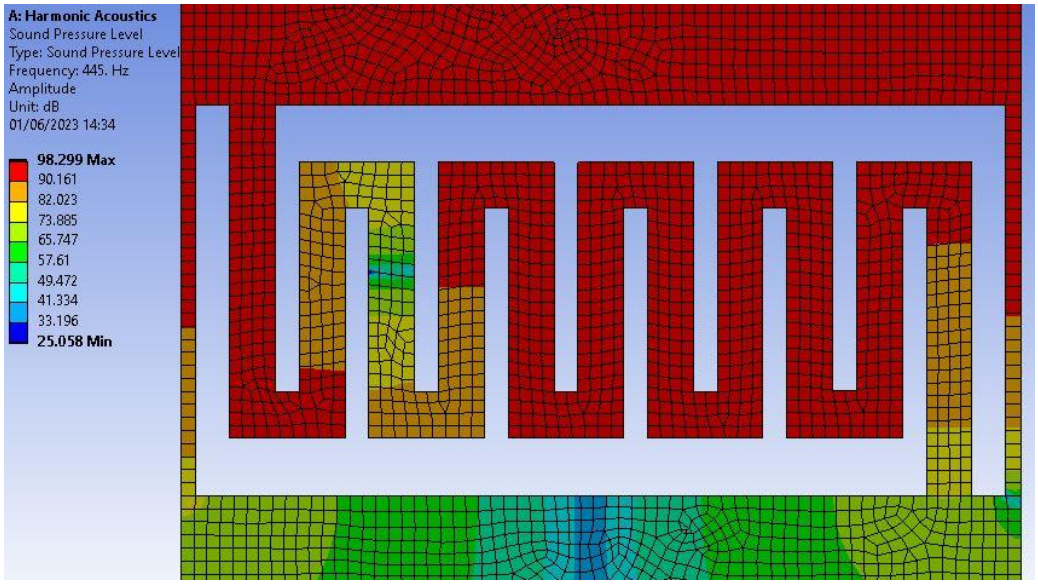

(b)

Figure 3.3. (a) Sound pressure level at the first resonance frequency ($f_{r1} = 343$ Hz), (b) Sound pressure level at the first antiresonance frequency ($f_{a1} = 445$ Hz).

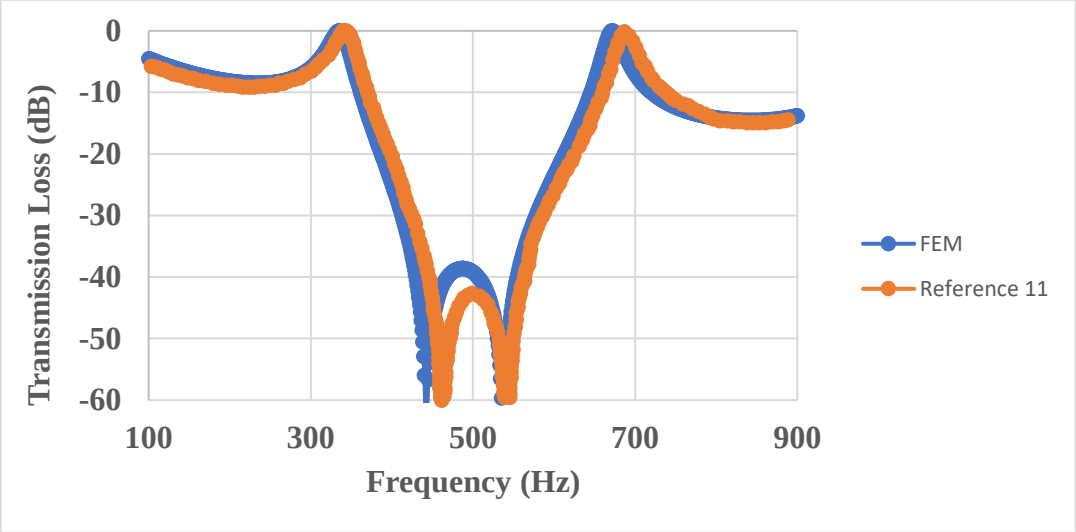

Figure 3.4. The resulting transmission loss graphs of the coupled straight and space-coiled channels via FEM, and reference article [11]. The width of the overall design domain is 129 mm.

As it can be seen from Figure 3.3, the third design involves both a straight channel and a space-coiled channel, which are considered in the same design domain. In fact, these channels are the ones in Figure 3.1 and Figure 3.2. It can be noticed that when these resonators are coupled, greater level of attenuation is obtained. The resulting transmission loss graph in Figure 3.4 is similar to the one in Figure 2.3.

4. METHODOLOGY

In the previous section, the finite element simulation results match the results in reference article [11] and benchmarking is completed. In order to achieve coupling with more than two resonators an analytical model of the problem that is based on transfer matrices will be formed using MATLAB. Once the analytical model is formed, transmission loss characteristics will be compared with ANSYS for model verification. Then, the analytical model will be used to obtain coupling among more than two different resonators at the same time. A methodology will be proposed that will allow coupling of multiple resonators systematically in a given frequency range. In all cases, normal incidence will be considered. Optimization of the design will be done with MATLAB by changing the number and/or the dimensions of space-coiled resonators to achieve isolation in the widest frequency range for a given transmission loss constraint. After finding the proper number and dimensions of coupled space-coiled resonators, the proposed design will be constructed by using ANSYS. The transmission loss graphs of MATLAB and ANSYS will be compared. Finally, the air pressure loss characteristics will be investigated.

In order to obtain an analytical model of the design which involves one resonator, transfer matrix method is used. Transfer matrix of the resonator (T_1) is constituted with four variables A_1, B_1, C_1, D_1 as follows

$$T_1 = \begin{bmatrix} A_1 & B_1 \\ C_1 & D_1 \end{bmatrix}, \tag{4.1}$$

$$A_1 = \cos(kl_1)\,, \tag{4.2}$$

$$B_1 = \frac{i\rho c \sin(kl_1)}{m_1}, \tag{4.3}$$

$$C_1 = \frac{im_1 \sin(kl_1)}{\rho c}, \tag{4.4}$$

$$D_1 = \cos(kl_1)\,. \tag{4.5}$$

In these equations, k is the wave number and is expressed by $k = 2\pi f/c$ where the terms f and c are the frequency and wave speed, respectively. m_1 is the slit ratio of the resonator and is expressed by $m_1 = d_o/d_1$ where d_o and d_1 are the width of the overall design domain and the slit width of the resonator, respectively. l_1 is the total length of the resonator and ρ

is air density. Transfer matrix is used to connect the acoustic pressures P and the acoustic velocities U on each side of the resonator.

$$\begin{Bmatrix} P_o \\ U_o \end{Bmatrix} = T_1 \begin{Bmatrix} P_i \\ U_i \end{Bmatrix} \tag{4.6}$$

where the subscripts *i* and *o* represent the inlet and outlet of the resonator, respectively. By using A_1, B_1, C_1, D_1, transmission loss for one resonator can be written as [51]

$$TL_1 = 10 \log_{10} \left(0.25 \left(A_1 + \frac{B_1}{\rho c} + C_1 \rho c + D_1 \right)^2 \right). \tag{4.7}$$

4.1. Effect of End Correction

Once the analytical model is formed, transmission loss characteristics can be compared with ANSYS for model verification. In order to verify the model, the following dimensions are chosen.

$$l_1 = 100 \text{ mm} \;\; d_1 = 10 \text{ mm}$$

where l_1 and d_1 are the total length of straight channel and the width of straight channel, respectively. The width of the overall design domain is taken as 129 mm. The proposed design according to these dimensions is shown in Figure 4.1.

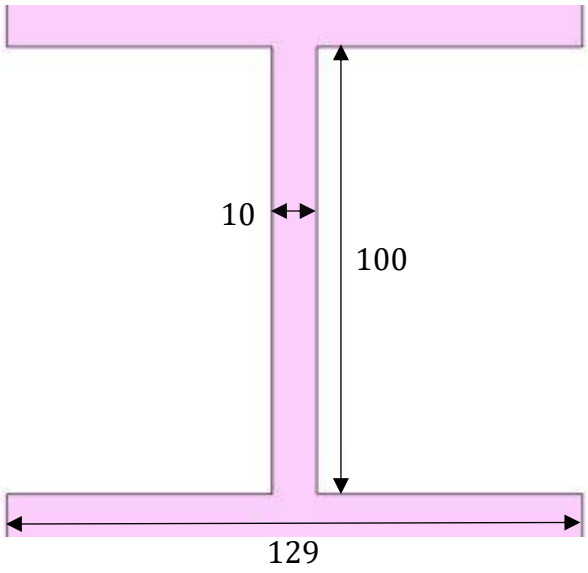

Figure 4.1. The proposed design without end correction. The dimensions are in mm.

As it can be seen from Figure 4.1, this design involves only a straight channel. The comparison of transmission losses between analytical model via MATLAB and finite element response via ANSYS without end correction is given in Figure 4.2.

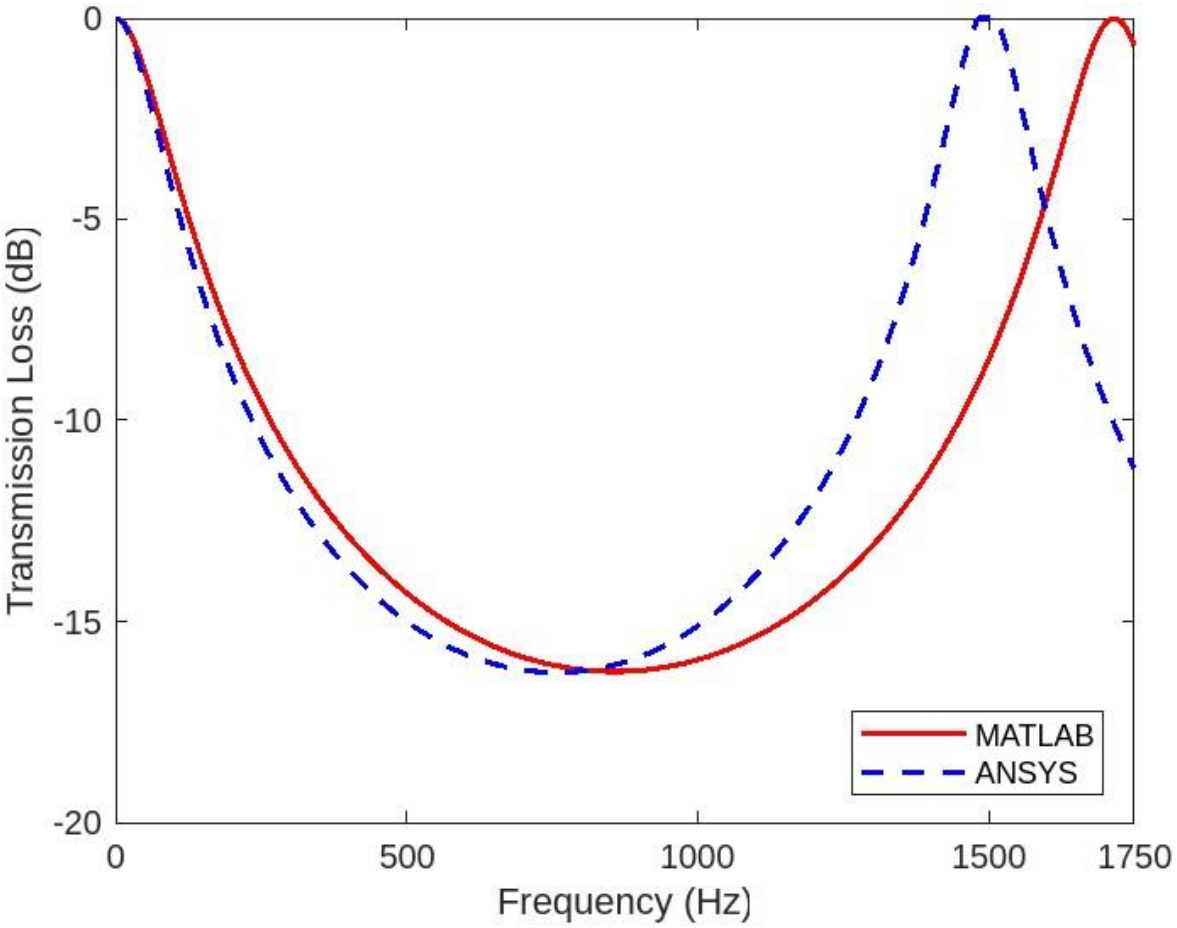

Figure 4.2. Transmission loss graphs of one straight channel via MATLAB and via ANSYS without end correction for 129 mm overall design domain width and 10 mm channel width.

As it can be seen from Figure 4.2, finite element response in ANSYS and transfer matrix response in MATLAB are different from each other. In order to match these responses, genetic algorithm is used via MATLAB. After matching with genetic algorithm, corresponding dimensions in ANSYS for the same acoustic response with transfer matrix model are given as follows

$$l_1 = 85.66 \text{ mm} \quad d_1 = 10 \text{ mm}\,.$$

The proposed design according to these dimensions is shown in Figure 4.3. As there are two open ends of the channel, end correction term at each end is $(100 - 85.66)/2 = 7.17$ mm, which is approximately 70% of the channel width. According to the end correction formula, end correction term at each end can be calculated as follows [14]

$$l_{end} = \mathrm{d}_1\left(e^{-(1.31906 d_1/d_o)} - 0.26148\right), \tag{4.8}$$

where d_1 and d_o are the widths of straight channel and the width of the overall design domain, respectively. By inserting the dimensions for this design, which are $d_1 = 10$ and $d_o = 129$, into this equation, l_{end} is calculated as 6.41 mm. This calculated end correction is approximately 64% of the channel width. Therefore, it can be concluded that the end correction term of the proposed design is close to the end correction term obtained through the formula [14].

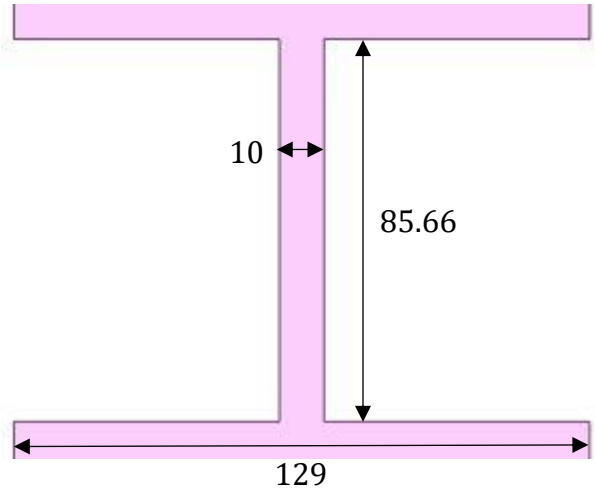

Figure 4.3. The proposed design with end correction. The dimensions are in mm.

As it can be seen from Figure 4.3, this design involves only a straight channel which is shorter than the case without end correction shown in Figure 4.1. The comparison of transmission losses between analytical model via MATLAB and finite element response via ANSYS with end correction is given in Figure 4.4.

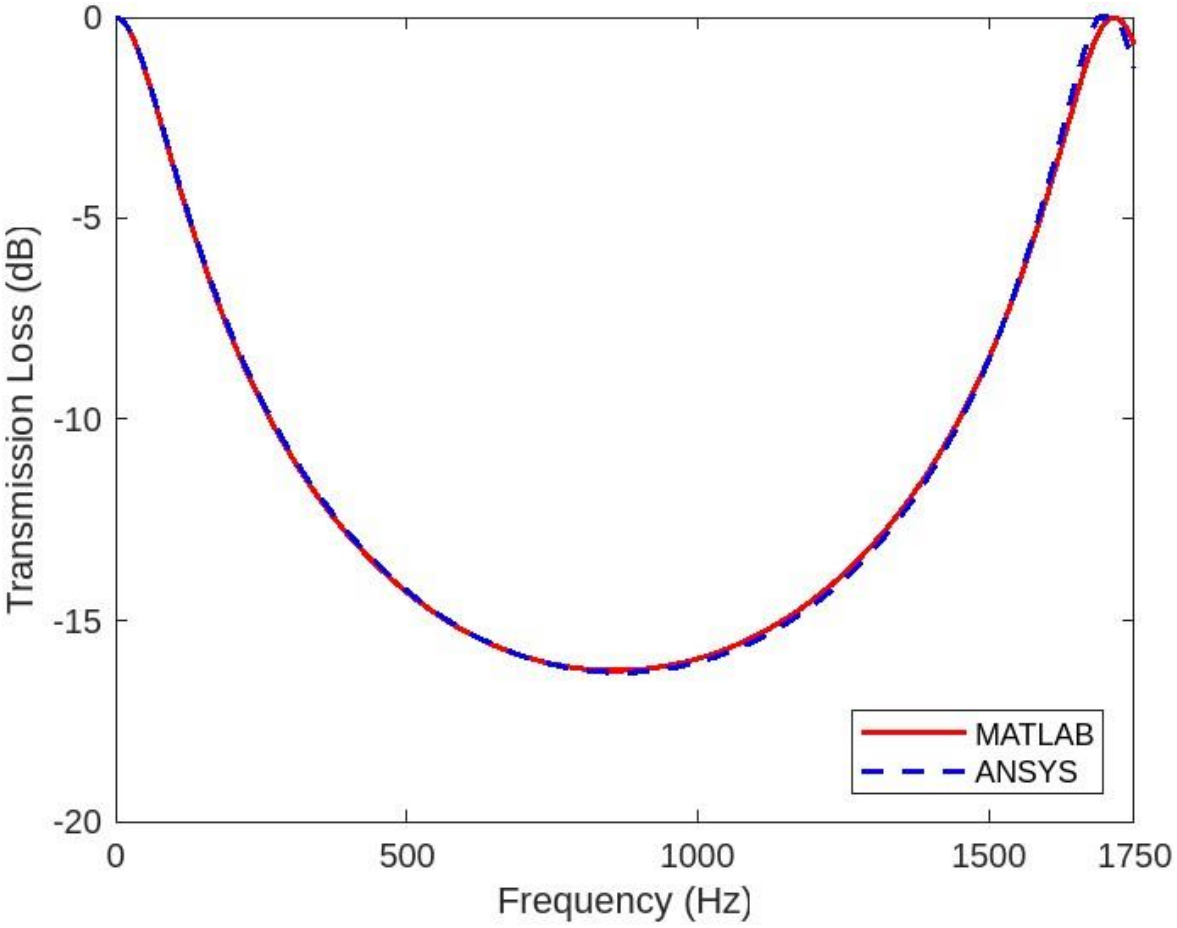

Figure 4.4. Transmission loss graphs of one straight channel via MATLAB and via ANSYS with end correction for 129 mm overall design domain width and 10 mm channel width.

As it can be seen from Figure 4.4, the frequency peaks and the maximum dB value in the transmission loss graph are almost the same for analytical model response via MATLAB and finite element response via ANSYS. In both graphs, a resonance occurs at the frequency of $f = 1716$ Hz and the maximum dB value is 16 dB. End correction is found by following the flowchart, which is given in Figure 4.5.

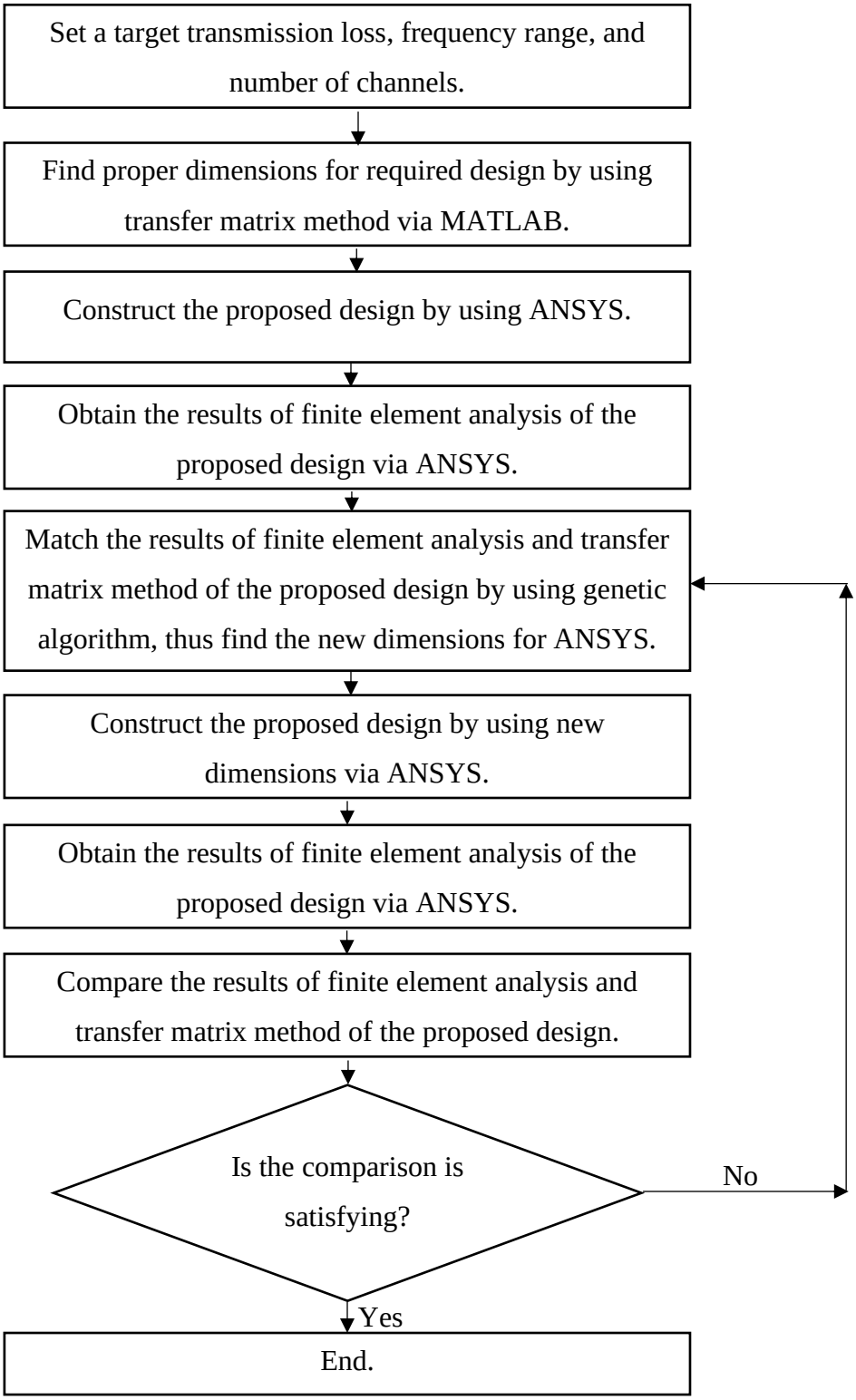

Figure 4.5. The flowchart for finding end correction.

4.2. Parallel Connection of Two Resonators

In order to obtain an analytical model of the design which involves two resonators, parallel connection of transfer matrices is used. In the literature, there exist some studies related to parallel assembly of transfer matrices [51,52] based on admittance sum method. In this thesis, a new derivation is given for parallel connection of transfer matrices. Transfer matrix for the second resonator (T_2) is constituted with A_2, B_2, C_2, D_2 as follows

$$T_2 = \begin{bmatrix} A_2 & B_2 \\ C_2 & D_2 \end{bmatrix}, \tag{4.9}$$

$$A_2 = \cos(kl_2)\,, \tag{4.10}$$

$$B_2 = \frac{i\rho c \sin(kl_2)}{m_2}, \tag{4.11}$$

$$C_2 = \frac{im_2 \sin(kl_2)}{\rho c}, \tag{4.12}$$

$$D_2 = \cos(kl_2)\,. \tag{4.13}$$

In these equations, m_2 is the slit ratio of the second resonator and is expressed by $m_2 = d_o/d_2$ where d_o and d_2 are the width of the overall design domain and the slit width of the second resonator, respectively. l_2 is the total length of the second resonator. The entries of the parallel transfer matrix of two coupled resonators (T_{p2}) is given as

$$T_{p2} = \begin{bmatrix} A_{p2} & B_{p2} \\ C_{p2} & D_{p2} \end{bmatrix}. \tag{4.14}$$

The main aim is to obtain these four entries in terms of the entries of the two individual resonators, i.e., A_1, B_1, C_1, D_1 in Equations (4.2)-(4.5) and A_2, B_2, C_2, D_2 in Equations (4.10)-(4.13). Notice that T_{p2} is used to connect the acoustic pressures P and acoustic velocities U on each side of the coupled resonators as follows

$$\begin{Bmatrix} P_o \\ U_o \end{Bmatrix} = T_{p2} \begin{Bmatrix} P_i \\ U_i \end{Bmatrix} = \begin{bmatrix} A_{p2} & B_{p2} \\ C_{p2} & D_{p2} \end{bmatrix} \begin{Bmatrix} P_i \\ U_i \end{Bmatrix}, \tag{4.15}$$

where the subscripts i and o represent the inlet and outlet of the coupled resonators, respectively. Inlet velocity (U_i) and outlet velocity (U_o) is the same for the first resonator and the second resonator. On the other hand, inlet pressure (P_i) is the sum of the inlet pressure of the first resonator (P_{i1}) and the second resonator (P_{i2}). Moreover, outlet pressure (P_o) is the sum of the outlet pressure of the first resonator (P_{o1}) and the second resonator (P_{o2}). These equalities can be written as

$$P_{i1} + P_{i2} = P_i \,, \tag{4.16}$$

$$P_{o1} + P_{o2} = P_o \,. \tag{4.17}$$

By using A_1, B_1, C_1, D_1 in Equations (4.2-4.5) and A_2, B_2, C_2, D_2 in Equations (4.10)-(4.13) the four entries (A_{p2}, B_{p2}, C_{p2}, D_{p2}) of the parallel connection of transfer matrices (T_{p2}) is calculated with the following steps.

The transfer matrix of the first resonator (T_1) can be seen in Equation (4.18) and the two equations corresponding to the rows of Equation (4.18) can be seen in Equations (4.19) and (4.20). Similarly, the transfer matrix of the second resonator (T_2) can be seen in Equation (4.21) and the two equations corresponding to the rows of Equation (4.21) can be seen in Equations (4.22) and (4.23) as follows

$$\begin{Bmatrix} P_{o1} \\ U_o \end{Bmatrix} = T_1 \begin{Bmatrix} P_{i1} \\ U_i \end{Bmatrix} = \begin{bmatrix} A_1 & B_1 \\ C_1 & D_1 \end{bmatrix} \begin{Bmatrix} P_{i1} \\ U_i \end{Bmatrix} = \begin{bmatrix} A_1 P_{i1} + B_1 U_i \\ C_1 P_{i1} + D_1 U_i \end{bmatrix}, \tag{4.18}$$

$$P_{o1} = A_1 P_{i1} + B_1 U_i \,, \tag{4.19}$$

$$U_o = C_1 P_{i1} + D_1 U_i \,, \tag{4.20}$$

$$\begin{Bmatrix} P_{o2} \\ U_o \end{Bmatrix} = T_2 \begin{Bmatrix} P_{i2} \\ U_i \end{Bmatrix} = \begin{bmatrix} A_2 & B_2 \\ C_2 & D_2 \end{bmatrix} \begin{Bmatrix} P_{i2} \\ U_i \end{Bmatrix} = \begin{bmatrix} A_2 P_{i2} + B_2 U_i \\ C_2 P_{i2} + D_2 U_i \end{bmatrix}, \tag{4.21}$$

$$P_{o2} = A_2 P_{i2} + B_2 U_i \,, \tag{4.22}$$

$$U_o = C_2 P_{i2} + D_2 U_i \,. \tag{4.23}$$

Equations (4.20) and (4.23) can be rewritten as

$$P_{i1} = \frac{U_o - D_1 U_i}{C_1} \,, \tag{4.24}$$

$$P_{i2} = \frac{U_o - D_2 U_i}{C_2} \,. \tag{4.25}$$

Equations (4.24) and (4.25) are used in Equation (4.16) as

$$\frac{U_o - D_1 U_i}{C_1} + \frac{U_o - D_2 U_i}{C_2} = P_i \,, \tag{4.26}$$

$$\frac{U_o C_2 - C_2 D_1 U_i + U_o C_1 - C_1 D_2 U_i}{C_1 C_2} = P_i \,, \tag{4.27}$$

$$\frac{U_o (C_1 + C_2)}{C_1 C_2} - \frac{U_i (C_2 D_1 + C_1 D_2)}{C_1 C_2} = P_i \,. \tag{4.28}$$

Consequently, second row of T_{p2} in Equation (4.15) is obtained as follows

$$U_o = \left(\frac{C_1 C_2}{C_1 + C_2}\right) P_i + \left(\frac{C_2 D_1 + C_1 D_2}{C_1 + C_2}\right) U_i \,. \tag{4.29}$$

Therefore, C_{p2} and D_{p2} are determined as

$$C_{p2} = \frac{C_1 C_2}{C_1 + C_2}, \tag{4.30}$$

$$D_{p2} = \frac{C_2 D_1 + C_1 D_2}{C_1 + C_2}. \tag{4.31}$$

In order to find the two remaining unknowns (A_{p2} and B_{p2}), Equations (4.24) and (4.25) are substituted in Equation (4.19) and Equation (4.22), respectively,

$$P_{o1} = A_1 \left(\frac{U_o - D_1 U_i}{C_1}\right) + B_1 U_i, \tag{4.32}$$

$$P_{o2} = A_2 \left(\frac{U_o - D_2 U_i}{C_2}\right) + B_2 U_i. \tag{4.33}$$

Moreover, Equations (4.32) and (4.33) are substituted in Equation (4.17),

$$P_o = A_1 \left(\frac{U_o - D_1 U_i}{C_1}\right) + B_1 U_i + A_2 \left(\frac{U_o - D_2 U_i}{C_2}\right) + B_2 U_i, \tag{4.34}$$

$$P_o = \left(\frac{A_1}{C_1} + \frac{A_2}{C_2}\right) U_o + \left(B_1 + B_2 - \frac{A_1 D_1}{C_1} - \frac{A_2 D_2}{C_2}\right) U_i. \tag{4.35}$$

Equation (4.29) is substituted in Equation (4.35) as follows

$$P_o = \left(\frac{A_1 C_2 + A_2 C_1}{C_1 C_2}\right)\left(\frac{C_1 C_2}{C_1 + C_2}\right) P_i + \left(\frac{A_1 C_2 + A_2 C_1}{C_1 C_2}\right)\left(\frac{C_2 D_1 + C_1 D_2}{C_1 + C_2}\right) U_i + \left(B_1 + B_2 - \frac{A_1 D_1 C_2 + A_2 D_2 C_1}{C_1 C_2}\right) U_i, \tag{4.36}$$

$$P_o = \left(\frac{A_1 C_2 + A_2 C_1}{C_1 + C_2}\right) P_i + \left(B_1 + B_2 + \frac{A_1 C_2^2 D_1}{(C_1 C_2)(C_1 + C_2)} + \frac{A_1 D_2 C_1 C_2 + A_2 D_1 C_1 C_2 + A_2 D_2 C_1^2}{(C_1 C_2)(C_1 + C_2)} - \frac{A_1 D_1 C_2 + A_2 D_2 C_1}{C_1 C_2}\right) U_i, \tag{4.37}$$

$$P_o = \left(\frac{A_1 C_2 + A_2 C_1}{C_1 + C_2}\right) P_i + \left(B_1 + B_2 + \frac{A_1 D_2 - A_1 D_1}{C_1 + C_2} + \frac{A_2 D_1 - A_2 D_2}{C_1 + C_2}\right) U_i. \tag{4.38}$$

Consequently, first row of T_{p2} in Equation (4.15) is obtained as follows

$$P_o = \left(\frac{A_1 C_2 + A_2 C_1}{C_1 + C_2}\right) P_i + \left(B_1 + B_2 + \frac{(A_1 - A_2)(D_2 - D_1)}{C_1 + C_2}\right) U_i. \tag{4.39}$$

Therefore, A_{p2} and B_{p2} are determined as

$$A_{p2} = \frac{A_1 C_2 + A_2 C_1}{C_1 + C_2}, \tag{4.40}$$

$$B_{p2} = B_1 + B_2 + \frac{(A_1 - A_2)(D_2 - D_1)}{C_1 + C_2}. \tag{4.41}$$

As all the entries of the parallel connection of transfer matrices are determined (see Equations (4.30), (4.31), (4.40), (4.41)), transmission loss of the acoustic metamaterial, which involves two coupled resonators, can be written as [51]

$$TL_{p2} = 10 \log_{10}\left(0.25 \left(A_{p2} + \frac{B_{p2}}{\rho c} + C_{p2} \rho c + D_{p2}\right)^2\right). \tag{4.42}$$

This analytical model can be verified with the results in reference article [11]. The dimensions for two coupled channels design are given below.

$$l_1 = 72 \text{ mm } \; l_2 = 500 \text{ mm } \; d_o = 129 \text{ mm } \; d_1 = 4.7 \text{ mm } \; d_2 = 7 \text{ mm}$$

where l_1 and l_2 are the total length of the first resonator, which is straight channel, and the total length of the second resonator, which is space-coiled channel, respectively. d_o, d_1 and d_2 are widths of overall design domain, straight channel and space-coiled channel, respectively. The design according to these dimensions is given in Figure 4.6.

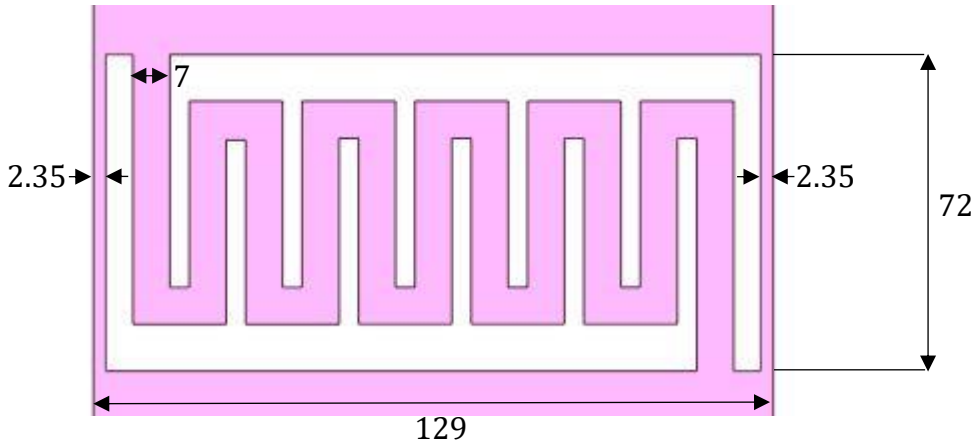

Figure 4.6. The design according to the given dimensions. The dimensions are in mm.

By inserting these dimensions into Equation (4.42), the resulting transmission loss which is given in Figure 4.7 is obtained.

As it can be seen from Figure 4.7, according to the MATLAB calculations, this design theoretically generates an attenuation band, which is centered at 492 Hz, with a transmission loss more than 40 dB of attenuation over a bandwidth which is 123 Hz between 436 Hz and 559 Hz. Normalized bandwidth of this design is $(559 - 436)/((559 + 436)/2) = 24.7\%$. Thus, the resulting transmission loss graph is quite similar to the finite element results without losses in Figure 2.3. Therefore, the analytical model for parallel connection of transfer matrices is verified.

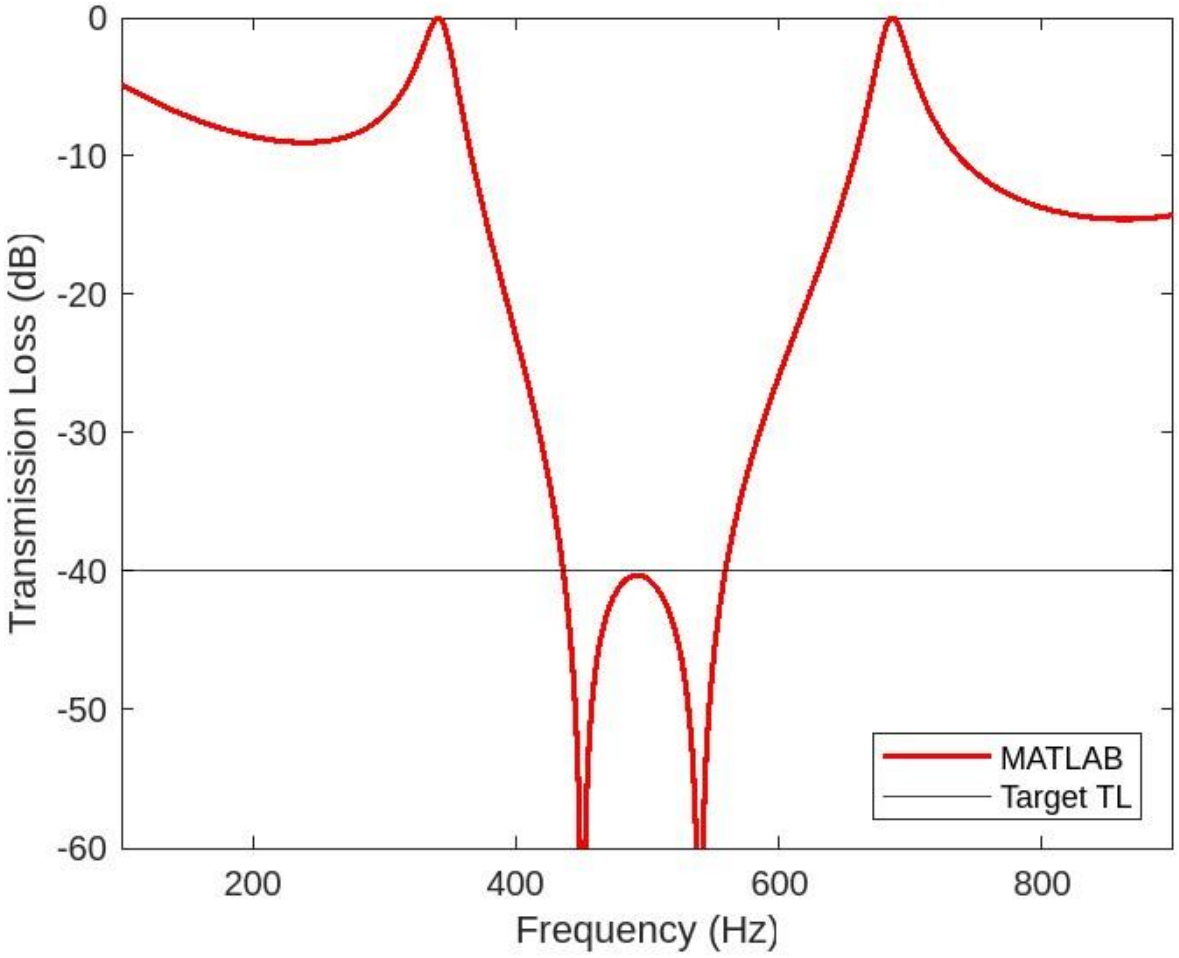

Figure 4.7. The resulting transmission loss graph of the coupled channels design [11] according to the proposed analytical model for parallel connection of transfer matrices.

Once the analytical model for coupled resonators is formed, transmission loss characteristics can be compared with ANSYS for model verification. For the design in reference article, the overall width of the design domain was 129 mm, the transmission loss target was 40 dB and the upper limit of the isolation bandwidth was 559 Hz [11]. In a general optimization problem, target transmission loss, overall width of the design domain and the upper limit of the isolation bandwidth can be set as constraints so that the lower limit of the isolation bandwidth can be minimized to achieve the maximum bandwidth by varying the dimensions of the channels in the acoustic metamaterial.

As a first design example, the aim is to achieve at least 30 dB transmission loss below 250 Hz. Hence, upper limit of the isolation bandwidth should be 250 Hz while the lower limit is to be minimized to achieve broadband response. The width of the overall design domain is 250 mm, which is fixed in the optimization code. For the optimization strategy, d_1 and d_2 are taken as fixed parameters while l_1 and l_2 are taken as variables. The resulting dimensions of the two channels according to the optimization in MATLAB are given in Table 4.1. In order to achieve similar acoustic response in the ANSYS model, genetic algorithm is used to vary the channel lengths, which are also listed in Table 4.1. The proposed design is shown in Figure 4.8.

Table 4.1. Comparison of channel lengths in MATLAB and ANSYS models of the design with two channels for 30 dB target TL below 250 Hz and 250 mm overall design domain width. In both designs, $d_1 = 40$ mm, $d_2 = 36$ mm.

	l_1 (mm)	l_2 (mm)
MATLAB	392.1	1176.3
ANSYS	354.7	1148.1

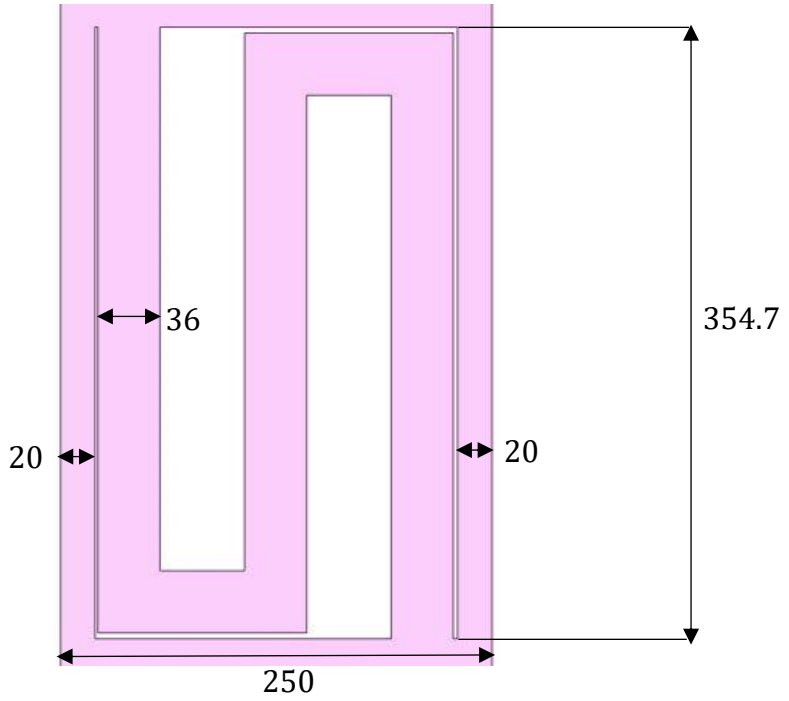

Figure 4.8. The proposed design with two channels for 250 mm overall design domain width, 250 Hz upper frequency limit and 30 dB target transmission loss within the isolation bandwidth. The dimensions are in mm.

As it can be seen from Figure 4.8, this design involves a straight channel and a space-coiled channel, which are considered in the same design domain. The comparison of transmission losses between analytical and finite element responses after matching operation is given in Figure 4.9.

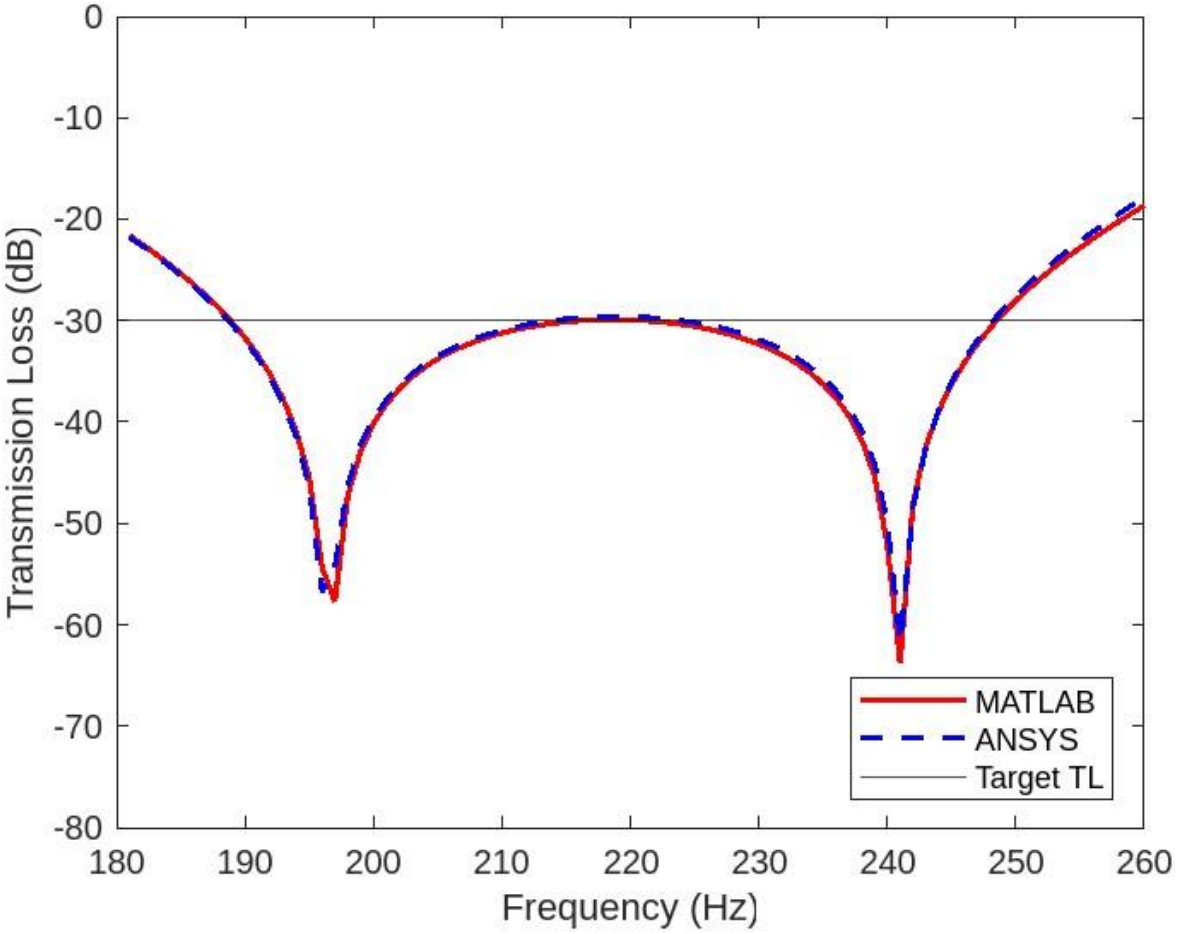

Figure 4.9. Transmission loss graphs of the design involving one straight channel and one space-coiled channel via MATLAB and ANSYS for 250 mm overall design domain width, 250 Hz upper frequency limit and 30 dB target transmission loss within the isolation bandwidth. Here, $d_1 = 40$ mm, $d_2 = 36$ mm.

As it can be seen from Figure 4.9, MATLAB and ANSYS results are very close to each other. Isolation frequency ranges in MATLAB and ANSYS models of the design are given in Table 4.2.

Table 4.2. Comparison of isolation frequency ranges and normalized bandwidth in MATLAB and ANSYS models of the two channels with 30 dB target TL below 250 Hz. In both designs, $d_1 = 40$ mm, $d_2 = 36$ mm.

	Isolation frequency range (Hz)	Normalized bandwidth (%)
MATLAB	189 – 249	27.4
ANSYS	189 – 248	27.0

4.3. Parallel Connection of More Than Two Resonators

In order to make an analytical model of the design which involves more than two resonators, parallel connection of transfer matrices can be used. Transfer matrix for a third resonator (T_3) is constituted with A_3, B_3, C_3, D_3.

$$T_3 = \begin{bmatrix} A_3 & B_3 \\ C_3 & D_3 \end{bmatrix}, \tag{4.43}$$

$$A_3 = \cos(kl_3)\,, \tag{4.44}$$

$$B_3 = \frac{i\rho c \sin(kl_3)}{m_3}, \tag{4.45}$$

$$C_3 = \frac{im_3 \sin(kl_3)}{\rho c}, \tag{4.46}$$

$$D_3 = \cos(kl_3)\,. \tag{4.47}$$

In these equations, m_3 is the slit ratio of the third resonator and is expressed by $m_3 = d_o/d_3$ where d_o and d_3 are the width of the overall design domain and the slit width of the third resonator, respectively. l_3 is the total length of the third resonator. By using A_{p2}, B_{p2}, C_{p2}, D_{p2} in Equations (4.30), (4.31), (4.40), (4.41) and A_3, B_3, C_3, D_3 in Equations (4.44) - (4.47) parallel connection of transfer matrices (T_{p3}) can be obtained as

$$T_{p3} = \begin{bmatrix} A_{p3} & B_{p3} \\ C_{p3} & D_{p3} \end{bmatrix}, \tag{4.48}$$

$$A_{p3} = \frac{C_{p2}A_3 + C_3A_{p2}}{C_{p2}+C_3}, \tag{4.49}$$

$$B_{p3} = B_{p2} + B_3 + \frac{A_{p2}(D_3 - D_{p2}) + A_3(D_{p2} - D_3)}{C_{p2}+C_3}, \tag{4.50}$$

$$C_{p3} = \frac{C_{p2}C_3}{C_{p2}+C_3}, \tag{4.51}$$

$$D_{p3} = \frac{C_{p2}D_3 + C_3D_{p2}}{C_{p2}+C_3}\,. \tag{4.52}$$

Parallel transfer matrix of three coupled resonators (T_{p3}) is used to connect the acoustic pressures P and acoustic velocities U on each side of the coupled resonators.

$$\begin{Bmatrix} P_o \\ U_o \end{Bmatrix} = T_{p3} \begin{Bmatrix} P_i \\ U_i \end{Bmatrix} \tag{4.53}$$

where the subscripts i and o represent the inlet and outlet of the coupled resonators, respectively.

After parallel connection of three transfer matrices is established, then by using these equations, transmission loss of the acoustic metamaterial, which involves three resonators, can be written as [51]

$$TL_3 = 10 \log_{10} \left(0.25 \left(A_{p3} + \frac{B_{p3}}{\rho c} + C_{p3} \rho c + D_{p3} \right)^2 \right). \tag{4.54}$$

Therefore, a methodology can be proposed that will allow coupling of multiple resonators systematically in a given frequency range. Let the number of resonators in an acoustic metamaterial be n. When one more resonator is to be added to this acoustic metamaterial, then transfer matrix for parallel combination of n resonators (T_{pn}) and (n+1)th resonator (T_{n+1}) can be recursively obtained using A_{pn}, B_{pn}, C_{pn}, D_{pn}, A_{n+1}, B_{n+1}, C_{n+1}, D_{n+1} where

$$T_{n+1} = \begin{bmatrix} A_{n+1} & B_{n+1} \\ C_{n+1} & D_{n+1} \end{bmatrix}, \tag{4.55}$$

$$A_{n+1} = \cos(k l_{n+1}), \tag{4.56}$$

$$B_{n+1} = \frac{i \rho c \sin(k l_{n+1})}{m_{n+1}}, \tag{4.57}$$

$$C_{n+1} = \frac{i m_{n+1} \sin(k l_{n+1})}{\rho c}, \tag{4.58}$$

$$D_{n+1} = \cos(k l_{n+1}). \tag{4.59}$$

In these equations, m_{n+1} is the slit ratio of the (n+1)th resonator and is expressed by $m_{n+1} = d_o / d_{n+1}$ where d_o and d_{n+1} are the width of the overall design domain and the slit width of the (n+1)th resonator, respectively. l_{n+1} is the total length of the (n+1)th resonator. The components of the parallel connection of (n+1) transfer matrices are calculated as

$$T_{p(n+1)} = \begin{bmatrix} A_{p(n+1)} & B_{p(n+1)} \\ C_{p(n+1)} & D_{p(n+1)} \end{bmatrix}, \tag{4.60}$$

$$A_{p(n+1)} = \frac{C_{pn} A_{n+1} + C_{n+1} A_{pn}}{C_{pn} + C_{n+1}}, \tag{4.61}$$

$$B_{p(n+1)} = B_{pn} + B_{n+1} + \frac{A_{pn}(D_{n+1}-D_{pn})+A_{n+1}(D_{pn}-D_{n+1})}{C_{pn}+C_{n+1}}, \quad (4.62)$$

$$C_{p(n+1)} = \frac{C_{pn}C_{n+1}}{C_{pn}+C_{n+1}}, \quad (4.63)$$

$$D_{p(n+1)} = \frac{C_{pn}D_{n+1}+C_{n+1}D_{pn}}{C_{pn}+C_{n+1}}. \quad (4.64)$$

After parallel connection of transfer matrices is established, then by using these equations, transmission loss of the acoustic metamaterial, which involves (n+1) resonators, can be written as [51]

$$TL_{n+1} = 10\log_{10}\left(0.25\left(A_{p(n+1)} + \frac{B_{p(n+1)}}{\rho c} + C_{p(n+1)}\rho c + D_{p(n+1)}\right)^2\right). \quad (4.65)$$

5. RESULTS AND DISCUSSION

By using the methodology for coupling of multiple resonators proposed in the previous section, an example will be shown for the analytical model of the design in MATLAB, which involves four resonators. Transmission loss characteristics will be compared with the ANSYS model for verification.

5.1. Effect of Transmission Loss

In this section, optimization of the design is done with MATLAB by varying the lengths of straight and space-coiled resonators to achieve isolation in the widest frequency range for a given transmission loss constraint. The width of the overall design is taken as 129 mm as in reference article [11] and the width of the channels is 3 mm. The upper limit of the isolation bandwidth is set as 500 Hz. The resulting dimensions of the four channels according to the optimization for targeted transmission loss level of 60 dB are given as

$$l_1 = 108.8 \text{ mm } \; l_2 = 517.6 \text{ mm } \; l_3 = 642.3 \text{ mm } \; l_4 = 985.7 \text{ mm},$$
$$d_1 = 3 \text{ mm } \; d_2 = 3 \text{ mm } \; d_3 = 3 \text{ mm } \; d_4 = 3 \text{ mm}.$$

One of the four channels is straight, and the others are space-coiled. After finding the proper number and dimensions of coupled straight and space-coiled resonators, the proposed design is constructed by using ANSYS. This design is shown in Figure 5.1.

As it can be seen from Figure 5.1, this design involves a straight channel and three space-coiled channels, which are considered in the same design domain. The aim of this design is to use the coupled resonator effect in a more powerful way. After matching with genetic algorithm via MATLAB, corresponding dimensions in ANSYS for the same acoustic response with transfer matrix model are given as follows

$$l_1 = 102.02 \text{ mm } \; l_2 = 515.22 \text{ mm } \; l_3 = 640.46 \text{ mm } \; l_4 = 995.08 \text{ mm},$$
$$d_1 = 3 \text{ mm } \; d_2 = 3 \text{ mm } \; d_3 = 3 \text{ mm } \; d_4 = 3 \text{ mm}.$$

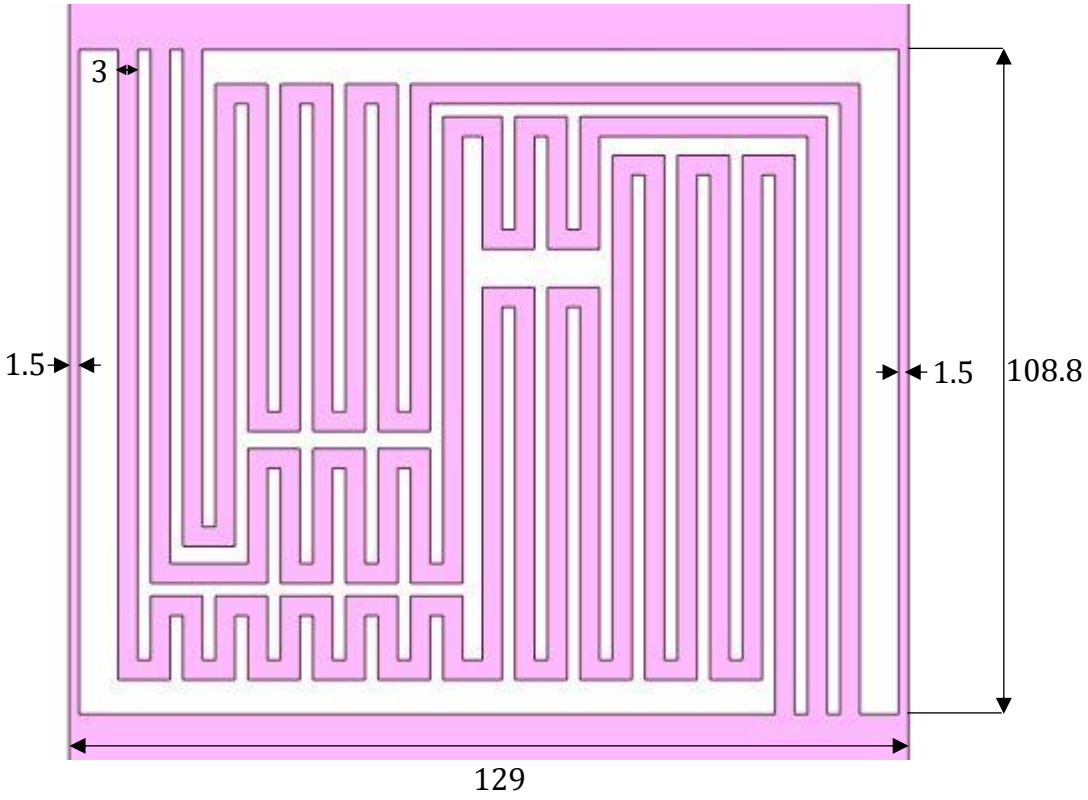

Figure 5.1. The proposed design with four channels for 129 mm overall design domain width, 500 Hz upper frequency limit and 60 dB target transmission loss within the isolation bandwidth. The dimensions are in mm.

The comparison of transmission losses between analytical model via MATLAB and finite element response via ANSYS after matching operation is given in Figure 5.2.

As it can be seen from Figure 5.2, according to the MATLAB calculations, this design theoretically generates an attenuation band, which is centered at 435 Hz, with a transmission loss more than 60 dB of attenuation over a bandwidth which is 112 Hz between 379 Hz and 491 Hz. Thus, normalized bandwidth is $(491-379)/((491+379)/2) = 25.7\%$. As it can be seen from Figure 5.2, according to the ANSYS analysis, the resulting transmission loss graph shows an attenuation band, which is centered at 435 Hz, with a transmission loss more than 60 dB of attenuation over a bandwidth which is 112 Hz between 379 Hz and 491 Hz. Thus, normalized bandwidth is again 25.7%. Therefore, it can be concluded that the frequency interval and the transmission loss are exactly same for analytical model response and finite element response.

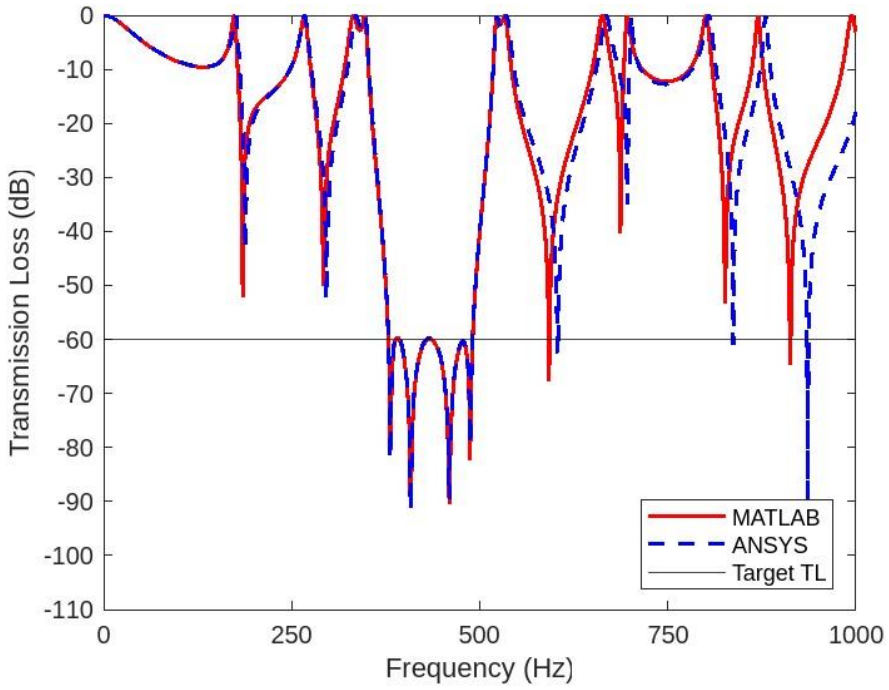

(a)

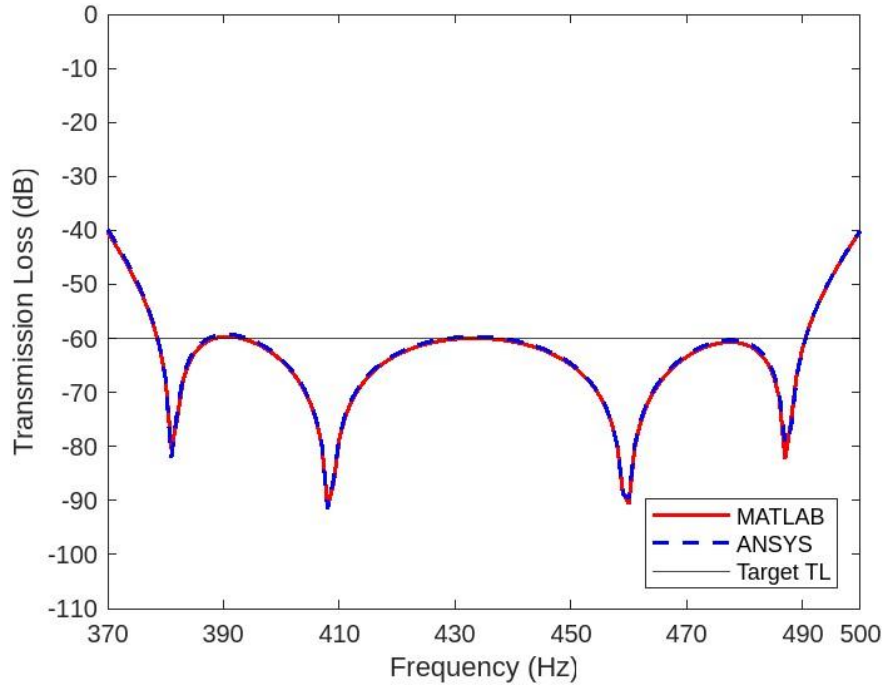

(b)

Figure 5.2. Transmission loss graphs of the design with four channels via MATLAB and ANSYS for 129 mm overall design domain width, 500 Hz upper frequency limit and 60 dB target transmission loss within the isolation bandwidth (a) At frequencies between 0 Hz and 1000 Hz, (b) At frequencies between 370 Hz and 500 Hz. Here, $d_1 = 3$ mm, $d_2 = 3$ mm, $d_3 = 3$ mm, $d_4 = 3$ mm.

For this specific design, the value of the end correction term at each end of the straight channel is $(108.8 - 102.02)/2 = 3.39$ mm, which is slightly larger than channel width. Moreover, the space-coiled channels do not have the same length difference between the MATLAB and ANSYS models as these channels have different shapes and different number of turns. Table 5.1 shows the lengths of the channels in the MATLAB and ANSYS models. Notice that for the longest channel, the length in ANSYS model is larger than the MATLAB model as this space-coiled channel involves more turns than the other channels.

Table 5.1. Comparison of channel lengths in MATLAB and ANSYS models of the design with four channels for 60 dB target TL below 500 Hz and 129 mm overall design domain width.

	l_1 (mm)	l_2 (mm)	l_3 (mm)	l_4 (mm)
MATLAB	108.8	517.6	642.3	985.7
ANSYS	102.02	515.22	640.46	995.08
Difference	6.78	2.38	1.84	-9.38

Table 5.2 shows the channel widths, target transmission loss and isolation bandwidth frequency ranges of various designs investigated via MATLAB. In order to have a fair comparison, all designs have the same upper limit for the isolation frequencies range (559 Hz) and same overall width (129 mm) corresponding to Design-1 shown in Figure 4.6. In Design-2, the straight channel width is increased (from 4.7 mm to 7 mm), with the same target TL of 40 dB, optimum straight channel length is significantly increased (from 72 mm to 126 mm); however, normalized bandwidth remained almost the same (24.7% vs 24.9%). Wider channels are better for reducing pressure loss in the case of airflow. However, when the channels become wider, the optimum length of the channel becomes longer, as well. Hence, compactness is undermined. In Design-3, target TL value is lowered to 30 dB. Compared to Design-2, optimum straight channel length is significantly reduced (compactness is improved) and normalized bandwidth is significantly increased. If significantly lower pressure loss is sought after in the case of airflow, the channel widths should be significantly increased. The design in Figure 4.8, has an overall width of 250 mm and the upper limit of the isolation bandwidth is at 249 Hz. In order to achieve 559 Hz upper limit, the optimum channel lengths can be scaled by 249/559=0.445, and to achieve 129 mm overall width, the optimum channel widths can be scaled by 129/250=0.516 as in Design-4.

Compared to Design-3, the channel widths are almost tripled, so pressure loss in the case of airflow will be much lower. On the other hand, normalized bandwidth of the system and compactness of the straight channel are sacrificed. In order to achieve higher target TL values, narrower channels are required. In Design-5, the channel widths are reduced to 3 mm and the target TL is set at 60 dB. Notice that the optimum straight channel length is significantly increased and the normalized bandwidth is significantly reduced. In Figure 5.1, a design with four channels (one straight channel and three space-coiled channels) is shown. The transmission loss graph of this design was given in Figure 5.2. The upper limit of the isolation bandwidth of this design is at 491 Hz. In order to achieve 559 Hz upper limit, the optimum channel lengths can be scaled by 491/559=0.878 as in Design-6. Note that the straight channel length is considerably shorter in Design-6 when compared to Design-5. As there are more channels, the airflow will be easier. Besides, the normalized bandwidth is almost doubled when four channels are used instead of two channels.

Table 5.2. Comparison of channel widths, target transmission loss and isolation bandwidth frequency ranges of various designs investigated in MATLAB. The first channel dimension in the rows belong to the straight channel and the others belong to the space-coiled channels. In all the analyses, the overall width of the design domain is 129 mm and the upper limit of the isolation bandwidth is 559 Hz.

	Channel widths (mm)	Channel lengths (mm)	Target TL (dB)	Isolation frequency range (Hz)	Normalized bandwidth (%)
Design-1 in Figure 4.6 [11]	4.7 – 7	72 – 500	40	436 – 559	24.7
Design-2	7 – 7	126 – 507	40	435 – 559	24.9
Design-3	7 – 7	104 – 538	30	378 – 559	38.6
Design-4	20.6 – 18.6	174 – 522	30	424 – 559	27.4
Design-5	3 – 3	141 – 483	60	491– 559	13.0
Design-6	3 – 3 – 3 – 3	95.6 – 454.6 – 564.2 – 865.8	60	432 – 559	25.7

The aim of the thesis is to design an acoustic metamaterial which allows airflow while attenuating sound. For high transmission loss targets, having high number of channels can be advantageous whereas for low transmission loss targets two channels can offer the best solution. In the next section, the comparison of pressure responses will be explained in detail.

5.2. Effect of Pressure Loss

Although the normalized bandwidth in the four channels design in Figure 5.2 is wide (25.7%), and transmission loss is high (60 dB), there will be significant pressure loss in the case of airflow as the channel widths are quite narrow (3 mm). Wider channels can offer lower pressure loss in the expense of reduced normalized bandwidth. In the next subsections, various designs will be compared both in terms of acoustic transmission loss and pressure loss. In all the analyses, overall width of the design domain is set as 250 mm and the upper limit of the isolation bandwidth is chosen as 250 Hz.

5.2.1. 10 dB Transmission Loss Target

In this subsection, optimization of the design is done for 10 dB transmission loss constraint with MATLAB by changing the number and/or the dimensions of straight and space-coiled resonators to achieve isolation in the widest frequency range while keeping the air pressure loss at minimum. When target TL is set as 10 dB, widest isolation bandwidth is obtained with the two channels design (a straight channel and a space-coiled channel) in MATLAB. The resulting dimensions of the two channels according to the optimization in MATLAB are given in Table 5.3. In order to achieve similar acoustic response in the ANSYS model, genetic algorithm is used to vary the channel lengths, which are also listed in Table 5.3.

By using the dimensions in Table 5.3, acoustic transmission loss and pressure loss analyses are done via ANSYS. For the acoustic part of the analyses, the comparison of transmission losses between analytical model and finite element response after matching operation is given in Figure 5.3. It can be seen that MATLAB and ANSYS results are very close to each other.

Table 5.3. Comparison of channel lengths and isolation frequency ranges in MATLAB and ANSYS models of the design with two channels for 10 dB target TL below 250 Hz and 250 mm overall design domain width. In both designs, $d_1 = 90$ mm, $d_2 = 49.8$ mm.

	l_1 (mm)	l_2 (mm)	Isolation frequency range (Hz)	Normalized bandwidth (%)
MATLAB	445.2	1310.5	144 – 249	53.4
ANSYS	433.6	1297.3	144 – 248	53.1

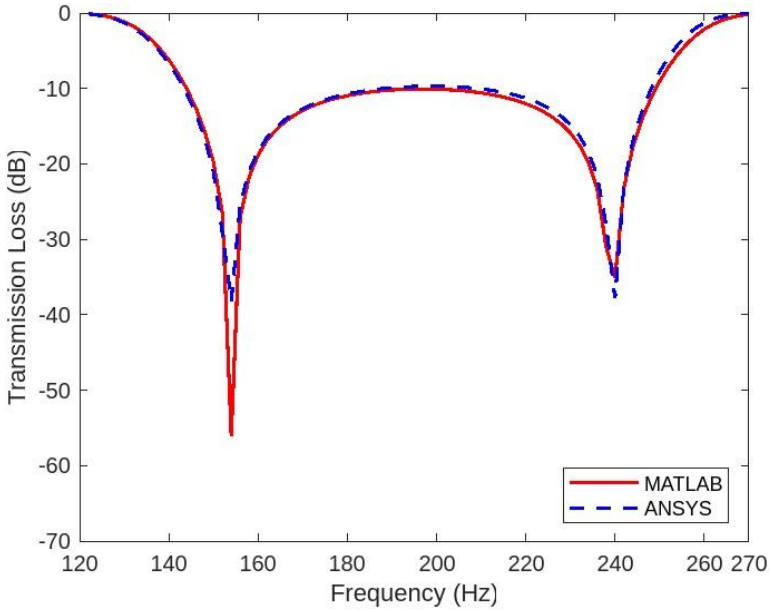

Figure 5.3. Transmission loss graphs of the design involving one straight channel and one space-coiled channel via MATLAB and ANSYS for 250 mm overall design domain width, 250 Hz upper frequency limit and 10 dB target transmission loss within the isolation bandwidth. Here, $d_1 = 90$ mm, $d_2 = 49.8$ mm.

For the pressure part of the analyses, inlet speed and the shape of the design are varied in the analyses. The following flow analysis is done for zero shear boundary conditions as

$$v_i = 3 \text{ m/s} \;\; t_{op} = 200 \text{ mm} \;\; shape_{coiled} = rectangular\ corner\ ,$$

where v_i and t_{op} are inlet speed and out-of-plane thickness of the design, respectively. In this analysis, the shape of the space-coiled channel involves rectangular corners. The resulting pressure response of the flow is given in Figure 5.4.

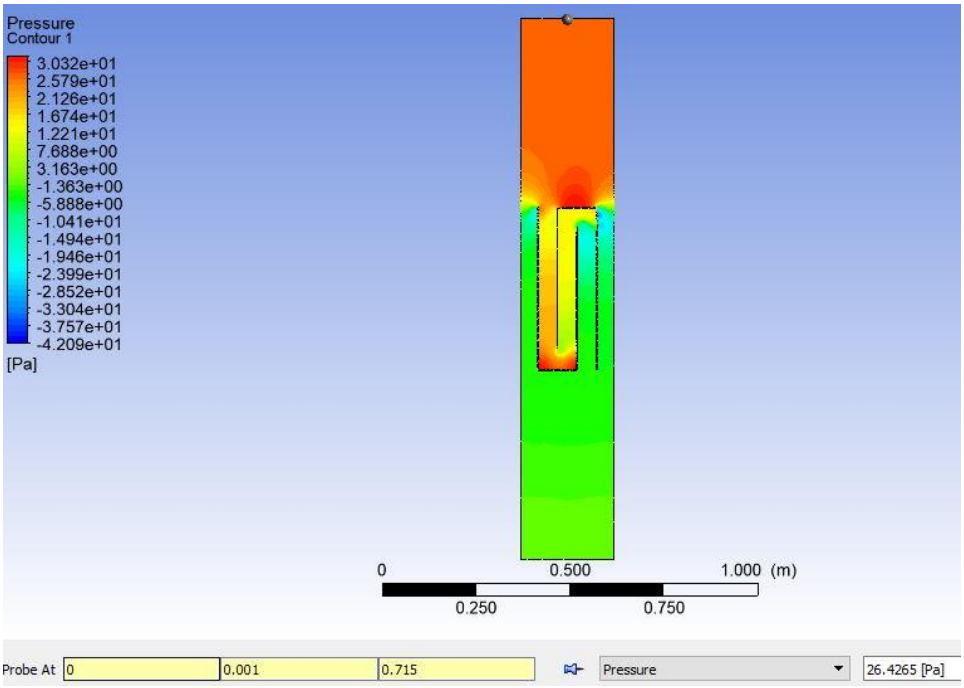

(a)

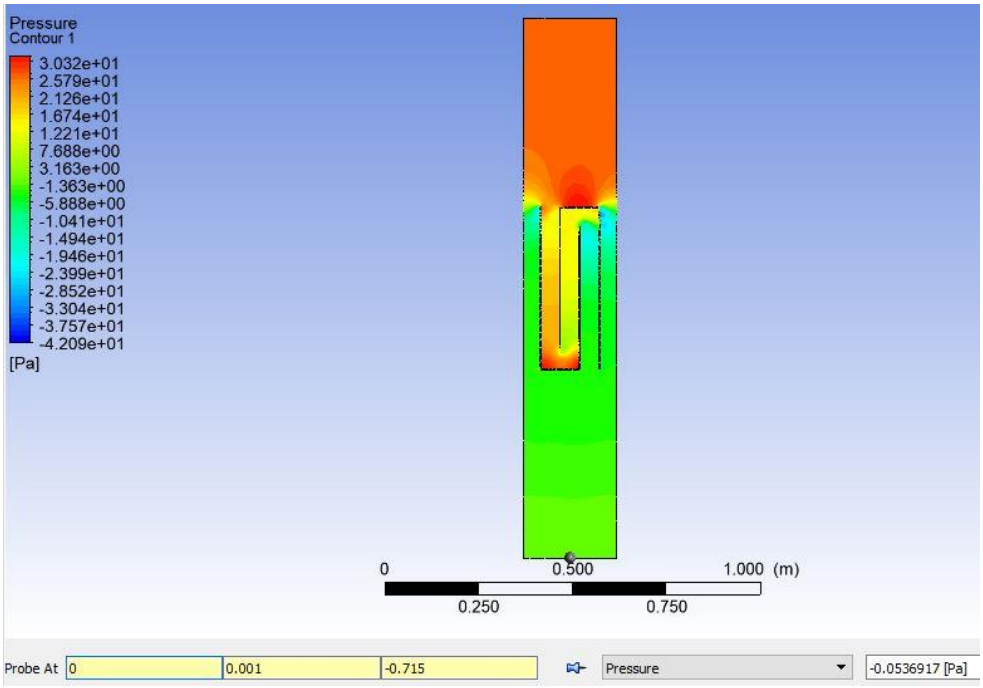

(b)

Figure 5.4. The pressure response of the flow for 3 m/s inlet speed, (a) Showing inlet pressure, (b) Showing outlet pressure, for the design with one straight channel and one space-coiled channel with rectangular corners for 10 dB target transmission loss, 250 mm overall design domain width and 250 Hz upper frequency limit. Here, $d_1 = 90$ mm, $d_2 = 49.8$ mm.

As it can be seen from Figure 5.4, the resulting pressure loss between inlet and outlet is 26.481 Pa. In order to decrease the pressure loss between inlet and outlet, rounded corners are used as shown in Figure 5.6. The next analysis is also done for zero shear boundary conditions as follows

$$v_i = 3 \text{ m/s} \;\; t_{op} = 200 \text{ mm} \;\; shape_{coiled} = rounded\ corner\ ,$$

where v_i and t_{op} are inlet speed and out-of-plane thickness of the design with rounded corners, respectively. Since the acoustic response of the design changes with rounded corners, matching operation between analytical model in MATLAB and finite element response in ANSYS is required. The dimensions of straight and space-coiled channels are revised such that they produce the same acoustic response as analytical model and so rectangular corner model. The resulting isolation frequency ranges and normalized bandwidth are listed in Table 5.4. For the acoustic part of the rounded corner analyses, the comparison of transmission losses between analytical model and finite element response after matching operation is given in Figure 5.5.

Table 5.4. Comparison of isolation frequency ranges and normalized bandwidth in MATLAB and ANSYS models of the two channels with rounded corners design with 10 dB target TL below 250 Hz. In both designs, $d_1 = 90$ mm $\;d_2 = 49.8$ mm.

	l_1 (mm)	l_2 (mm)	Isolation frequency range (Hz)	Normalized bandwidth (%)
MATLAB	445.2	1310.5	144 – 249	53.4
ANSYS	434.9	1299.5	144 – 248	53.1

As it can be seen from Figure 5.5, according to the MATLAB calculations, this design theoretically generates an attenuation band, which is centered at 196.5 Hz, with a transmission loss more than 10 dB of attenuation over a bandwidth which is 105 Hz between 144 Hz and 249 Hz. As it can be seen from Figure 5.5, according to the ANSYS analysis, the resulting transmission loss graph shows an attenuation band, which is centered at 196 Hz, with a transmission loss more than 10 dB of attenuation over a bandwidth which is 104 Hz between 144 Hz and 248 Hz.

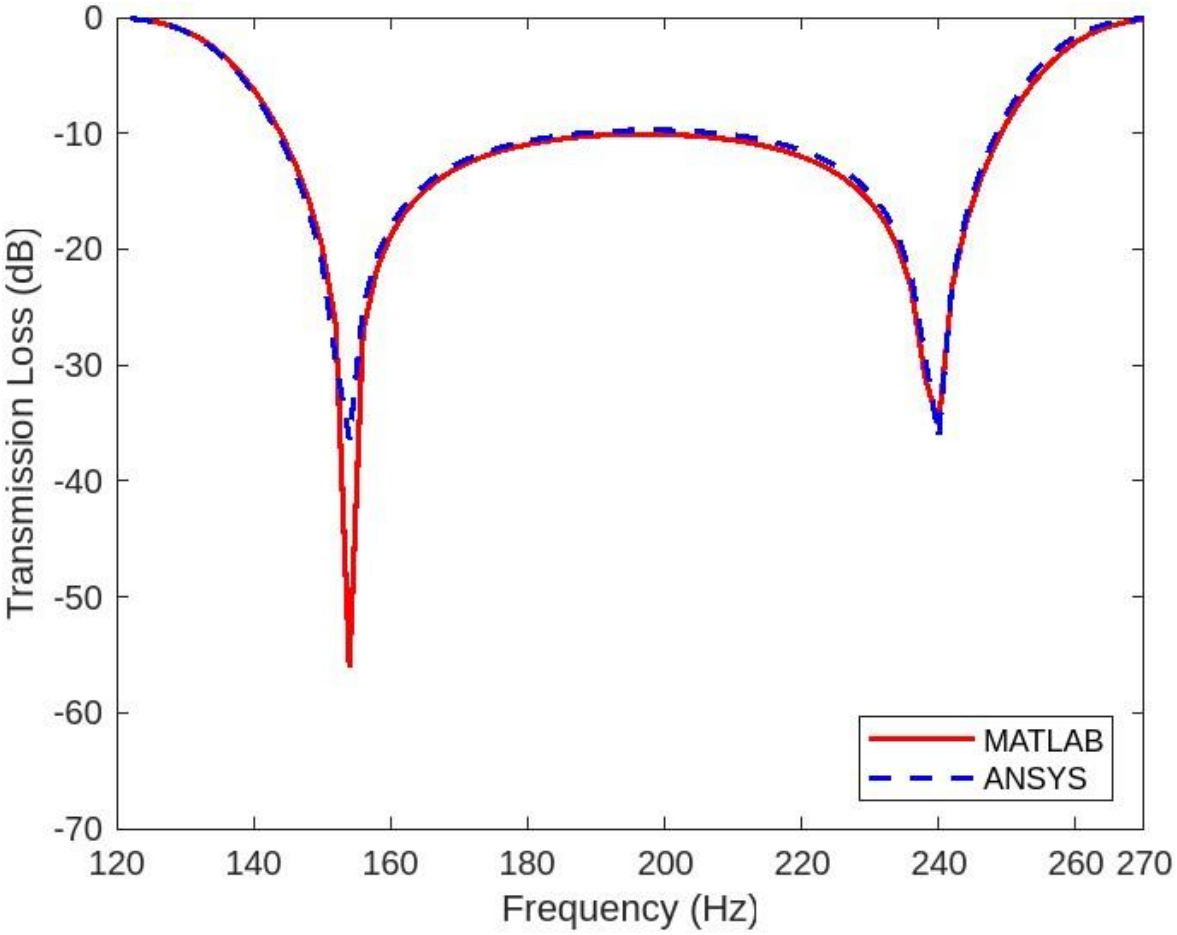

Figure 5.5. Transmission loss graphs of the design involving one straight channel and one space-coiled channel with rounded corners via MATLAB and ANSYS for 250 mm overall design domain width, 250 Hz upper frequency limit and 10 dB target transmission loss within the isolation bandwidth. Here, $d_1 = 90$ mm, $d_2 = 49.8$ mm.

Therefore, it can be concluded that the frequency interval and the transmission loss are almost the same for analytical model response and finite element response. The resulting pressure response of the flow is given in Figure 5.6.

As it can be seen from Figure 5.6, the design with rounded corners produces a pressure loss between inlet and outlet is 21.081 Pa at 3 m/s inlet speed. Hence, lower pressure loss is obtained than the design with rectangular corners which produces a pressure loss of 26.481 Pa.

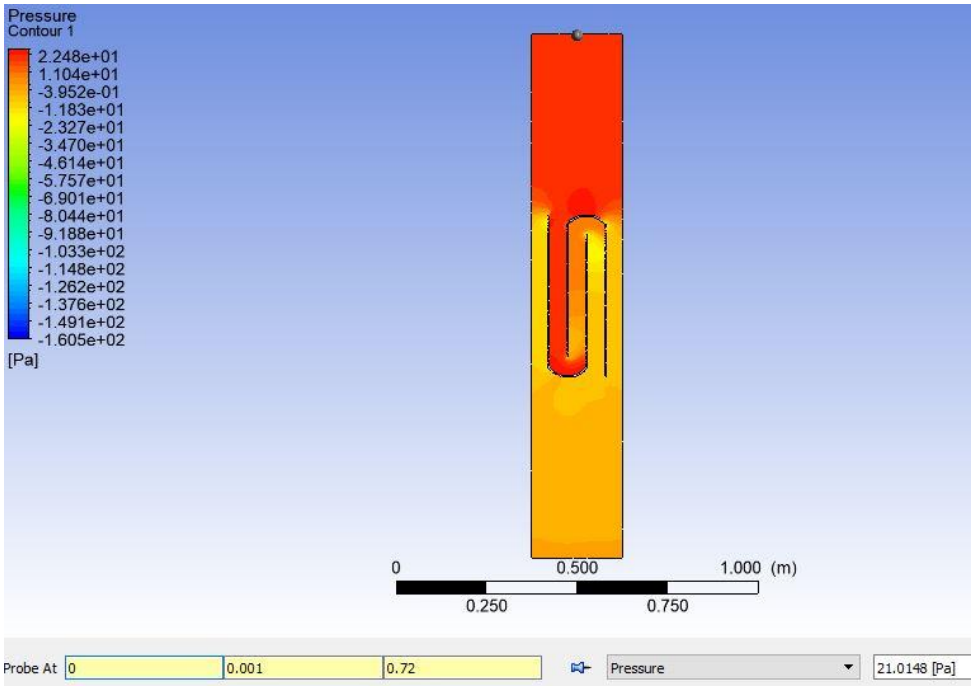

(a)

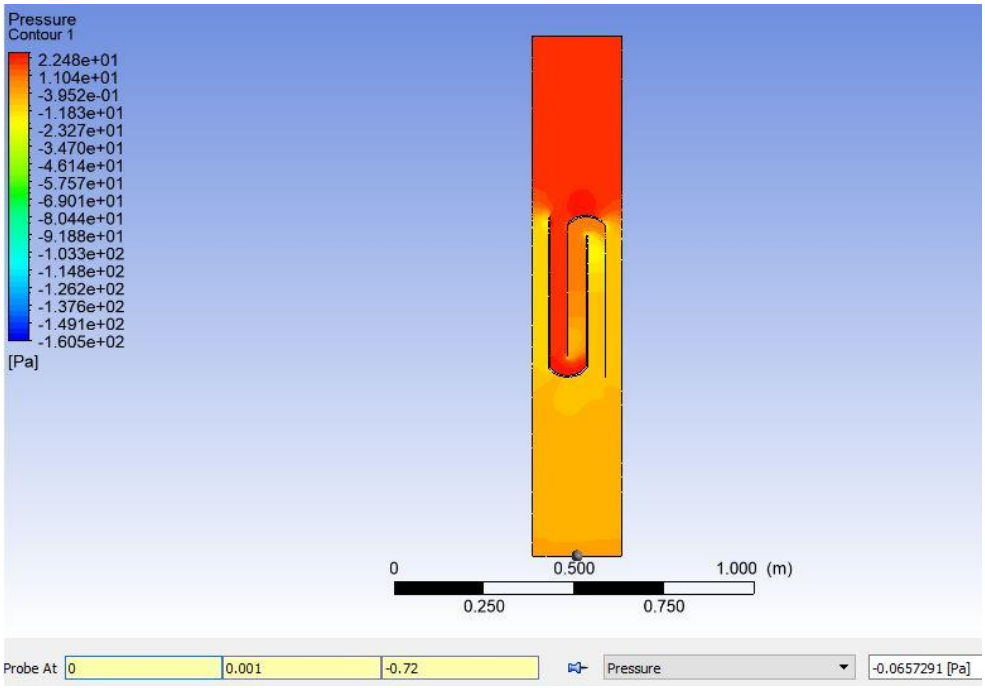

(b)

Figure 5.6. The pressure response of the flow for 3 m/s inlet speed, (a) Showing inlet pressure, (b) Showing outlet pressure, for the design with one straight channel and one space-coiled channel with rounded corners for 10 dB target transmission loss, 250 mm overall design domain width and 250 Hz upper frequency limit. Here, $d_1 = 90$ mm, $d_2 = 49.8$ mm.

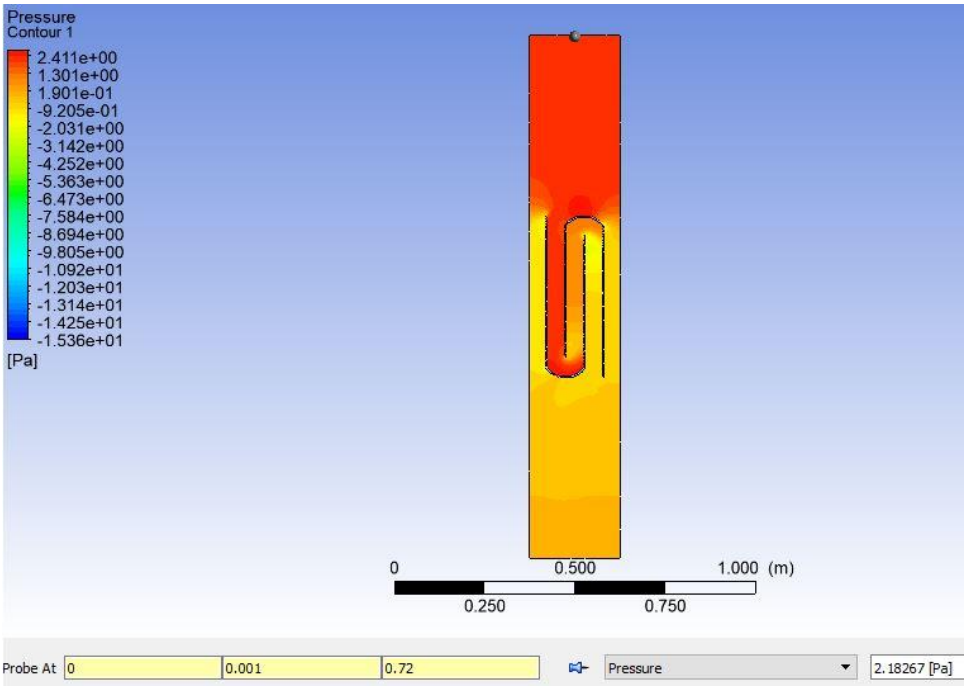

(a)

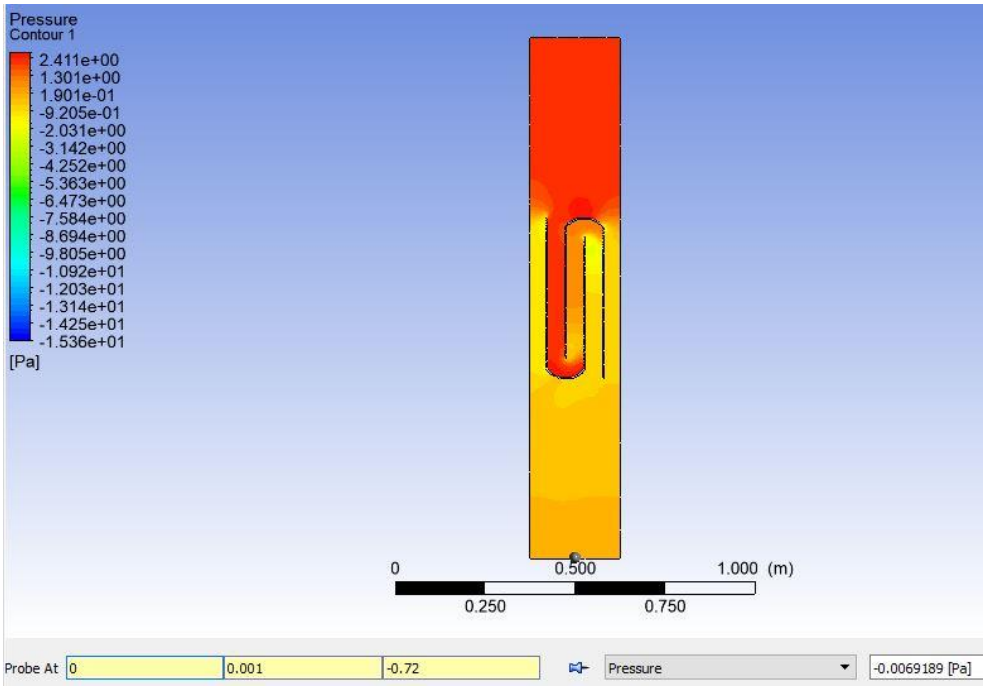

(b)

Figure 5.7. The pressure response of the flow for 1 m/s inlet speed, (a) Showing inlet pressure, (b) Showing outlet pressure, for the design with one straight channel and one space-coiled channel with rounded corners for 10 dB target transmission loss, 250 mm overall design domain width and 250 Hz upper frequency limit. Here, $d_1 = 90$ mm, $d_2 = 49.8$ mm.

The pressure loss of the design with rounded corners can be calculated for a different inlet speed and the result can be investigated using Equation (2.1). According to Equation (2.1), pressure loss is proportional to the square of inlet speed. Hence, the following flow analysis is done for zero shear boundary conditions as follows

$$v_i = 1 \text{ m/s } \; t_{op} = 200 \text{ mm } \; shape_{coiled} = rounded\ corner\ ,$$

where v_i and t_{op} are inlet speed and out-of-plane thickness of the design with rounded corners, respectively. The resulting pressure response of the flow is given in Figure 5.7.

As it can be seen from Figure 5.7, the resulting pressure loss between inlet and outlet is 2.187 Pa. The ratio between the two designs, which have velocities of 1 m/s and 3 m/s, is $21.081/2.187 = 9.639$. This ratio is close to the ideal ratio of $(3/1)^2 = 9$ according to Equation (2.1). Therefore, it can be concluded that pressure loss response in finite element model is verified since the pressure loss ratio in finite element model is approximately proportional to the square of inlet speed ratio.

5.2.2. 30 dB Transmission Loss Target

In this second subsection, optimization of the design is done for 30 dB transmission loss constraint with MATLAB by changing the number and/or the dimensions of straight and space-coiled resonators to achieve isolation in the widest frequency range while keeping the air pressure loss at minimum. The second subsection includes two design solutions, which have different numbers of channels. The aim of the first design is to inspect pressure loss response with the increasing transmission loss. This will be done by comparing the pressure loss responses of the designs having transmission losses of 10 dB and 30 dB. The aim of the second design is to inspect maximum frequency bandwidth with the increasing number of space-coiled channels while keeping the transmission loss the same. According to these aims, two resulting designs are obtained. The first design involves two channels (one straight channel and one space-coiled). The second design involves three channels (one straight channel and two space-coiled channels). The width of the overall design domain is 250 mm for both designs.

In the first design, the resulting dimensions of the two channels according to the optimization in MATLAB are given in Table 5.5. In order to achieve similar acoustic response in the ANSYS model, genetic algorithm is used to vary the channel lengths, which are also listed in Table 5.5.

Table 5.5. Comparison of channel lengths and isolation frequency ranges in MATLAB and ANSYS models of the two channels design with 30 dB target TL below 250 Hz and 250 mm overall design domain width. In both designs, $d_1 = 40$ mm, $d_2 = 36$ mm.

	l_1 (mm)	l_2 (mm)	Isolation frequency range (Hz)	Normalized bandwidth (%)
MATLAB	392.1	1176.3	189 – 249	27.4
ANSYS	354.7	1148.1	189 – 248	27.0

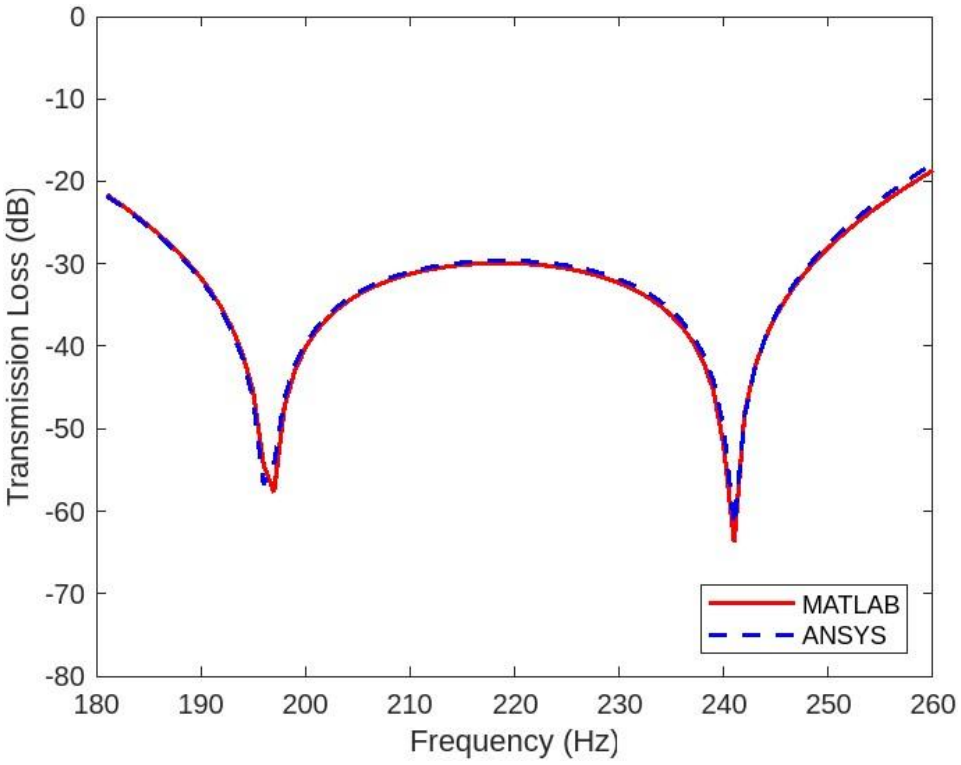

Figure 5.8. Transmission loss graphs of the design involving one straight channel and one space-coiled channel via MATLAB and ANSYS for 250 mm overall design domain width, 250 Hz upper frequency limit and 30 dB target transmission loss within the isolation bandwidth. Here, $d_1 = 40$ mm, $d_2 = 36$ mm.

By using the dimensions in Table 5.5, acoustic transmission loss and pressure loss analyses are done via ANSYS. For the acoustic part of the analyses, the comparison of transmission losses between analytical model and finite element response after matching operation is given in Figure 5.8. It can be seen that MATLAB and ANSYS results are very close to each other.

For the pressure part of the analyses, the shape of the design is varied in the analyses. The following flow analysis is done for zero shear boundary conditions as follows

$$v_i = 3\ m/s\ \ t_{op} = 200\ \text{mm}\ \ shape_{coiled} = rectangular\ corner\ ,$$

where v_i and t_{op} are inlet speed and out-of-plane thickness of the design, respectively. In this analysis, the shape of the space-coiled channel involves rectangular corners. The resulting pressure response of the flow is given in Figure 5.9.

As it can be seen from Figure 5.9, the resulting pressure loss between inlet and outlet is 109.520 Pa. In order to decrease the pressure loss between inlet and outlet, rounded corners are used as shown in Figure 5.11. The next analysis is also done for zero shear boundary conditions as follows

$$v_i = 3\ m/s\ \ t_{op} = 200\ \text{mm}\ \ shape_{coiled} = rounded\ corner\ ,$$

where v_i and t_{op} are inlet speed and out-of-plane thickness of the design with rounded corners, respectively. Since the acoustic response of the design changes with rounded corners like in the case of 10 dB transmission level, matching operation between analytical model in MATLAB and finite element response in ANSYS is required. The dimensions of straight and space-coiled channels are revised such that they produce the same acoustic response as analytical model and the rectangular corner model. The resulting isolation frequency ranges and normalized bandwidth are listed in Table 5.6. For the acoustic part of the rounded corner analyses, the comparison of transmission losses between analytical model and finite element response after matching operation is given in Figure 5.10.

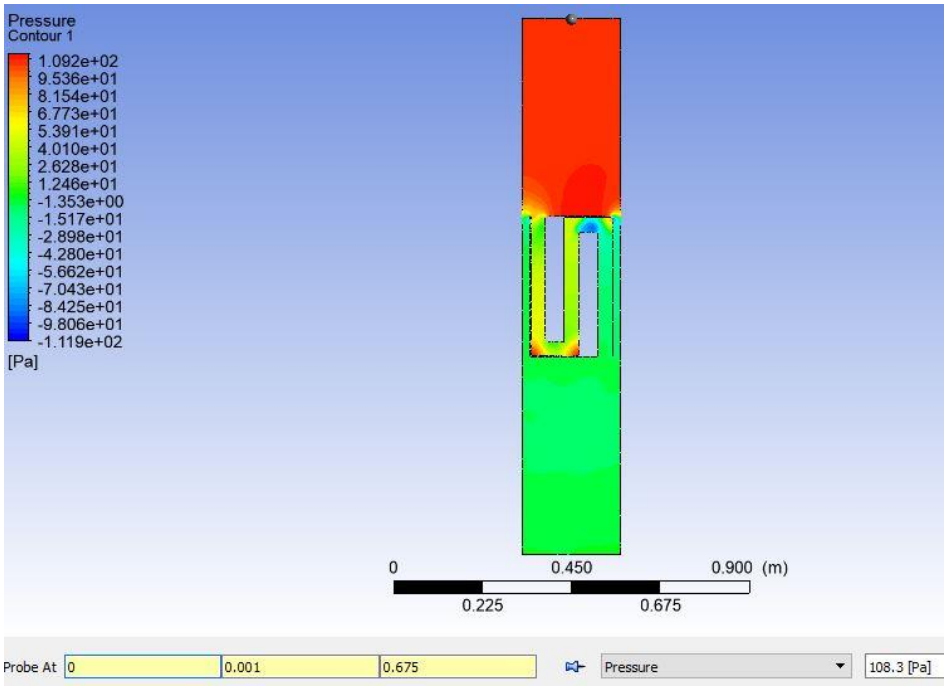

(a)

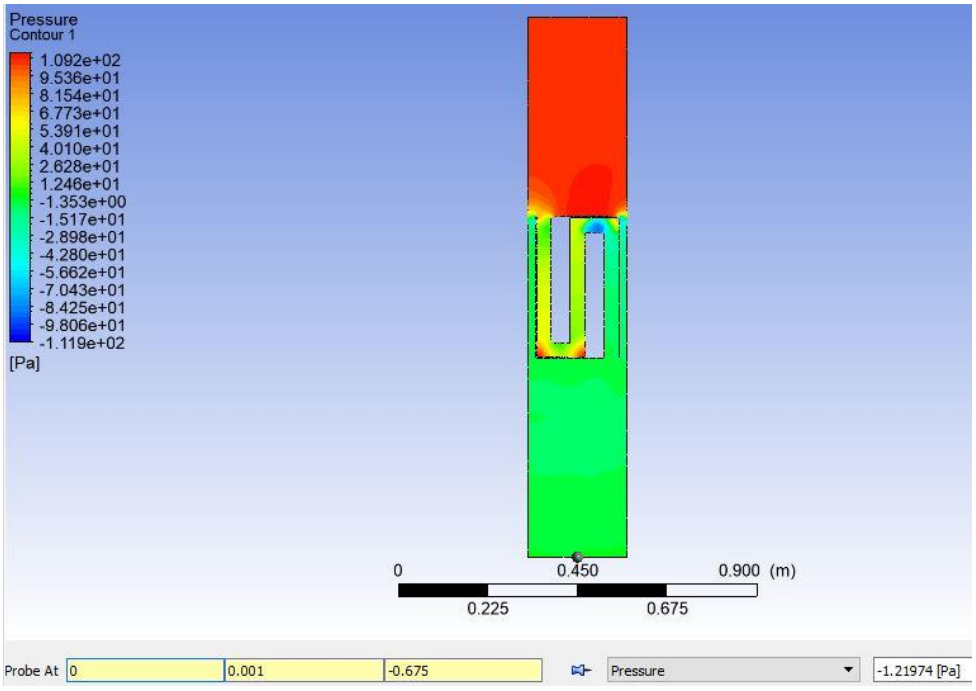

(b)

Figure 5.9. The pressure response of the flow for 3 m/s inlet speed, (a) Showing inlet pressure, (b) Showing outlet pressure, for the design with one straight channel and one space-coiled channel with rectangular corners for 30 dB target transmission loss, 250 mm overall design domain width and 250 Hz upper frequency limit. Here, $d_1 = 40$ mm, $d_2 = 36$ mm.

Table 5.6. Comparison of isolation frequency ranges and normalized bandwidth in MATLAB and ANSYS models of the two channels with rounded corners design with 30 dB target TL below 250 Hz. In both designs, $d_1 = 40$ mm, $d_2 = 36$ mm.

	l_1 (mm)	l_2 (mm)	Isolation frequency range (Hz)	Normalized bandwidth (%)
MATLAB	392.1	1176.3	189 – 249	27.4
ANSYS	359.5	1147.0	188 – 248	27.5

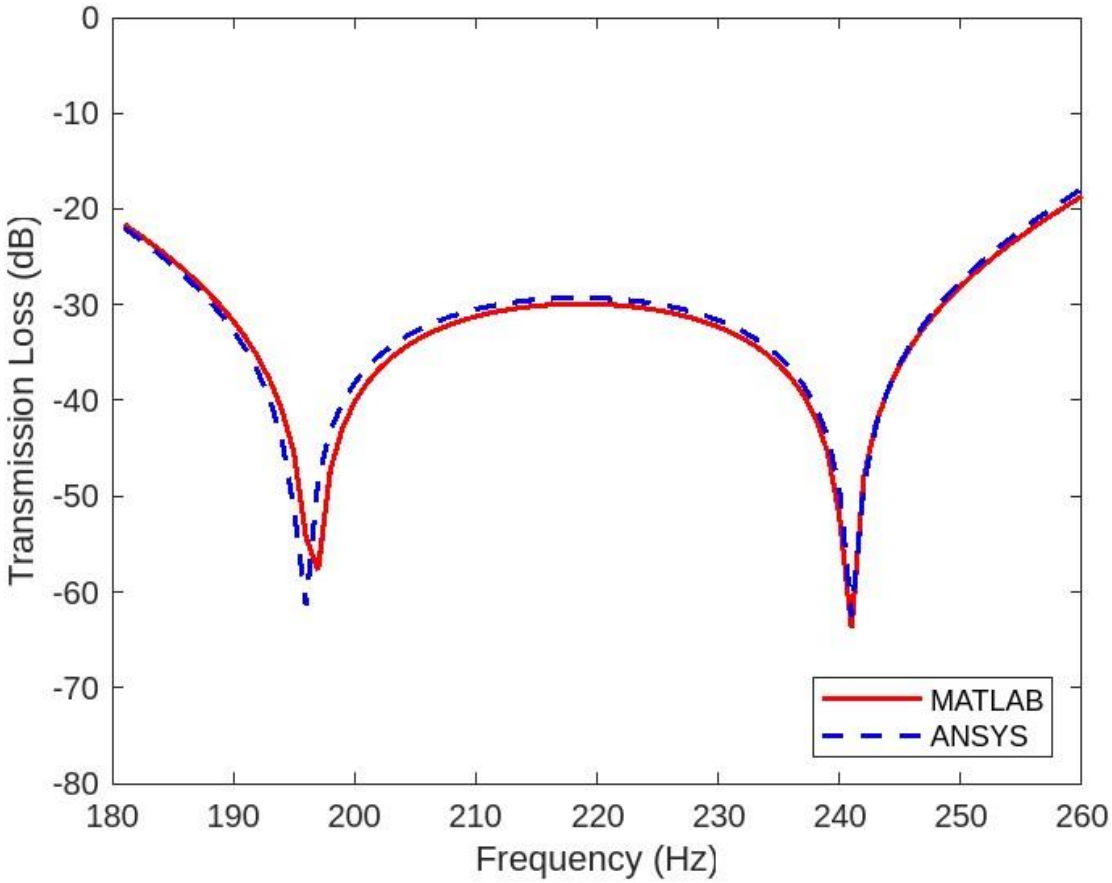

Figure 5.10. Transmission loss graphs of the design involving one straight channel and one space-coiled channel with rounded corners via MATLAB and ANSYS for 250 mm overall design domain width, 250 Hz upper frequency limit and 30 dB target transmission loss within the isolation bandwidth. Here, $d_1 = 40$ mm, $d_2 = 36$ mm.

As it can be seen from Figure 5.10, according to the MATLAB calculations, this design theoretically generates an attenuation band, which is centered at 219 Hz, with a transmission loss more than 30 dB of attenuation over a bandwidth which is 60 Hz between 189 Hz and

249 Hz. As it can be seen from Figure 5.10, according to the ANSYS analysis, the resulting transmission loss graph shows an attenuation band, which is centered at 218 Hz, with a transmission loss more than 30 dB of attenuation over a bandwidth which is 60 Hz between 188 Hz and 248 Hz. Therefore, it can be concluded that the frequency interval and the transmission loss are almost the same for analytical model response and finite element response. The resulting pressure response of the flow is given in Figure 5.11.

As it can be seen from Figure 5.11, the design with rounded corners produces a pressure loss between inlet and outlet 52.509 Pa at 3 m/s inlet speed. This pressure loss is significantly lower than the one with rectangular corners (109.520 Pa). On the other hand, the pressure loss of the design having a target transmission loss of 10 dB and one rounded space-coiled channel with one straight channel, 21.081 Pa, is smaller than the pressure loss of the design having a target transmission loss of 30 dB and one rounded space-coiled channel with one straight channel, 52.509 Pa. Moreover, the frequency bandwidth of the design having transmission loss of 10 dB and one rounded space-coiled channel with one straight channel, 104 Hz, is larger than the frequency bandwidth of the design having transmission loss of 30 dB and one rounded space-coiled channel with one straight channel, 60 Hz. Therefore, it can be concluded that there is a tradeoff between transmission loss and pressure loss by comparing the designs having transmission losses of 10 dB and 30 dB.

In the second design, the resulting dimensions of the three channels according to the optimization in MATLAB are given in Table 5.7. In order to achieve similar acoustic response in the ANSYS model, genetic algorithm is used to vary the channel lengths, which are also listed in Table 5.7.

By using the dimensions in Table 5.7, acoustic transmission loss and pressure loss analyses are done via ANSYS. For the acoustic part of the analyses, the comparison of transmission losses between analytical model and finite element response after matching operation is given in Figure 5.12. It can be seen that MATLAB and ANSYS results are very close to each other.

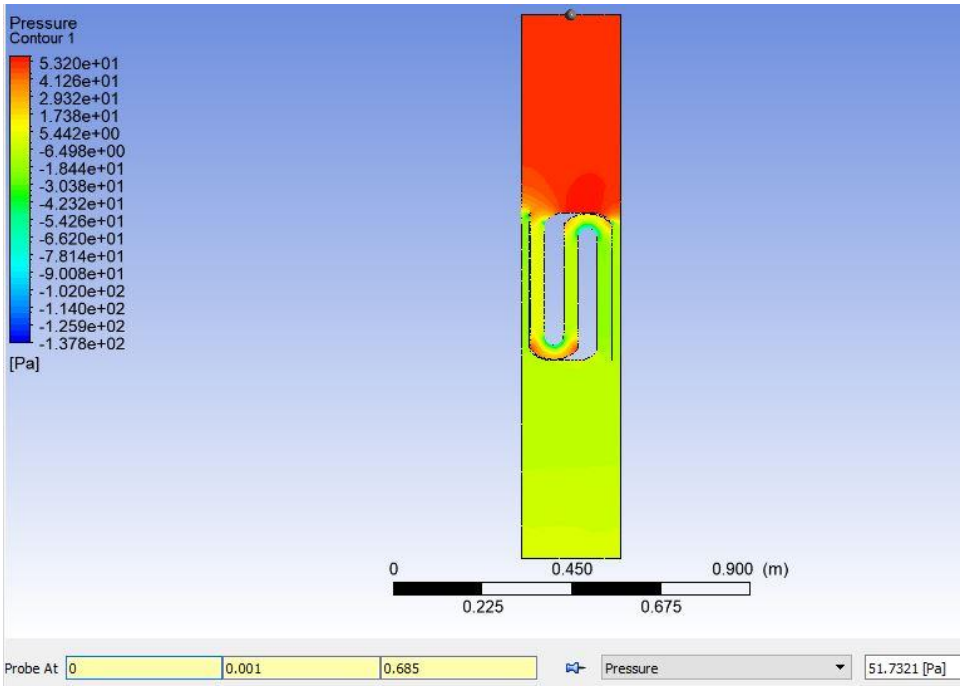

(a)

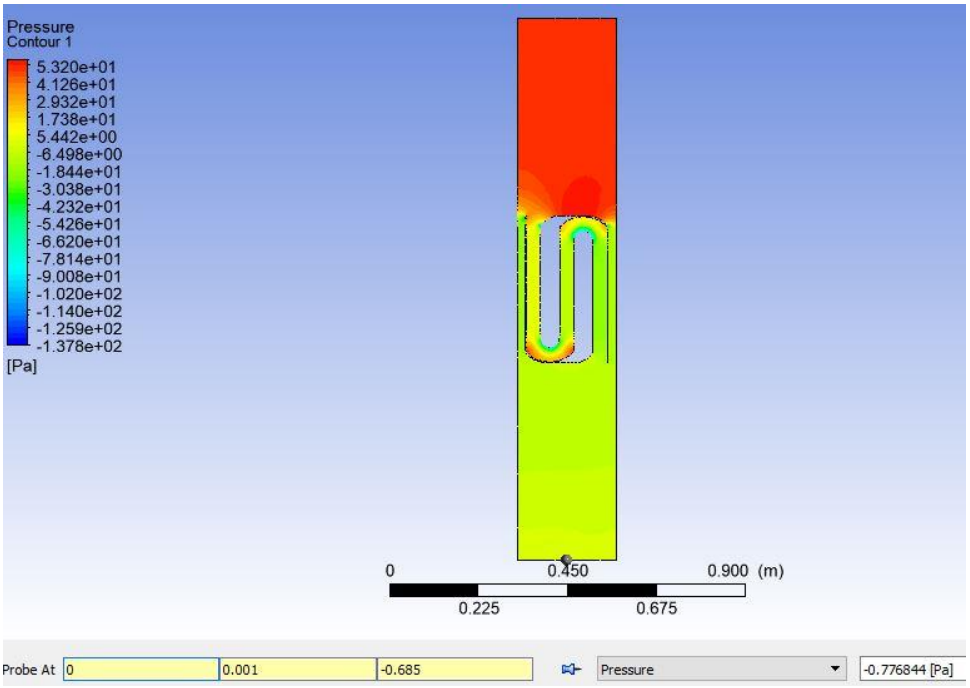

(b)

Figure 5.11. The pressure response of the flow for 3 m/s inlet speed, (a) Showing inlet pressure, (b) Showing outlet pressure, for the design with one straight channel and one space-coiled channel with rounded corners for 30 dB target transmission loss, 250 mm overall design domain width and 250 Hz upper frequency limit. Here, $d_1 = 40$ mm, $d_2 = 36$ mm.

Table 5.7. Comparison of channel lengths and isolation frequency ranges in MATLAB and ANSYS models of the three channels design with 30 dB target TL below 250 Hz and 250 mm overall design domain width. In both designs, $d_1 = 37$ mm, $d_2 = 35$ mm, $d_3 = 1.78$ mm.

	l_1 (mm)	l_2 (mm)	l_3 (mm)	Isolation frequency range (Hz)	Normalized bandwidth (%)
MATLAB	408	1224	2040	170 – 250	38.1
ANSYS	371	1195	2036	170 – 250	38.1

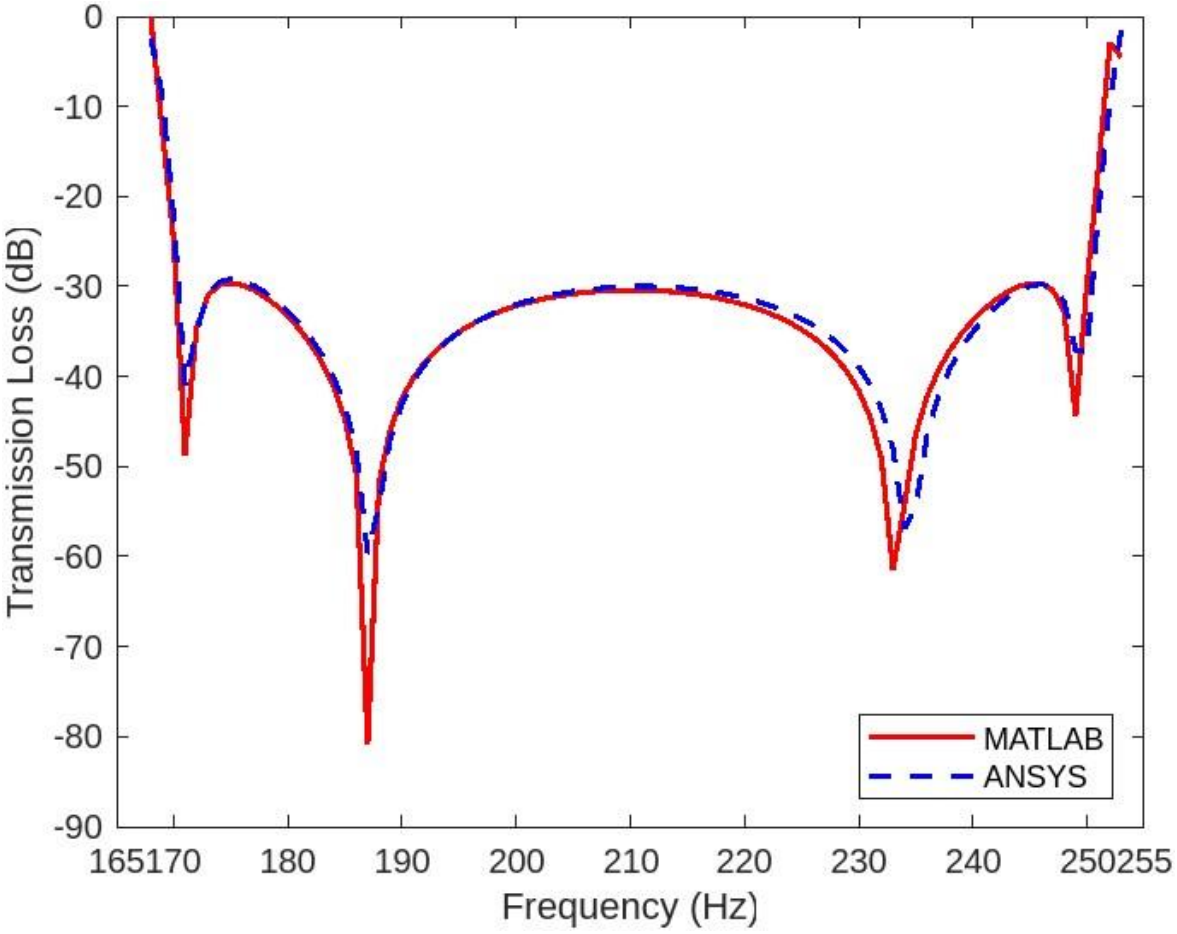

Figure 5.12. Transmission loss graphs of the design involving one straight channel and two space-coiled channels with rectangular corners via MATLAB and ANSYS for 250 mm overall design domain width, 250 Hz upper frequency limit and 30 dB target transmission loss within the isolation bandwidth. Here, $d_1 = 37$ mm, $d_2 = 35$ mm, $d_3 = 1.78$ mm.

The aim of the second design was to inspect maximum frequency bandwidth with the increasing number of space-coiled channels while keeping the transmission loss the same. Maximum frequency bandwidth of the design having one straight and one rectangular space-coiled channel, 59 Hz, is smaller than maximum frequency bandwidth of the design having one straight and two rectangular space-coiled channels, 80 Hz. Therefore, it can be concluded that for the target transmission loss of 30 dB, increasing the number of space-coiled channels has a positive effect. Moreover, the comparison of pressure responses is done in the following step.

For the pressure part of the analyses, the shape of the design is varied in the analyses. The following flow analysis is done for zero shear boundary conditions as follows

$$v_i = 3\ m/s\ \ t_{op} = 200\ \text{mm}\ \ shape_{coiled} = rectangular\ corner\ ,$$

where v_i and t_{op} are inlet speed and out-of-plane thickness of the design, respectively. In this analysis, the shape of the space-coiled channel involves rectangular corners. The resulting pressure response of the flow is given in Figure 5.13.

As it can be seen from Figure 5.13, the resulting pressure loss between inlet and outlet is 122.671 Pa. In order to decrease the pressure loss between inlet and outlet, rounded corners are used as shown in Figure 5.16. The next analysis is also done for zero shear boundary conditions as follows

$$v_i = 3\ m/s\ \ t_{op} = 200\ \text{mm}\ \ shape_{coiled} = rounded\ corner\ ,$$

where v_i and t_{op} are inlet speed and out-of-plane thickness of the design with rounded corners, respectively. Since the acoustic response of the design changes with rounded corners, matching operation between analytical model in MATLAB and finite element response in ANSYS is done. The dimensions of straight and space-coiled channels are revised such that they produce the same acoustic response as analytical model and so rectangular corner model. The resulting isolation frequency ranges and normalized bandwidth are listed in Table 5.8. For the acoustic part of the rounded corner analyses, the comparison of transmission losses between analytical model and finite element response after matching operation is given in Figure 5.15.

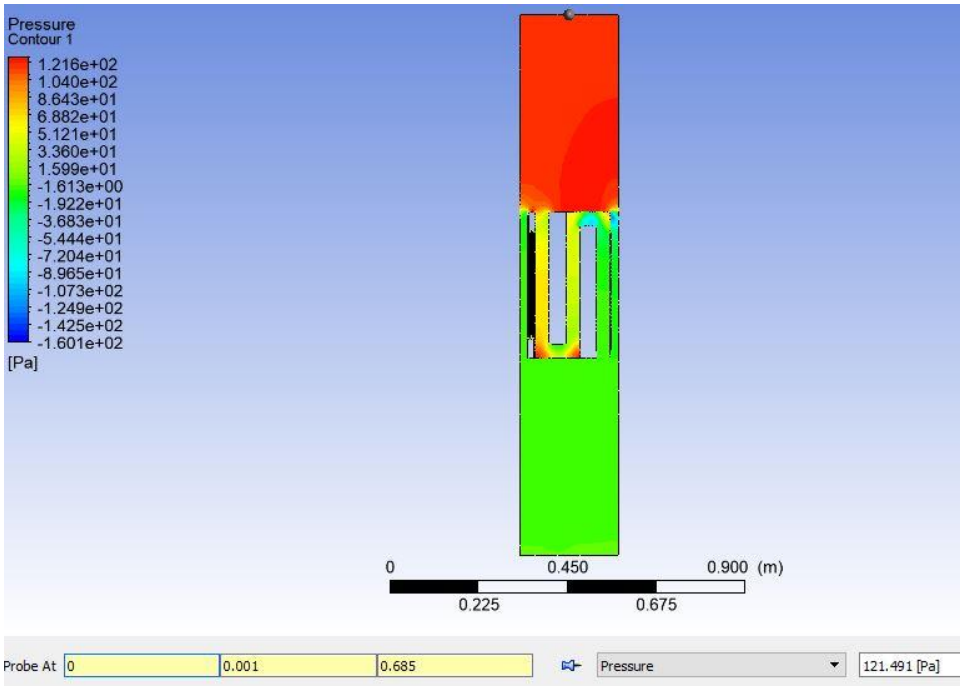

(a)

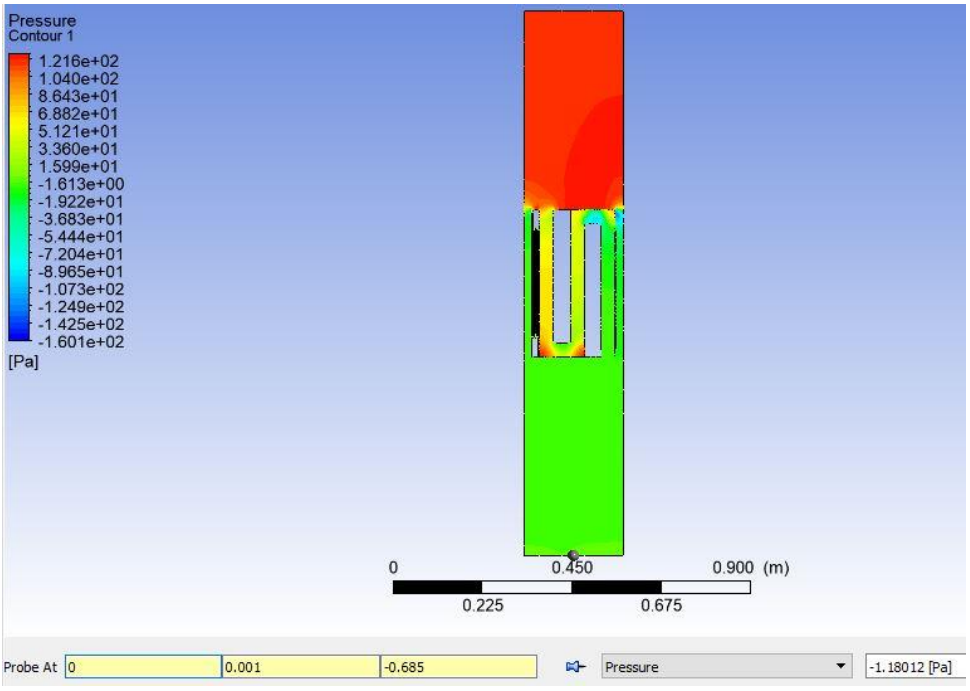

(b)

Figure 5.13. The pressure response of the flow for 3 m/s inlet speed, (a) Showing inlet pressure, (b) Showing outlet pressure, for the design with one straight channel and two rectangular space-coiled channels with rectangular corners for 30 dB target transmission loss, 250 mm overall design domain width and 250 Hz upper frequency limit. Here, $d_1 = 37$ mm, $d_2 = 35$ mm, $d_3 = 1.78$ mm.

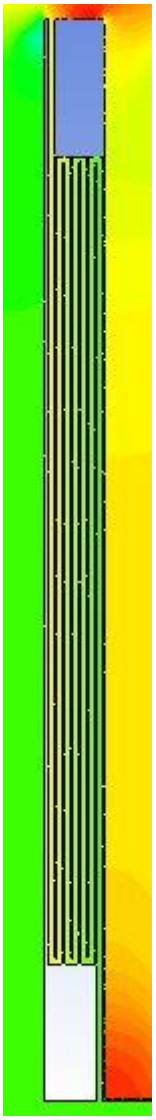

Figure 5.14. Zoom of the space-coiled channel having 1.78 mm width, for the design in Figure 5.13.

Table 5.8. Comparison of isolation frequency ranges and normalized bandwidth in MATLAB and ANSYS models of the three channels with rounded corners design with 30 dB target TL below 250 Hz. In both designs, $d_1 = 37$ mm, $d_2 = 35$ mm, $d_3 = 1.78$ mm.

	l_1 (mm)	l_2 (mm)	l_3 (mm)	Isolation frequency range (Hz)	Normalized bandwidth (%)
MATLAB	408	1224	2040	170 – 250	38.1
ANSYS	380.4	1198.0	2036.0	170 – 250	38.1

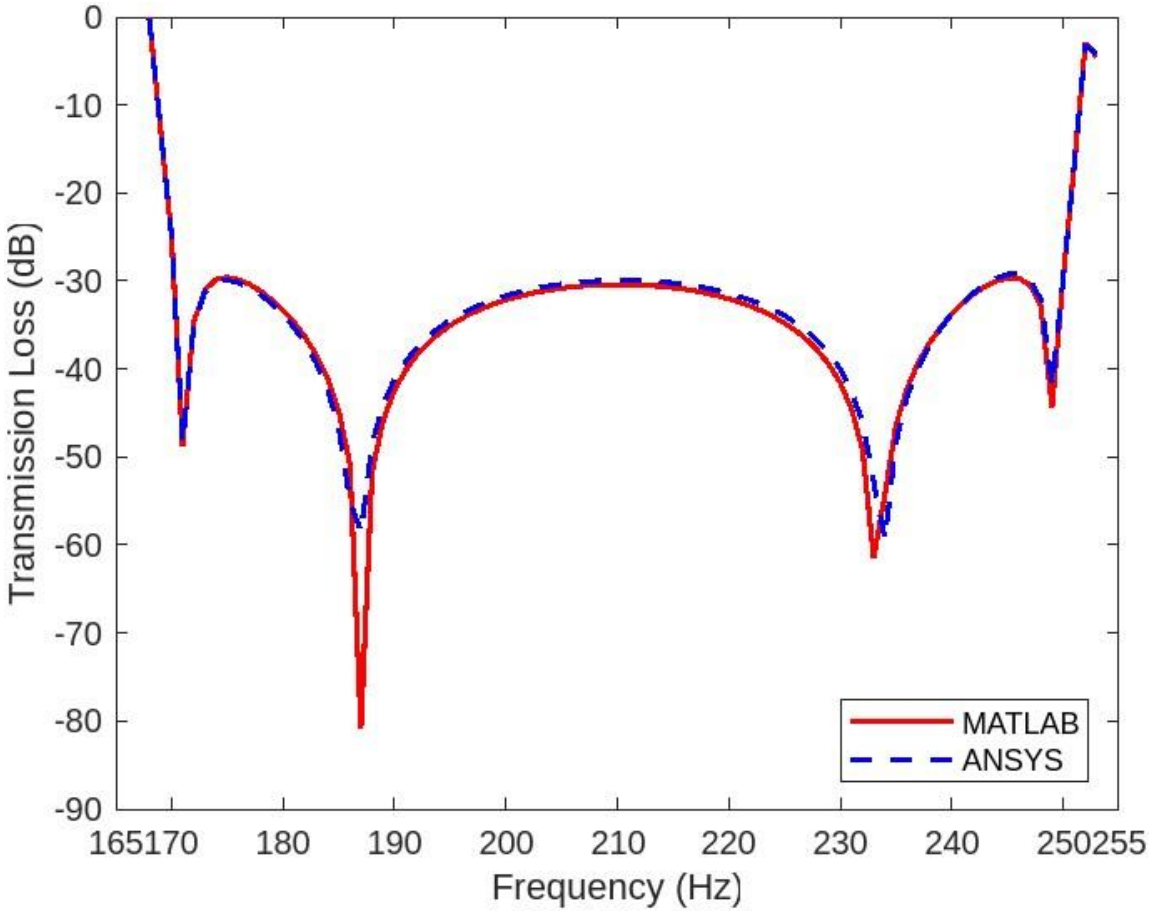

Figure 5.15. Transmission loss graphs of the design involving one straight channel and two space-coiled channels with rounded corners via MATLAB and ANSYS for 250 mm overall design domain width, 250 Hz upper frequency limit and 30 dB target transmission loss within the isolation bandwidth. Here, $d_1 = 37$ mm, $d_2 = 35$ mm, $d_3 = 1.78$ mm.

As it can be seen from Figure 5.15, according to the MATLAB calculations, this design theoretically generates an attenuation band, which is centered at 210 Hz, with a transmission loss more than 30 dB of attenuation over a bandwidth which is 80 Hz between 170 Hz and 250 Hz. As it can be seen from Figure 5.15, according to the ANSYS analysis, the resulting transmission loss graph shows an attenuation band, which is centered at 210 Hz, with a transmission loss more than 30 dB of attenuation over a bandwidth which is 80 Hz between 170 Hz and 250 Hz. Therefore, it can be concluded that the frequency interval and the transmission loss are exactly the same for analytical model response and finite element response. The resulting pressure response of the flow is given in Figure 5.16.

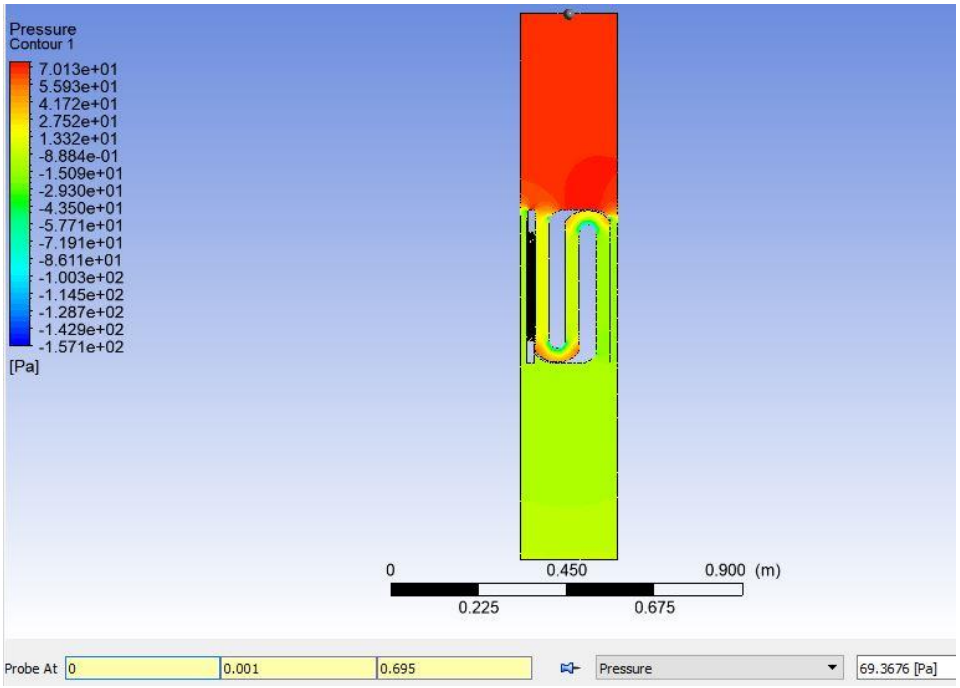

(a)

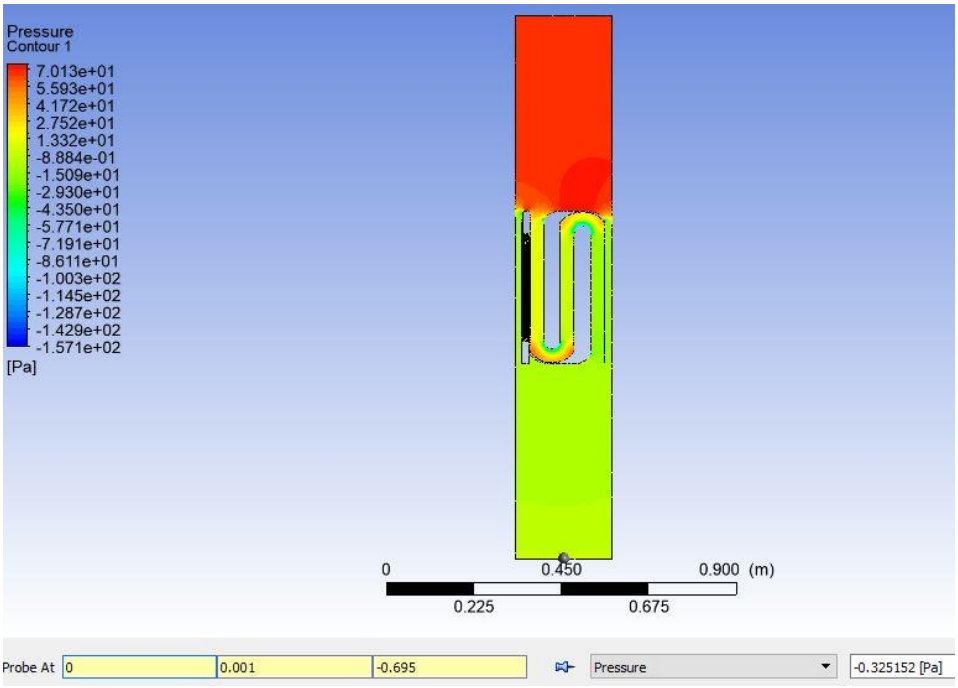

(b)

Figure 5.16. The pressure response of the flow for 3 m/s inlet speed, (a) Showing inlet pressure, (b) Showing outlet pressure, for the design with one straight channel and two space-coiled channels with rounded corners for 30 dB target transmission loss, 250 mm overall design domain width and 250 Hz upper frequency limit. Here, $d_1 = 37$ mm, $d_2 = 35$ mm, $d_3 = 1.78$ mm.

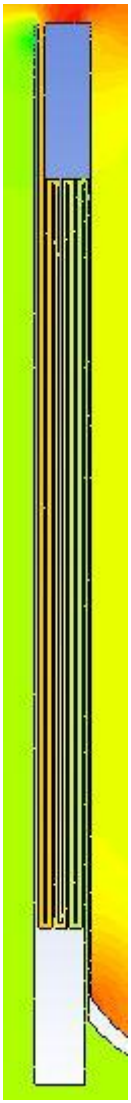

Figure 5.17. Zoom of the space-coiled channel having 1.78 mm width, for the design in Figure 5.16.

As it can be seen from Figure 5.16, the design with rounded corners produces a pressure loss between inlet and outlet is 69.693 Pa at 3 m/s inlet speed. The pressure loss of the design having one straight and one rounded space-coiled channels, 52.509 Pa, is smaller than the pressure loss of the design having one straight and two rounded space-coiled channels, 69.693 Pa. Therefore, it can be concluded that there is a negative relation between the number of space-coiled channels and the pressure loss by comparing the designs having one and two rounded space-coiled channels.

All in all, it can be concluded that although there is a positive relation between maximum frequency bandwidth and number of space-coiled channels, there is a negative relation between the pressure loss and the number of space-coiled channels.

5.2.3. 50 dB Transmission Loss Target

In this third subsection, optimization of the design is done for 50 dB transmission loss constraint with MATLAB by changing the number and/or the dimensions of space-coiled resonators to achieve isolation in the widest frequency range while keeping the air pressure loss at minimum. The third subsection includes three design solutions, which have different numbers of channels. The aim of the first design is to inspect pressure loss response with the further increasing of transmission loss while having two channels (one straight and one space-coiled). This will be done by comparing the pressure loss responses of the designs having transmission losses of 30 dB and 50 dB. The aim of the second design is to inspect maximum frequency bandwidth and pressure loss response with changing number of channels for high transmission loss targets. This will be done by comparing the maximum frequency bandwidth and pressure loss responses of the second design and the third design. The aim of the third design is to inspect maximum frequency bandwidth with the increasing number of space-coiled channels while keeping the target transmission loss at 50 dB. The reason why this third design is done is to check if the positive relation, which is found in the design of 30 dB transmission loss, between maximum frequency bandwidth and number of space-coiled channels exists also in the design with 50 dB transmission loss target. According to these aims, three resulting designs are obtained. The first and the second designs involve both a straight channel and a space-coiled channel. The third design involves a straight channel and two space-coiled channels. The width of the overall design domain is 250 mm for all three designs.

In the first design, the resulting dimensions of the two channels according to the optimization in MATLAB are given in Table 5.9. In order to achieve similar acoustic response in the ANSYS model, genetic algorithm is used to vary the channel lengths, which are also listed in Table 5.9.

Table 5.9. Comparison of channel lengths and isolation frequency ranges in MATLAB and ANSYS models of the two channels design with 50 dB target TL below 250 Hz and 250 mm overall design domain width. In both designs, $d_1 = 40$ mm, $d_2 = 40$ mm.

	l_1 (mm)	l_2 (mm)	Isolation frequency range (Hz)	Normalized bandwidth (%)
MATLAB	391.1	1084.0	229 – 251	9.17
ANSYS	323.9	1045.7	230 – 250	8.33

By using the dimensions in Table 5.9, acoustic transmission loss and pressure loss analyses are done via ANSYS. For the acoustic part of the analyses, the comparison of transmission losses between analytical model and finite element response after matching operation is given in Figure 5.18. It can be seen that MATLAB and ANSYS results are very close to each other.

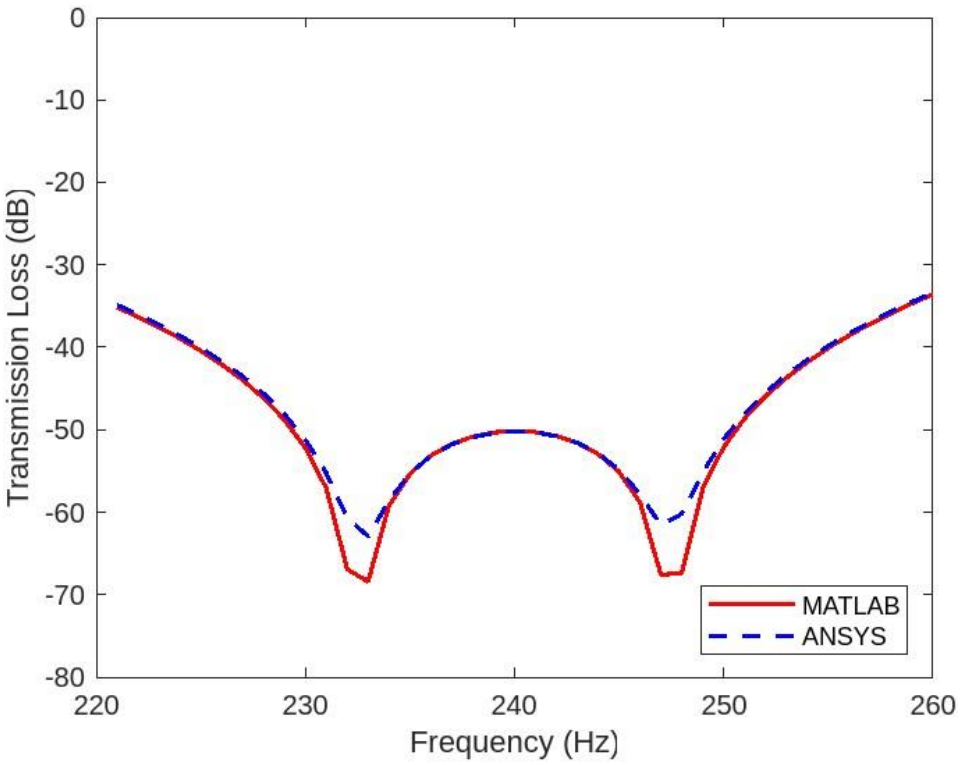

Figure 5.18. Transmission loss graphs of the design involving one straight channel and one space-coiled channel via MATLAB and ANSYS for 250 mm overall design domain width, 250 Hz upper frequency limit and 50 dB target transmission loss within the isolation bandwidth. Here, $d_1 = 40$ mm, $d_2 = 40$ mm.

According to these results, it can be concluded that the frequency bandwidth of the design having transmission loss of 30 dB and one rectangular space-coiled channel with one straight channel, 59 Hz, is larger than the frequency bandwidth of the design having transmission loss of 50 dB and one rectangular space-coiled channel with one straight channel, 20 Hz.

For the pressure part of the analyses, the shape of the design is varied in the analyses. The following flow analysis is done for zero shear boundary conditions as follows

$$v_i = 3\ m/s\ \ t_{op} = 200\ \text{mm}\ \ shape_{coiled} = rectangular\ corner\ ,$$

where v_i and t_{op} are inlet speed and out-of-plane thickness of the design, respectively. In this analysis, the shape of the space-coiled channel involves rectangular corners. The resulting pressure response of the flow is given in Figure 5.19.

As it can be seen from Figure 5.19, the resulting pressure loss between inlet and outlet is 100.903 Pa. In order to decrease the pressure loss between inlet and outlet, rounded corners are used as shown in Figure 5.21. The next analysis is also done for zero shear boundary conditions as follows

$$v_i = 3\ m/s\ \ t_{op} = 200\ \text{mm}\ \ shape_{coiled} = rounded\ corner\ ,$$

where v_i and t_{op} are inlet speed and out-of-plane thickness of the design with rounded corners, respectively. Since the acoustic response of the design changes with rounded corners like in the cases of 10 dB and 30 dB transmission levels, matching operation between analytical model in MATLAB and finite element response in ANSYS is required. The dimensions of straight and space-coiled channels are revised such that they produce the same acoustic response as analytical model and so rectangular corner model. The resulting isolation frequency ranges and normalized bandwidth are listed in Table 5.10. For the acoustic part of the rounded corner analyses, the comparison of transmission losses between analytical model via MATLAB and finite element response via ANSYS after matching operation is given in Figure 5.20.

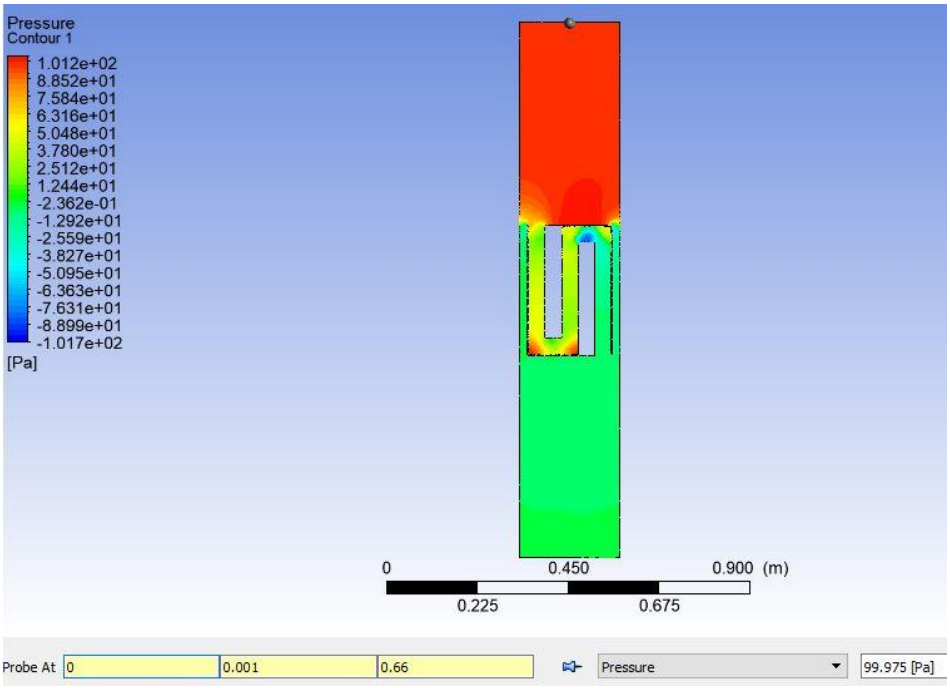

(a)

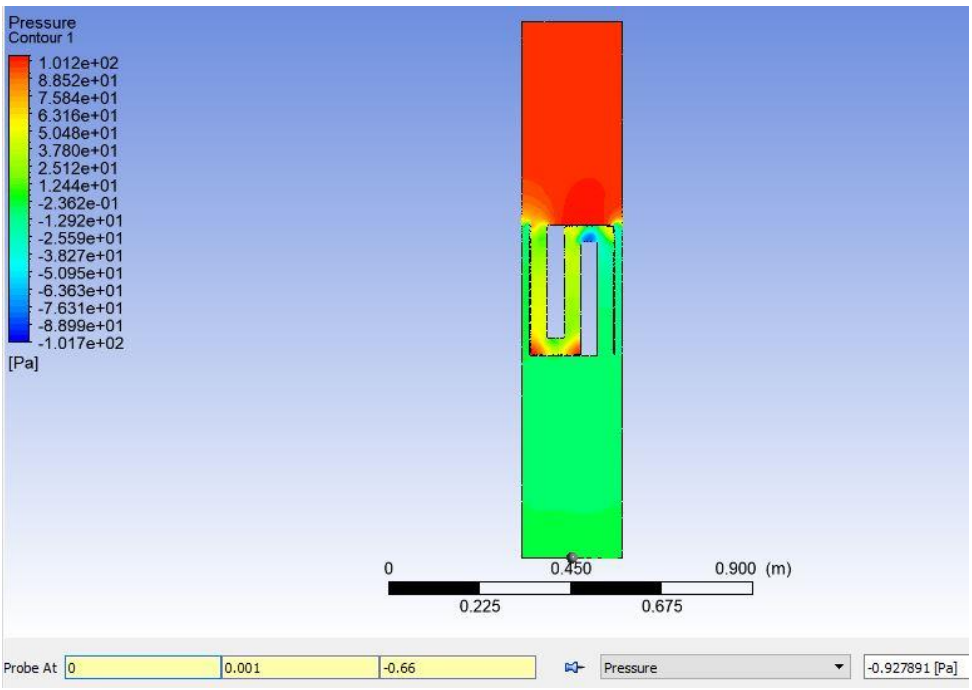

(b)

Figure 5.19. The pressure response of the flow for 3 m/s inlet speed, (a) Showing inlet pressure, (b) Showing outlet pressure, for the design with one straight channel and one space-coiled channel with rectangular corners for 50 dB target transmission loss, 250 mm overall design domain width and 250 Hz upper frequency limit. Here, $d_1 = 40$ mm, $d_2 = 40$ mm.

Table 5.10. Comparison of isolation frequency ranges and normalized bandwidth in MATLAB and ANSYS models of the two channels with rounded corners design with 50 dB target TL below 250 Hz. In both designs, $d_1 = 40$ mm, $d_2 = 40$ mm.

	l_1 (mm)	l_2 (mm)	Isolation frequency range (Hz)	Normalized bandwidth (%)
MATLAB	391.1	1084.0	229 – 251	9.17
ANSYS	341.8	1050.8	229 – 250	8.77

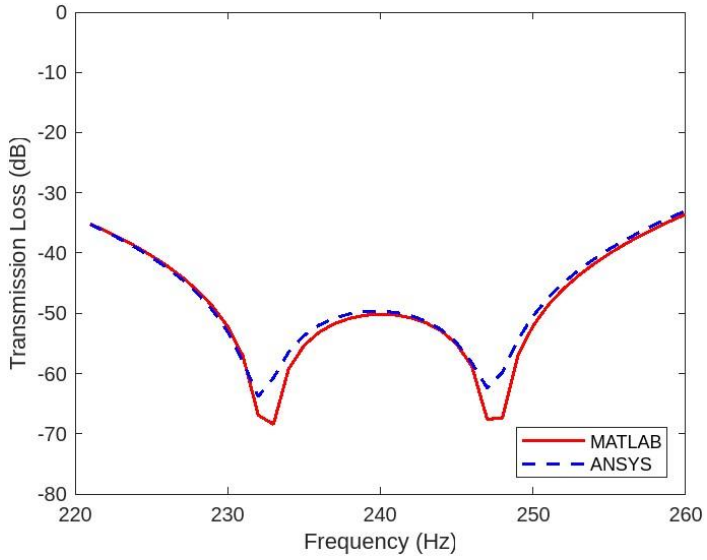

Figure 5.20. Transmission loss graphs of the design involving one straight channel and one space-coiled channel with rounded corners via MATLAB and ANSYS for 250 mm overall design domain width, 250 Hz upper frequency limit and 50 dB target transmission loss within the isolation bandwidth. Here, $d_1 = 40$ mm, $d_2 = 40$ mm.

As it can be seen from Figure 5.20, according to the MATLAB calculations, this design theoretically generates an attenuation band, which is centered at 240 Hz, with a transmission loss more than 50 dB of attenuation over a bandwidth which is 22 Hz between 229 Hz and 251 Hz. As it can be seen from Figure 5.20, according to the ANSYS analysis, the resulting transmission loss graph shows an attenuation band, which is centered at 239.5 Hz, with a transmission loss more than 50 dB of attenuation over a bandwidth which is 21 Hz between 229 Hz and 250 Hz. Therefore, it can be concluded that the frequency interval and the transmission loss are almost the same for analytical model response and finite element response. The resulting pressure response of the flow is given in Figure 5.21.

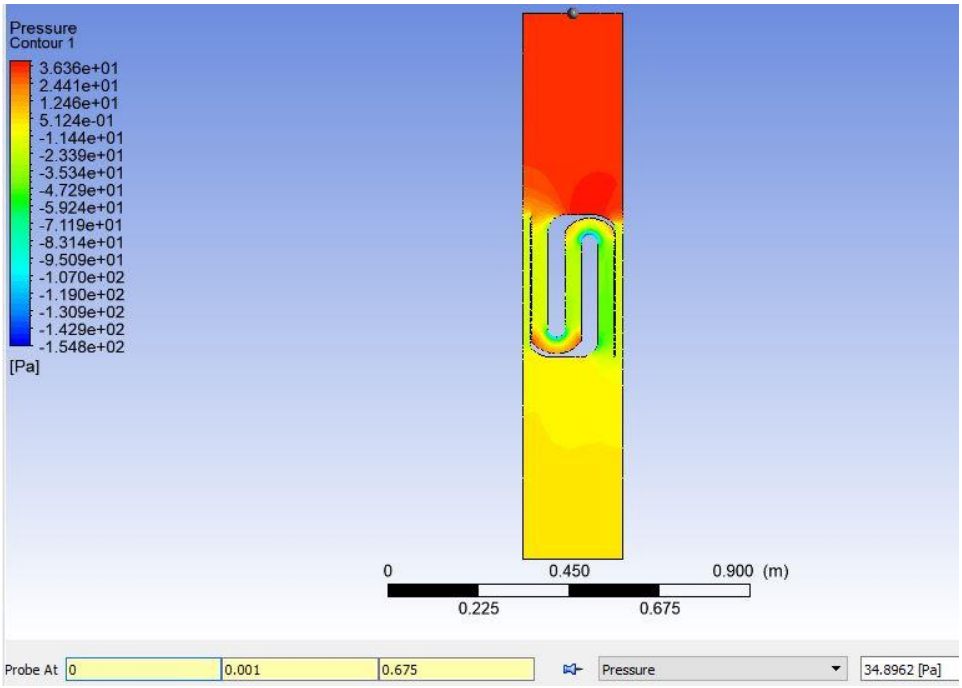

(a)

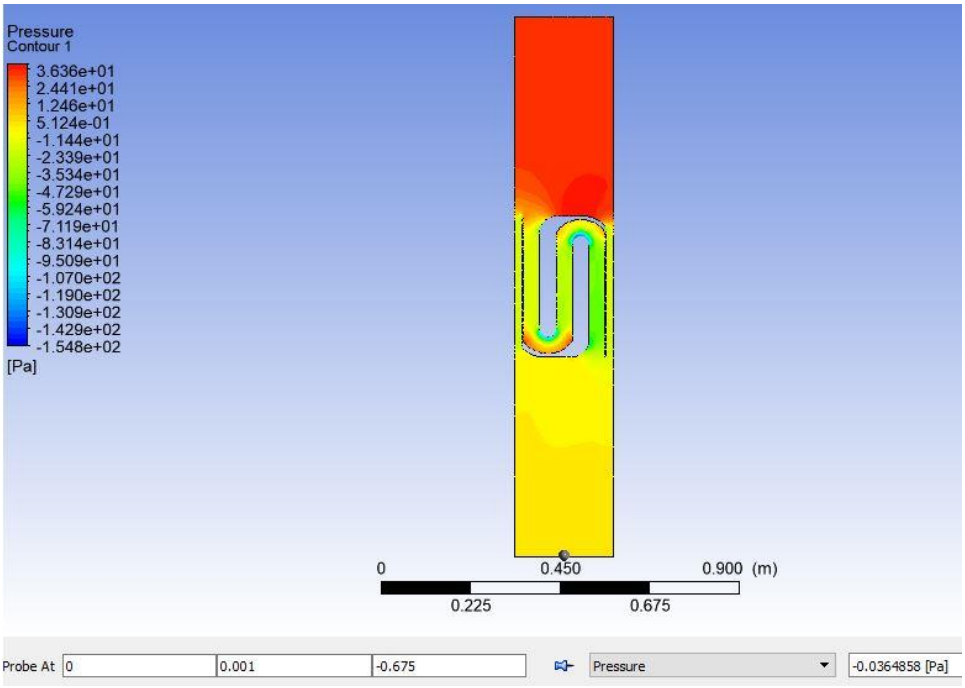

(b)

Figure 5.21. The pressure response of the flow for 3 m/s inlet speed, (a) Showing inlet pressure, (b) Showing outlet pressure, for the design with one straight channel and one space-coiled channel with rounded corners for 50 dB target transmission loss, 250 mm overall design domain width and 250 Hz upper frequency limit. Here, $d_1 = 40$ mm, $d_2 = 40$ mm.

As it can be seen from Figure 5.21, the design with rounded corners produces a pressure loss between inlet and outlet 34.932 Pa at 3 m/s inlet speed. The pressure loss of the design having transmission loss of 30 dB and one rounded space-coiled channel with one straight channel, 52.509 Pa, is larger than the pressure loss of the design having transmission loss of 50 dB and one rounded space-coiled channel with one straight channel, 34.932 Pa. Therefore, it can be concluded that pressure loss decreases with the further increasing of transmission loss by comparing the designs having transmission losses of 30 dB and 50 dB while having the same number of channels, i.e., two. However, the frequency bandwidth of the design having transmission loss of 30 dB and one rounded space-coiled channel with one straight channel, 60 Hz, is larger than the frequency bandwidth of the design having transmission loss of 50 dB and rounded one space-coiled channel with one straight channel, 21 Hz.

In the second design regarding 50 dB target transmission loss, the resulting dimensions of the two channels according to the optimization in MATLAB are given in Table 5.11. In order to achieve similar acoustic response in the ANSYS model, genetic algorithm is used to vary the channel lengths, which are also listed in Table 5.11.

Table 5.11. Comparison of channel lengths and isolation frequency ranges in MATLAB and ANSYS models of the two channels design with 50 dB target TL below 250 Hz and 250 mm overall design domain width. In both designs, $d_1 = 28$ mm, $d_2 = 27.68$ mm.

	l_1 (mm)	l_2 (mm)	Isolation frequency range (Hz)	Normalized bandwidth (%)
MATLAB	379.9	1093.5	224 – 249	10.6
ANSYS	318.0	1057.5	224 – 249	10.6

By using the dimensions in Table 5.11, acoustic transmission loss and pressure loss analyses are done via ANSYS. For the acoustic part of the analyses, the comparison of transmission losses between analytical model and finite element response after matching operation is given in Figure 5.22. It can be seen that MATLAB and ANSYS results are very close to each other.

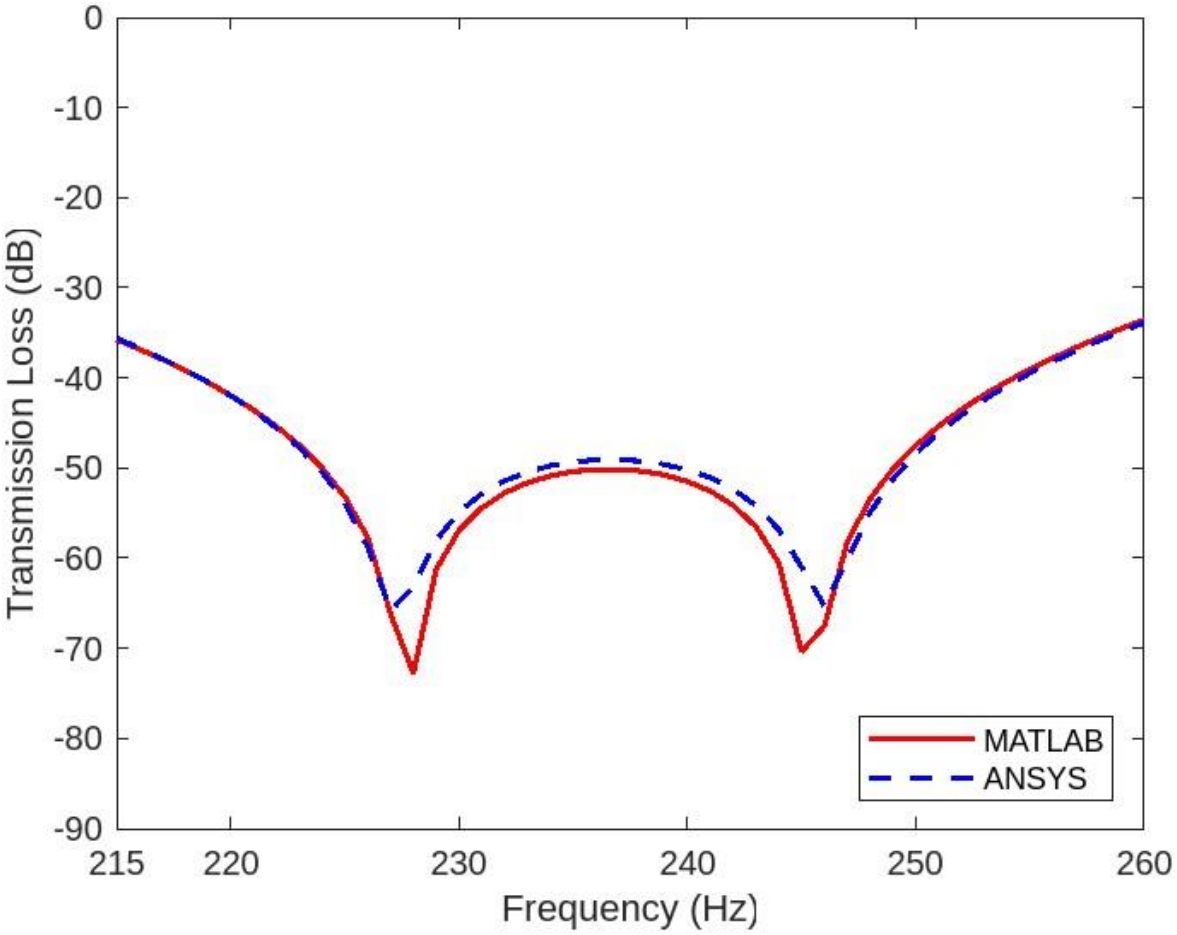

Figure 5.22. Transmission loss graphs of the design involving one straight channel and one space-coiled channel via MATLAB and ANSYS for 250 mm overall design domain width, 250 Hz upper frequency limit and 50 dB target transmission loss within the isolation bandwidth. Here, $d_1 = 28$ mm, $d_2 = 27.68$ mm.

For the pressure part of the analyses, the shape of the design is varied in the analyses. The following flow analysis is done for zero shear boundary conditions as follows

$$v_i = 3\ m/s\ \ t_{op} = 200\ \text{mm}\ \ shape_{coiled} = rectangular\ corner\ ,$$

where v_i and t_{op} are inlet speed and out-of-plane thickness of the design, respectively. In this analysis, the shape of the space-coiled channel involves rectangular corners. The resulting pressure response of the flow is given in Figure 5.23.

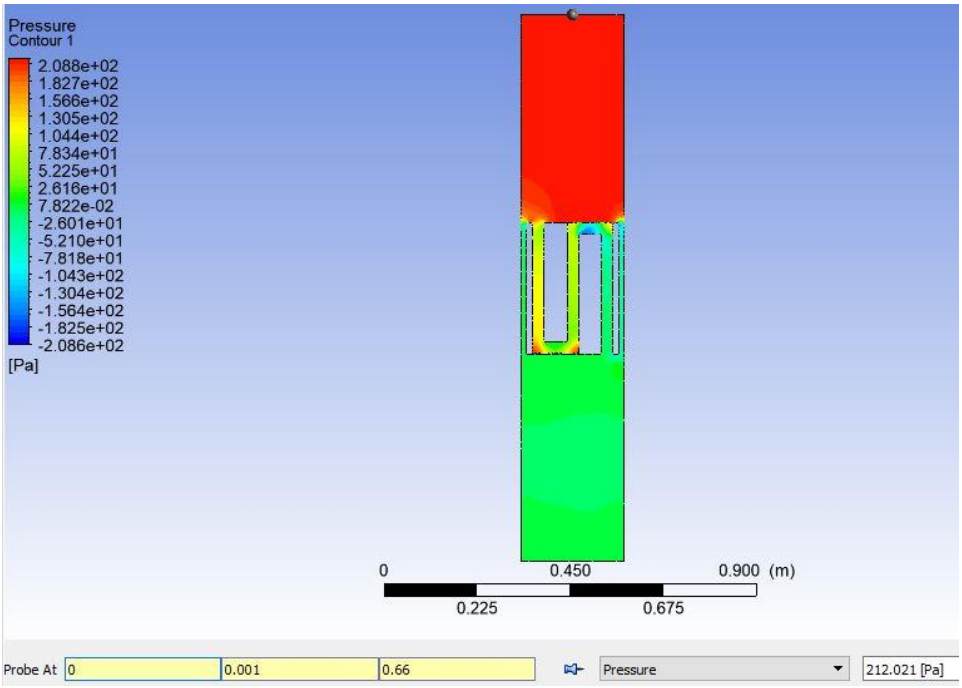

(a)

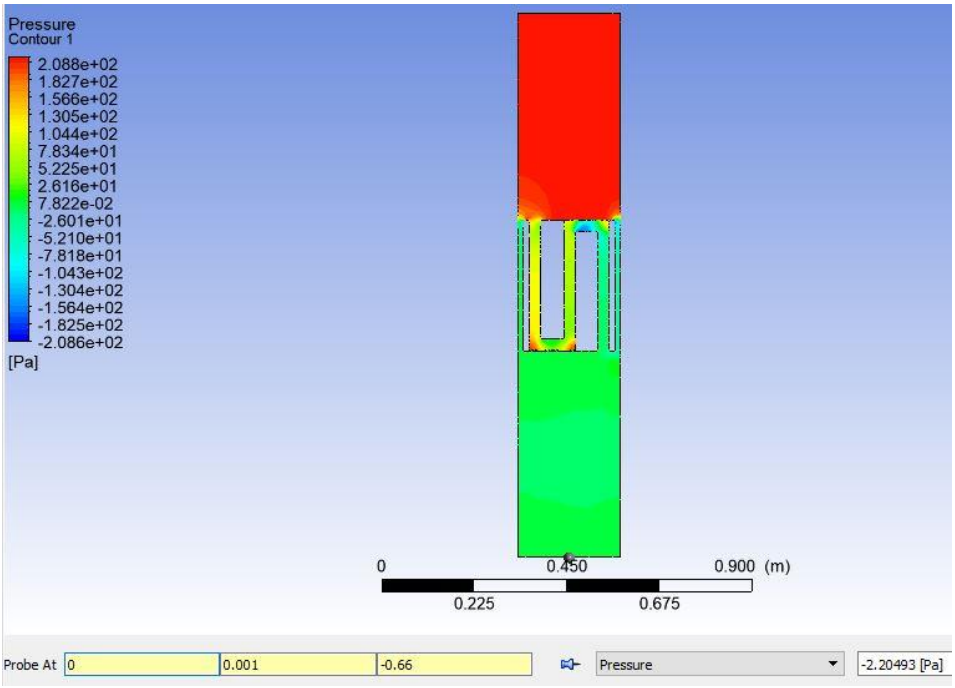

(b)

Figure 5.23. The pressure response of the flow for 3 m/s inlet speed, (a) Showing inlet pressure, (b) Showing outlet pressure, for the design with one straight channel and one space-coiled channel with rectangular corners for 50 dB target transmission loss, 250 mm overall design domain width and 250 Hz upper frequency limit. Here, $d_1 = 28$ mm, $d_2 = 27.68$ mm.

As it can be seen from Figure 5.23, the resulting pressure loss between inlet and outlet is 214.226 Pa. In order to decrease the pressure loss between inlet and outlet, rounded corners are used as shown in Figure 5.25. The next analysis is also done for zero shear boundary conditions as follows

$$v_i = 3\ m/s\ \ t_{op} = 200\ \text{mm}\ \ shape_{coiled} = rounded\ corner\ ,$$

where v_i and t_{op} are inlet speed and out-of-plane thickness of the design with rounded corners, respectively. Since the acoustic response of the design changes with rounded corners, matching operation between analytical model in MATLAB and finite element response in ANSYS is required. The dimensions of straight and space-coiled channels are revised such that they produce the same acoustic response as analytical model and so rectangular corner model. The resulting isolation frequency ranges and normalized bandwidth are listed in Table 5.12. For the acoustic part of the rounded corner analyses, the comparison of transmission losses between analytical model via MATLAB and finite element response via ANSYS after matching operation is given in Figure 5.24.

Table 5.12. Comparison of isolation frequency ranges and normalized bandwidth in MATLAB and ANSYS models of the two channels with rounded corners design with 50 dB target TL below 250 Hz. In both designs, $d_1 = 28$ mm, $d_2 = 27.68$ mm.

	l_1 (mm)	l_2 (mm)	Isolation frequency range (Hz)	Normalized bandwidth (%)
MATLAB	379.9	1093.5	224 – 249	10.6
ANSYS	351.9	1057.4	224 – 249	10.6

As it can be seen from Figure 5.24, according to the MATLAB calculations, this design theoretically generates an attenuation band, which is centered at 237 Hz, with a transmission loss more than 50 dB of attenuation over a bandwidth which is 25 Hz between 224 Hz and 249 Hz. As it can be seen from Figure 5.24, according to the ANSYS analysis, the resulting transmission loss graph shows an attenuation band, which is centered at 237 Hz, with a transmission loss more than 50 dB of attenuation over a bandwidth which is 25 Hz between 224 Hz and 249 Hz.

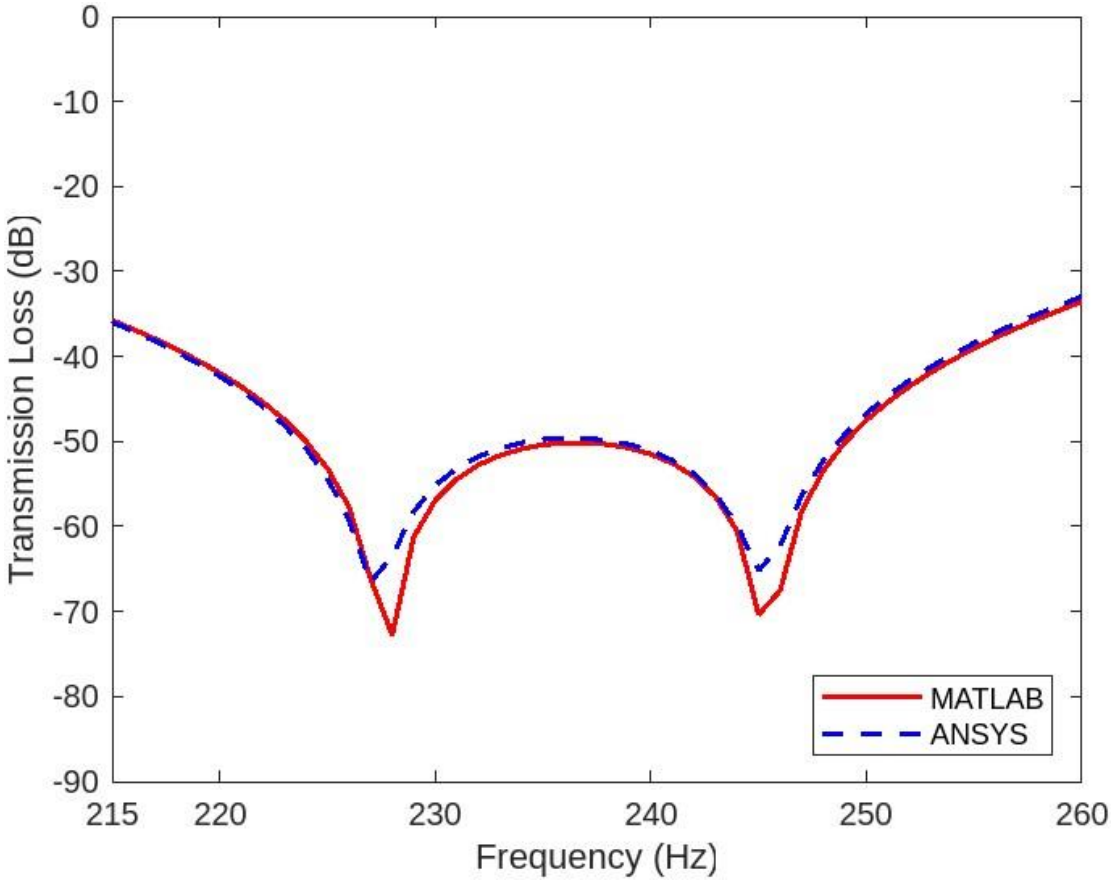

Figure 5.24. Transmission loss graphs of the design involving one straight channel and one space-coiled channel with rounded corners via MATLAB and ANSYS for 250 mm overall design domain width, 250 Hz upper frequency limit and 50 dB target transmission loss within the isolation bandwidth. Here, $d_1 = 28$ mm, $d_2 = 27.68$ mm.

Therefore, it can be concluded that the frequency interval and the transmission loss are the same for analytical model response and finite element response. The resulting pressure response of the flow is given in Figure 5.25.

As it can be seen from Figure 5.25, the design with rounded corners produces a pressure loss between inlet and outlet 101.945 Pa at 3 m/s inlet speed. It can be seen that when the channel widths are decreased from $d_1 = 40$ mm, $d_2 = 40$ mm to $d_1 = 28$ mm, $d_2 = 27.68$ mm, the isolation bandwidth increased but the pressure loss also increased. Hence, there is a trade-off between isolation bandwidth and pressure loss for the design with two channels. In order to circumvent this trade-off, an alternative design with three channels is introduced.

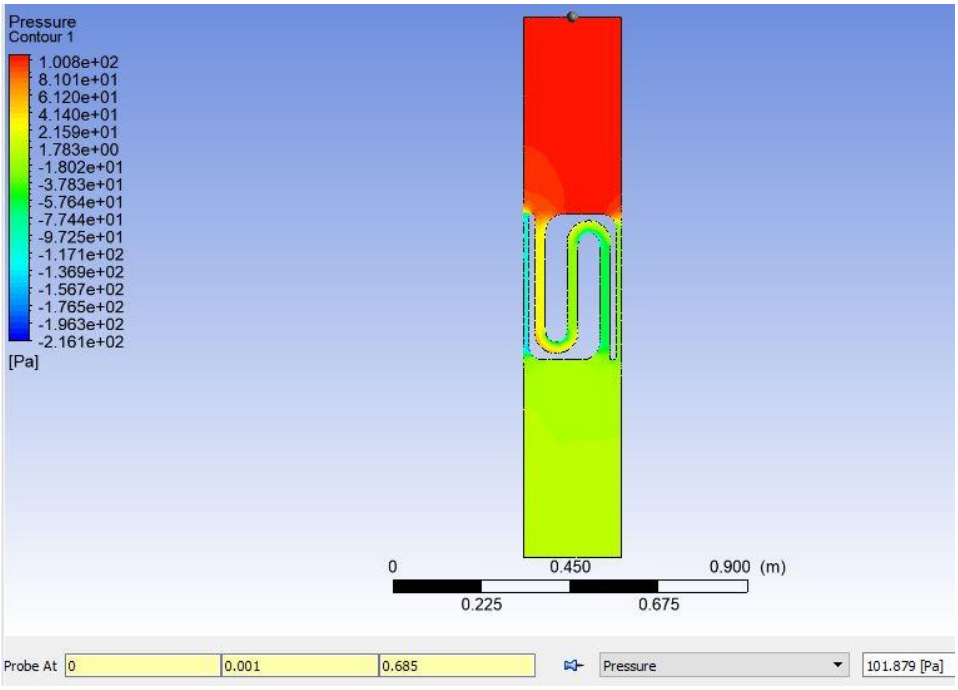

(a)

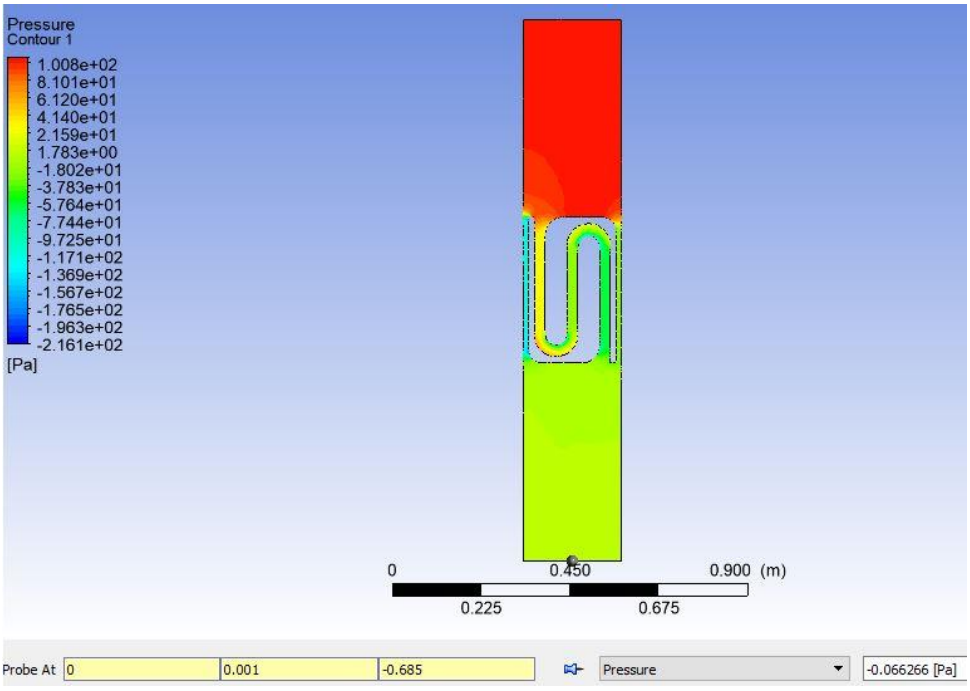

(b)

Figure 5.25. The pressure response of the flow for 3 m/s inlet speed, (a) Showing inlet pressure, (b) Showing outlet pressure, for the design with one straight channel and one space-coiled channel with rounded corners for 50 dB target transmission loss, 250 mm overall design domain width and 250 Hz upper frequency limit. Here, $d_1 = 28$ mm, $d_2 = 27.68$ mm.

In the third design regarding 50 dB target transmission loss, the resulting dimensions of the three channels according to the optimization in MATLAB are given in Table 5.13. In order to achieve similar acoustic response in the ANSYS model, genetic algorithm is used to vary the channel lengths, which are also listed in Table 5.13.

Table 5.13. Comparison of channel lengths and isolation frequency ranges in MATLAB and ANSYS models of the three channels design with 50 dB target TL below 250 Hz and 250 mm overall design domain width. In both designs, $d_1 = 28$ mm, $d_2 = 35.3$ mm, $d_3 = 7.68$ mm.

	l_1 (mm)	l_2 (mm)	l_3 (mm)	Isolation frequency range (Hz)	Normalized bandwidth (%)
MATLAB	389.1	1167.3	1945.5	191 – 250	26.7
ANSYS	371.74	1150.05	1947.74	191 – 249	26.4

By using the dimensions in Table 5.13, acoustic transmission loss and pressure loss analyses are done via ANSYS. For the acoustic part of the analyses, the comparison of transmission losses between analytical model via MATLAB and finite element response via ANSYS after matching operation is given in Figure 5.26. It can be seen that MATLAB and ANSYS results are very close to each other.

The aim of the third design was to inspect maximum frequency bandwidth with the increasing number of space-coiled channels while keeping the transmission loss is 50 dB. Maximum frequency bandwidth (25 Hz) of the design having one straight and one rectangular space-coiled channels ($d_1 = 28$ mm, $d_2 = 27.68$ mm), is smaller than maximum frequency bandwidth (58 Hz) of the design having one straight and two rectangular space-coiled channels ($d_1 = 28$ mm, $d_2 = 35.3$ mm, $d_3 = 7.68$ mm). This positive relation between maximum frequency bandwidth and number of space-coiled channels was also found in the design with 30 dB transmission loss target. Therefore, it can be concluded that there exists a positive relation between maximum frequency bandwidth and number of space-coiled channels by comparing the designs having one and two space-coiled channels for the cases of 30 dB or 50 dB transmission losses. Besides, the comparison of pressure responses is done in the next step.

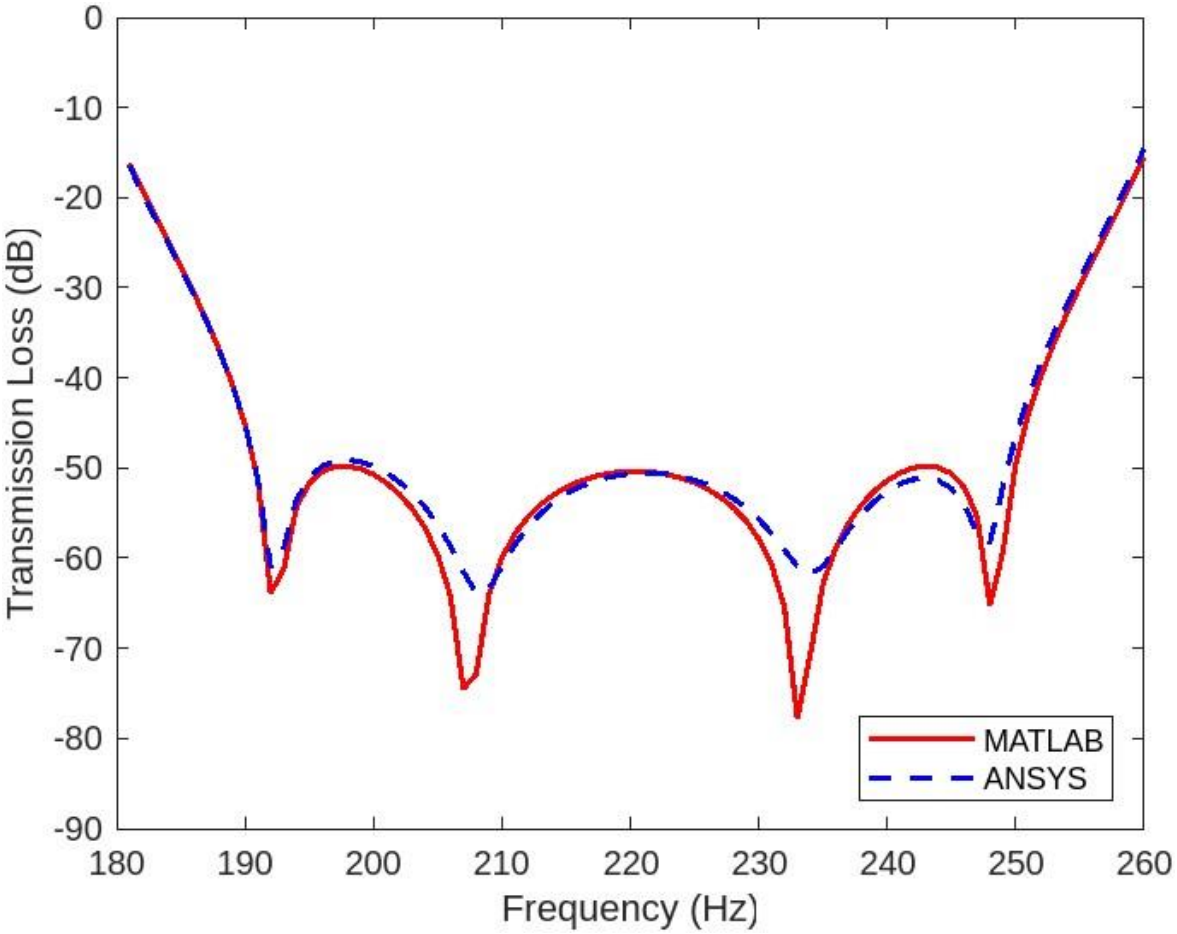

Figure 5.26. Transmission loss graphs of the design involving one straight channel and two space-coiled channels with rectangular corners via MATLAB and ANSYS for 250 mm overall design domain width, 250 Hz upper frequency limit and 50 dB target transmission loss within the isolation bandwidth. Here, $d_1 = 28$ mm, $d_2 = 35.3$ mm, $d_3 = 7.68$ mm.

For the pressure part of the analyses, the shape of the design is varied in the analyses. The following flow analysis is done for zero shear boundary conditions as follows

$$v_i = 3\ m/s \;\; t_{op} = 200 \text{ mm} \;\; shape_{coiled} = rectangular\ corner\ ,$$

where v_i and t_{op} are inlet speed and out-of-plane thickness of the design, respectively. In this analysis, the shape of the space-coiled channel involves rectangular corners. The resulting pressure response of the flow is given in Figure 5.27.

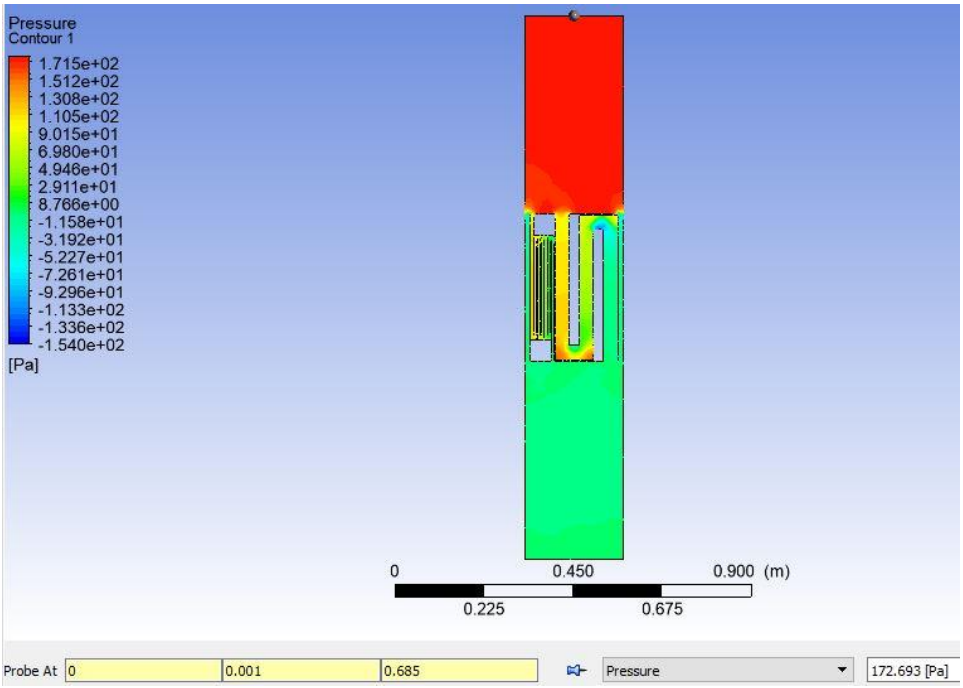

(a)

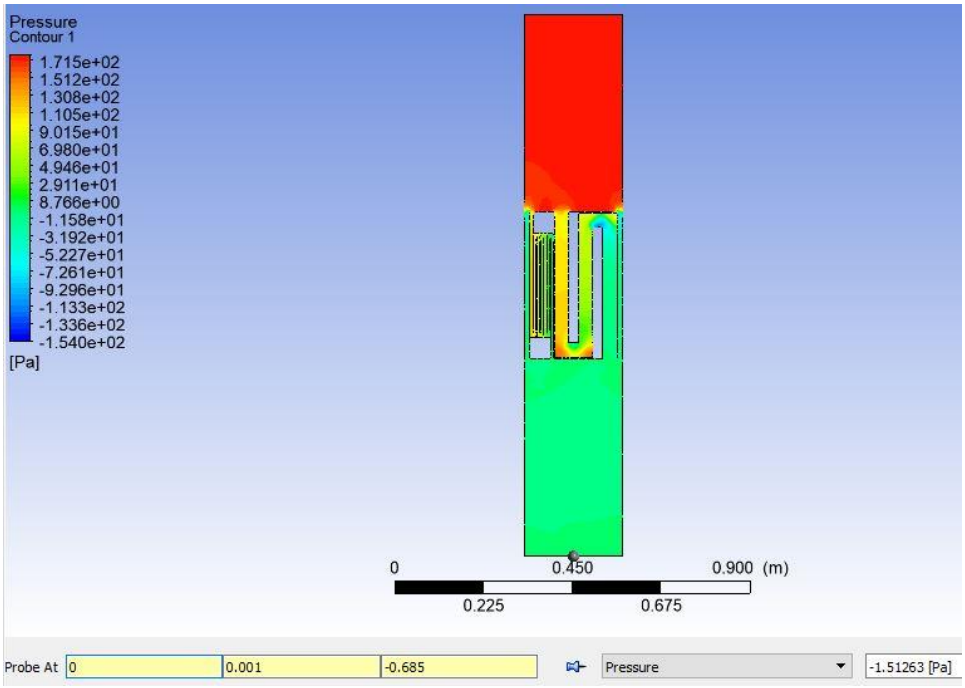

(b)

Figure 5.27. The pressure response of the flow for 3 m/s inlet speed, (a) Showing inlet pressure, (b) Showing outlet pressure, for the design with one straight channel and two space-coiled channels with rectangular corners for 50 dB target transmission loss, 250 mm overall design domain width and 250 Hz upper frequency limit. Here, $d_1 = 28$ mm, $d_2 = 35.3$ mm, $d_3 = 7.68$ mm.

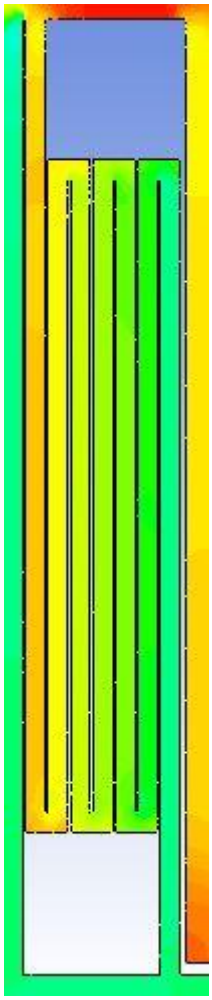

Figure 5.28. Zoom of the space-coiled channel having 7.68 mm width, for the design in Figure 5.27.

As it can be seen from Figure 5.27, the resulting pressure loss between inlet and outlet is 174.206 Pa. In order to decrease the pressure loss between inlet and outlet, rounded corners are used as shown in Figure 5.30. The next analysis is also done for zero shear boundary conditions as follows

$$v_i = 3\ m/s\ \ t_{op} = 200\ \text{mm}\ \ shape_{coiled} = rounded\ corner\ ,$$

where v_i and t_{op} are inlet speed and out-of-plane thickness of the design with rounded corners, respectively. Since the acoustic response of the design changes, matching operation between analytical model in MATLAB and finite element response in ANSYS is done. The dimensions of straight and space-coiled channels are revised such that they produce the same

acoustic response as analytical model and so rectangular corner model. The resulting isolation frequency ranges and normalized bandwidth are listed in Table 5.14. For the acoustic part of the rounded corner analyses, the comparison of transmission losses between analytical model and finite element response after matching operation is given in Figure 5.29.

Table 5.14. Comparison of isolation frequency ranges and normalized bandwidth in MATLAB and ANSYS models of the three channels with rounded corners design with 50 dB target TL below 250 Hz. In both designs, $d_1 = 28$ mm, $d_2 = 35.3$ mm, $d_3 = 7.68$ mm.

	l_1 (mm)	l_2 (mm)	l_3 (mm)	Isolation frequency range (Hz)	Normalized bandwidth (%)
MATLAB	389.1	1167.3	1945.5	191 – 250	26.7
ANSYS	370.8	1141.3	1947.7	191 – 249	26.4

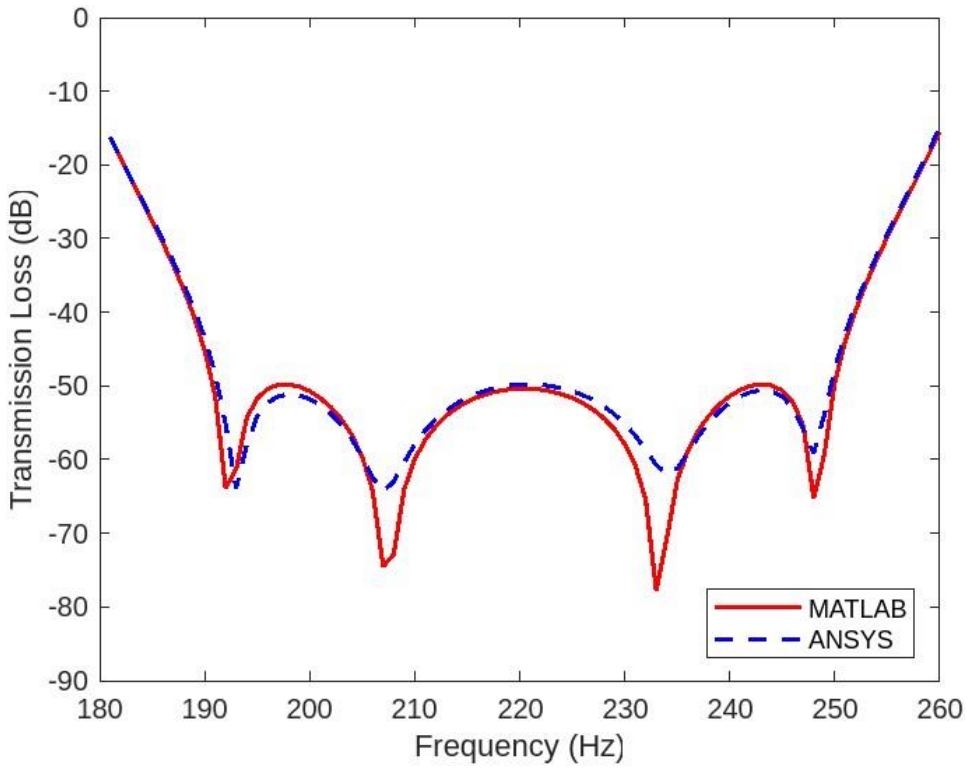

Figure 5.29. Transmission loss graphs of the design involving one straight channel and two space-coiled channels with rounded corners via MATLAB and ANSYS for 250 mm overall design domain width, 250 Hz upper frequency limit and 50 dB target transmission loss within the isolation bandwidth. Here, $d_1 = 28$ mm, $d_2 = 35.3$ mm, $d_3 = 7.68$ mm.

As it can be seen from Figure 5.29, according to the MATLAB calculations, this design theoretically generates an attenuation band, which is centered at 220.5 Hz, with a transmission loss more than 50 dB of attenuation over a bandwidth which is 59 Hz between 191 Hz and 250 Hz. As it can be seen from Figure 5.29, according to the ANSYS analysis, the resulting transmission loss graph shows an attenuation band, which is centered at 220.5 Hz, with a transmission loss more than 50 dB of attenuation over a bandwidth which is 58 Hz between 191 Hz and 249 Hz. Therefore, it can be concluded that the frequency interval and the transmission loss are almost the same for analytical model response and finite element response. The resulting pressure response of the flow is given in Figure 5.30.

As it can be seen from Figure 5.30, the design with rounded corners produces a pressure loss between inlet and outlet is 101.445 Pa at 3 m/s inlet speed. The pressure loss of the second design having one straight and one rounded space-coiled channel, 101.945 Pa, is larger than the pressure loss of the third design having one straight and two rounded space-coiled channels, 101.445 Pa. Moreover, the maximum frequency bandwidth (25 Hz) of the second design having one straight and one rounded space-coiled channel ($d_1 = 28$ mm, $d_2 = 27.68$ mm), is smaller than the maximum frequency bandwidth (58 Hz) of the third design having one straight and two rounded space-coiled channels ($d_1 = 28$ mm, $d_2 = 35.3$ mm, $d_3 = 7.68$ mm). Therefore, it can be concluded that for 50 dB transmission loss target, a three channel design results in wider isolation bandwidth and lower pressure loss than a two channel design.

All in all, it can be concluded that although there is a positive relation between maximum frequency bandwidth and number of space-coiled channels, there is a negative relation between the pressure loss and the number of space-coiled channels in the case of 30 dB. On the other hand, in the case of 50 dB, there exists both a positive relation between maximum frequency bandwidth and the number of space-coiled channels and a positive relation between the pressure loss and the number of space-coiled channels. Moreover, the pressure loss of the design having transmission loss of 30 dB and two rounded space-coiled channels with one straight channel, 69.693 Pa, is smaller than the pressure loss of the design having transmission loss of 50 dB and two rounded space-coiled channels with one straight channel, 101.445 Pa. Hence, there exists another conclusion regarding pressure loss and

further increasing of transmission loss by comparing the designs having transmission losses of 30 dB and 50 dB while keeping the number of channels as three.

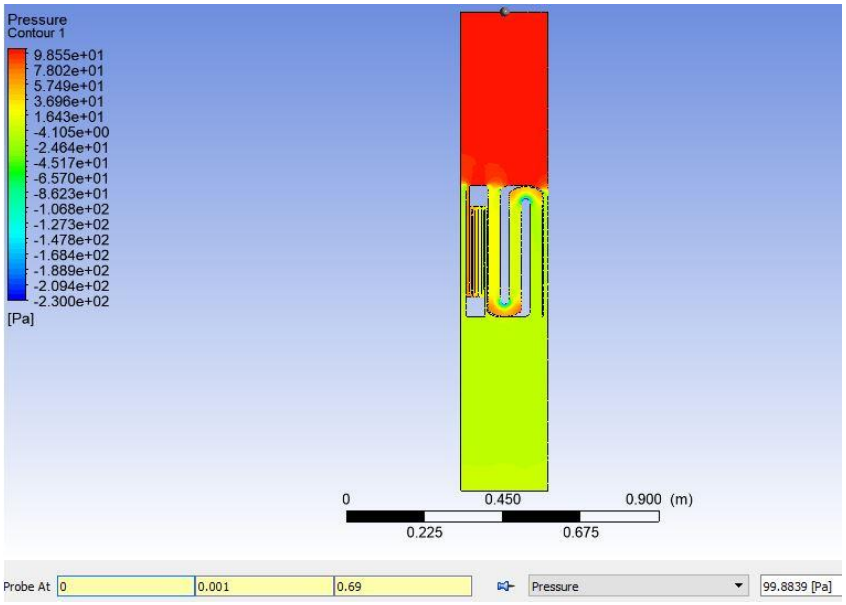

(a)

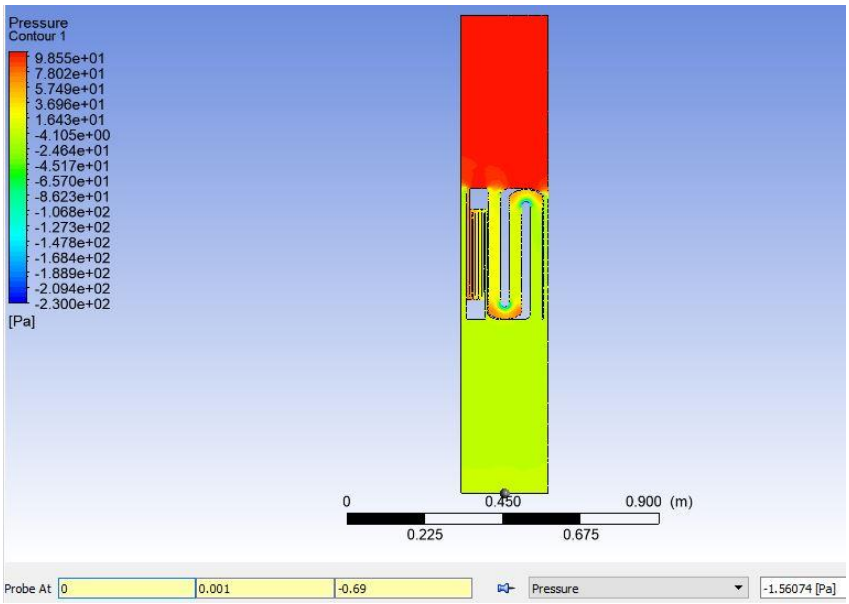

(b)

Figure 5.30. The pressure response of the flow for 3 m/s inlet speed, (a) Showing inlet pressure, (b) Showing outlet pressure, for the design with one straight channel and two space-coiled channels with rounded corners for 50 dB target transmission loss, 250 mm overall design domain width and 250 Hz upper frequency limit. Here, $d_1 = 28$ mm, $d_2 = 35.3$ mm, $d_3 = 7.68$ mm.

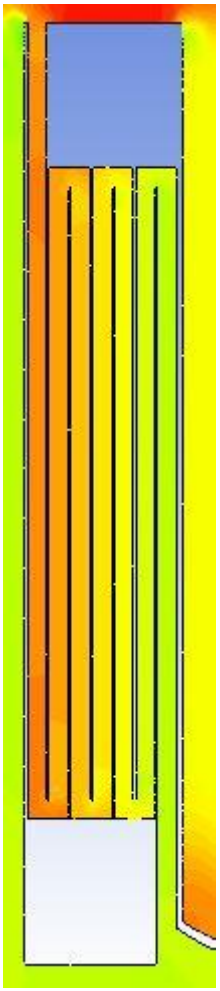

Figure 5.31. Zoom of the space-coiled channel having 7.68 mm width, for the design in Figure 5.30.

In conclusion, the pressure loss of the design having transmission loss of 30 dB and one rounded space-coiled channel with one straight channel, 52.509 Pa, is larger than the pressure loss of the first design having transmission loss of 50 dB and one rounded space-coiled channel with one straight channel, 34.932 Pa. Consequently, pressure loss response decreases with the further increasing of transmission loss by comparing the designs having transmission losses of 30 dB and 50 dB while keeping the number of channels as two. On the other hand, pressure loss increases with the further increasing of transmission loss by comparing the designs having target transmission losses of 30 dB and 50 dB while keeping the number of channels as three. The results of all acoustic and pressure loss analyses in this section are shown in Table 5.15.

Table 5.15. The results of all acoustic transmission loss and pressure loss analyses in Section 5. In all the analyses, the overall width of the design domain is 250 mm and the upper limit of the isolation bandwidth is 250 Hz.

	Inputs					Outputs				
						Bandwidth (Hz)			Pressure Loss (Pa)	
Target Transmission Loss (dB)	Channel Lengths for Rectangular Ones in MATLAB (mm)	Channel Lengths for Rectangular Ones in ANSYS (mm)	Channel Lengths for Rounded Ones in ANSYS (mm)	Channel Widths (mm)	Inlet Speed (m/s)	Rectangular Corner Finite Element	Rounded Corner Finite Element	Transfer Matrix Method	Rectangular Corner	Rounded Corner
10	445.2 - 1310.5	433.6 - 1297.3	434.9 - 1299.5	90 - 49.8	1	104	104	105		2.187
10	445.2 - 1310.5	433.6 - 1297.3	434.9 - 1299.5	90 - 49.8	3	104	104	105	26.481	21.081
30	392.1 - 1176.3	354.7 - 1148.1	359.5 - 1147.0	40 - 36	3	59	60	60	109.520	52.509
30	408.0 - 1224.0 - 2040.0	371 - 1195 - 2036	380.4 - 1198.0 - 2036.0	37 - 35 - 1.78	3	80	80	80	122.671	69.693
50	391.1 - 1084.0	323.9 - 1045.7	341.8 - 1050.8	40 - 40	3	20	21	22	100.903	34.932
50	379.9 - 1093.5	318.0 - 1057.5	351.9 - 1057.4	28 - 27.68	3	25	25	25	214.226	101.945
50	389.1 - 1167.3 - 1945.5	371.74 - 1150.05 - 1947.74	370.8 - 1141.3 - 1947.7	28 - 35.3 - 7.68	3	58	58	59	174.206	101.445

6. CONCLUSION

Broadband ventilated acoustic metamaterial design with coupled space-coiled resonators is studied in this thesis. The purpose of the thesis is to determine an acoustic metamaterial design, which produces large level of attenuation for a wide frequency bandwidth and provides minimum air pressure loss for effective ventilation. For this purpose, the number and/or dimensions of coupled space-coiled resonators is optimized. At the same time, the acoustic metamaterial, which is proposed according to acoustic optimization, is analyzed in terms of air pressure loss behavior.

Firstly, the three distinct designs are created by using ANSYS to benchmark the responses of the acoustic analysis with the results in reference article. In order to accomplish coupling with more than two channels, an analytical model of the problem for the design involving one channel is constructed by using transfer matrix method via MATLAB. After construction of the analytical model, the design is constructed by using ANSYS. The constructed design is analyzed by using finite element method. The transmission loss behaviors of the analytical model in MATLAB and finite element model in ANSYS are compared for model verification. The results are different due to the effect of the end correction. The methodology to determine the end correction is expressed with a flowchart.

The analytical model is utilized to get coupling two channels in the same design domain. For this utilization, transfer matrices are connected in parallel configuration. After the derivation related to parallel connection of transfer matrices is done, the methodology for constructing the analytical model of the design having more than two channels is proposed. By utilizing this methodology, the number and/or the dimensions of the coupled channels is optimized for the goal of obtaining sound isolation in the widest frequency range for a given transmission loss constraint. Once the proper number and dimensions of the channels are determined, the finite element model of the proposed design is constructed. The lengths in the analytical model are changed to calculate the lengths in the finite element model via genetic algorithm. Several analyses are made to show the relationship between isolation bandwidth, transmission loss and air pressure loss.

There exist trade-offs between isolation bandwidth, transmission loss and air pressure loss. In order to explain these trade-offs, possible design solutions with target transmission losses including 10 dB, 30 dB and 50 dB are determined. All of these following design solutions have 250 mm width of the overall design domain to be able to fit thick channels, which provide sufficient air flow. The analyses show that for low transmission loss targets such as 10 dB, a two channel design results in both large isolation bandwidth and low pressure loss. For instance, isolation bandwidth and pressure loss for 3 m/s inlet speed of the design with one straight channel and one space-coiled channel with rounded corners for 10 dB target transmission loss, 250 mm overall design domain width and 250 Hz upper frequency limit are 104 Hz and 21.081 Pa, respectively. On the other hand, these analyses also show that for high transmission loss targets including 50 dB or 60 dB, a three or four channel design results in wider isolation bandwidth and lower pressure loss than a two channel design. For example, isolation bandwidth and pressure loss for 3 m/s inlet speed of the second design with one straight channel and one space-coiled channel with rounded corners for 50 dB target transmission loss, 250 mm overall design domain width and 250 Hz upper frequency limit are 25 Hz and 101.945 Pa, respectively. However, isolation bandwidth and pressure loss for 3 m/s inlet speed of the design with one straight channel and two space-coiled channels with rounded corners for 50 dB target transmission loss, 250 mm overall design domain width and 250 Hz upper frequency limit are 58 Hz and 101.445 Pa, respectively. Therefore, depending on the target transmission loss constraint, the optimum number of channels and channel dimensions should be provided to both maximize isolation bandwidth and minimize pressure loss in case of airflow.

REFERENCES

1. Cummer, S. A., J. Christensen and A. Alu, “Controlling Sound with Acoustic Metamaterials”, *Nature Reviews Materials*, Vol. 1, No. 3, pp. 1-13, 2016.

2. Lee, D., D. M. Nguyen and J. Rho, “Acoustic Wave Science Realized by Metamaterials”, *Nano Convergence*, Vol. 4, No. 1, pp. 1-15, 2017.

3. Khelif, A., S. Mohammadi, A. A. Eftekhar, A. Adibi and B. Aoubiza, “Acoustic Confinement and Waveguiding with a Line-Defect Structure in Phononic Crystal Slabs”, *Journal of Applied Physics*, Vol. 108, No. 8, p. 084515, 2010.

4. Munk, B. A., *Metamaterials: Critique and Alternatives*, John Wiley & Sons, New York, 2009.

5. Iannace, G., G. Ciaburro and A. Trematerra, “Metamaterials Acoustic Barrier”, *Applied Acoustics*, Vol. 181, p. 108172, 2021.

6. Popov, E., *Introduction to Diffraction Gratings: Summary of Applications Gratings: Theory and Numeric Applications*, Institut Fresnel, France, 2012.

7. Lahiri, A., *Basic Optics: Principles and Concepts*, Elsevier, Amsterdam, 2016.

8. Wilm, M., A. Khelif, S. Ballandras, V. Laude and B. Djafari-Rouhani, “Out-of-Plane Propagation of Elastic Waves in Two-Dimensional Phononic Band-Gap Materials”, *Physical Review E*, Vol. 67, No. 6, p. 065602, 2003.

9. Martinez-Sala, R., J. Sancho, J. V. Sanchez, V. Gomez, J. Llinares and F. Meseguer, “Sound Attenuation by Sculpture”, *Nature*, Vol. 378, No. 6554, pp. 241-241, 1995.

10. Consoli, A. and C. López, “Lasing Optical Cavities Based on Macroscopic Scattering Elements”, *Scientific Reports*, Vol. 7, No. 1, pp. 1-7, 2017.

11. Elayouch, A., M. Addouche, M. Farhat and A. Khelif, “Subwavelength Sound Screening by Coupling Space-Coiled Fabry-Perot Resonators”, *Europhysics Letters*, Vol. 119, No. 3, p. 36001, 2017.

12. Liu, Z., X. Zhang, Y. Mao, Y. Y. Zhu, Z. Yang, C. T. Chan and P. Sheng, “Locally Resonant Sonic Materials”, *Science*, Vol. 289, No. 5485, pp. 1734-1736, 2000.

13. Munjal, M. L., *Acoustics of Ducts and Mufflers with Application to Exhaust and Ventilation System Design*, John Wiley & Sons, New York, 1987.

14. Torregrosa, A. J., A. Broatch, R. Payri and F. Gonza´ lez, “Numerical Estimation of End Corrections in Extended-Duct and Perforated-Duct Mufflers”, *Journal of Vibration and Acoustics*, Vol. 121, No.3, pp. 302-308, 1999.

15. Kang, Z. and Z. Ji, “Acoustic Length Correction of Duct Extension into a Cylindrical Chamber”, *Journal of Sound and Vibration*, Vol. 310, No.4-5, pp. 782-791, 2008.

16. Chaitanya, P. and M. L. Munjal, “Effect of Wall Thickness on the End Corrections of the Extended Inlet and Outlet of a Double-Tuned Expansion Chamber”, *Applied Acoustics*, Vol. 72, No.1, pp. 65-70, 2011.

17. Khelif, A., Y. Achaoui, S. Benchabane, V. Laude and B. Aoubiza, “Locally Resonant Surface Acoustic Wave Band Gaps in a Two-Dimensional Phononic Crystal of Pillars on a Surface”, *Physical Review B*, Vol. 81, No. 21, p. 214303, 2010.

18. Addouche, M., M. A. Al-Lethawe, A. Choujaa and A. Khelif, “Superlensing Effect for Surface Acoustic Waves in a Pillar-Based Phononic Crystal with Negative Refractive Index”, *Applied Physics Letters*, Vol. 105, No. 2, p. 023501, 2014.

19. Yang, Z., J. Mei, M. Yang, N. H. Chan and P. Sheng, “Membrane-Type Acoustic Metamaterial with Negative Dynamic Mass”, *Physical Review Letters*, Vol. 101, No. 20, p. 204301, 2008.

20. Liang, Z. and J. Li, “Extreme Acoustic Metamaterial by Coiling Up Space”, *Physical Review Letters*, Vol. 108, No. 11, p. 114301, 2012.

21. Song, K., S. H. Lee, K. Kim, S. Hur and J. Kim, “Emission Enhancement of Sound Emitters Using an Acoustic Metamaterial Cavity”, *Scientific Reports*, Vol 4, No. 1, pp. 1-6, 2014.

22. Frenzel, T., J. D. Brehm, T. Buckmann, R. Schittny, M. Kadic and M. Wegener, “Three-Dimensional Labyrinthine Acoustic Metamaterials”, *Applied Physics Letters*, Vol. 103, No. 6, p. 061907, 2013.

23. Liang, Z., T. Feng, S. Lok, F. Liu, K. B. Ng, C. H. Chan, J. Wang, S. Han, S. Lee and J. Li, “Space-Coiling Metamaterials with Double Negativity and Conical Dispersion”, *Scientific Reports*, Vol. 3, No. 1, pp. 1-6, 2013.

24. Xie, Y., B. I. Popa, L. Zigoneanu and S. A. Cummer, “Measurement of a Broadband Negative Index with Space-Coiling Acoustic Metamaterials”, *Physical Review Letters*, Vol. 110, No. 17, p. 175501, 2013.

25. Xie, Y., A. Konneker, B. I. Popa and S. A. Cummer, “Tapered Labyrinthine Acoustic Metamaterials for Broadband Impedance Matching”, *Applied Physics Letters*, Vol. 103, No. 20, p. 201906, 2013.

26. Li, Y., B. Liang, X. Zou and J. Cheng, “Extraordinary Acoustic Transmission through Ultrathin Acoustic Metamaterials by Coiling Up Space”, *Applied Physics Letters*, Vol. 103, No. 6, p. 063509, 2013.

27. Park, J. J., K. J. B. Lee, O. B. Wright, M. K. Jung and S. H. Lee, “Giant Acoustic Concentration by Extraordinary Transmission in Zero-Mass Metamaterials”, *Physical Review Letters*, Vol. 110, No. 24, p. 244302, 2013.

28. Lu, M. H., X. K. Liu, L. Feng, J. Li, C. P. Huang, Y. F. Chen, Y. Y. Zhu, S. N. Zhu and N. B. Ming, "Extraordinary Acoustic Transmission through a 1D Grating with Very Narrow Apertures", *Physical Review Letters*, Vol. 99, No. 17, p. 174301, 2007.

29. Miroshnichenko, A. E., S. Flach and Y. S. Kivshar, "Fano Resonances in Nanoscale Structures", *Reviews of Modern Physics*, Vol. 82, No. 3, pp. 2257-2298, 2010.

30. Fano, U., "Effects of Configuration Interaction on Intensities and Phase Shifts", *Physical Review*, Vol. 124, No. 6, pp. 1866-1878, 1961.

31. Ott, C., A. Kaldun, P. Raith, K. Meyer, M. Laux, J. Evers, C. H. Keitel, C. H. Greene and T. Pfeifer, "Lorentz Meets Fano in Spectral Line Shapes: A Universal Phase and Its Laser Control", *Science*, Vol. 340, No. 6133, pp. 716-720, 2013.

32. Liu, N., L. Langguth, T. Weiss, J. Kastel, M. Fleischhauer, T. Pfau and H. Giessen, "Plasmonic Analogue of Electromagnetically Induced Transparency at the Drude Damping Limit", *Nature Materials*, Vol. 8, No. 9, pp. 758-762, 2009.

33. Liu, F., M. Ke, A. Zhang, W. Wen, J. Shi, Z. Liu and P. Sheng, "Acoustic Analog of Electromagnetically Induced Transparency in Periodic Arrays of Square Rods", *Physical Review E*, Vol. 82, No. 2, p. 026601, 2010.

34. Santillan, A. and S. I. Bozhevolnyi, "Acoustic Transparency and Slow Sound Using Detuned Acoustic Resonators", *Physical Review B*, Vol. 84, No. 6, p. 064304, 2011.

35. Fleischhauer, M., A. Imamoglu and J. P. Marangos, "Electromagnetically Induced Transparency: Optics in Coherent Media", *Reviews of Modern Physics*, Vol. 77, No. 2, pp. 633-673, 2005.

36. Elayouch, A., M. Addouche, E. Herth and A. Khelif, "Experimental Evidence of Ultrasonic Opacity Using the Coupling of Resonant Cavities in a Phononic Membrane", *Applied Physics Letters*, Vol. 103, No. 8, p. 083504, 2013.

37. Ufimtsev, P. Y., *Fundamentals of the Physical Theory of Diffraction*, Second Edition, Wiley, New York, 2007.

38. Elayouch, A., M. Addouche, P. Lasaygues, Y. Achaoui, M. Ouisse and A. Khelif, "How Diffraction Limits Ultrasonic Screening in Phononic Plate Composed of a Periodic Array of Resonant Slits", *Comptes Rendus Physique*, Vol. 17, No. 5, pp. 518-523, 2016.

39. Li, Y. and B. M. Assouar, "Acoustic Metasurface-Based Perfect Absorber with Deep Subwavelength Thickness", *Applied Physics Letters*, Vol. 108, No. 6, p. 063502, 2016.

40. Zhu, X., K. Li, P. Zhang, J. Zhu, J. Zhang, C. Tian and S. Liu, "Implementation of Dispersion-Free Slow Acoustic Wave Propagation and Phase Engineering with Helical-Structured Metamaterials", *Nature Communications*, Vol. 7, No. 1, p. 11731, 2016.

41. Kumar, S. and H. P. Lee, "The Present and Future Role of Acoustic Metamaterials for Architectural and Urban Noise Mitigations", *Acoustics*, Vol. 1, No. 3, pp. 590-607, 2019.

42. Magnani, A., C. Marescotti and F. Pompoli, "Acoustic Absorption Modeling of Single and Multiple Coiled-Up Resonators", *Applied Acoustics*, Vol. 186, p. 108504, 2022.

43. Sun, M., X. Fang, D. Mao, X. Wang and Y. Li, "Broadband Acoustic Ventilation Barriers", *Physical Review Applied*, Vol. 13, No. 4, p. 044028, 2020.

44. Sun, M., X. Fang, D. Mao, X. Wang and Y. Li, "Ultra-Open Acoustic Metamaterial Silencer Based on Fano-Like Interference", *Physical Review B*, Vol. 99, No. 2, p. 024302, 2019.

45. Kumar, S. and H. P. Lee, "Recent Advances in Acoustic Metamaterials for Simultaneous Sound Attenuation and Air Ventilation Performances", *Crystals*, Vol. 10, No. 8, p. 686, 2020.

46. Dong, R., D. Mao, X. Wang and Y. Li, “Ultrabroadband Acoustic Ventilation Barriers via Hybrid-Functional Metasurfaces”, *Physical Review Applied*, Vol. 15, No. 2, p. 024044, 2021.

47. Fusaro, G., X. Yu, Z. Lu, F. Cui and J. Kang, “A Metawindow with Optimised Acoustic and Ventilation Performance”, *Applied Sciences*, Vol. 11, No. 7, p. 3168, 2021.

48. Dong, R., D. Mao, Y. Zhu, F. Mo, X. Wang and Y. Li, “A Ventilating Acoustic Barrier for Attenuating Broadband Diffuse Sound”, *Applied Physics Letters*, Vol. 119, No. 26, p. 263505, 2021.

49. Liu, C., H. Wang, B. Liang, J. Cheng and Y. Lai, “Low-Frequency and Broadband Muffler via Cascaded Labyrinthine Metasurfaces”, *Applied Physics Letters*, Vol. 120, No. 23, p. 231702, 2022.

50. Elnady, T., S. Elsaadany and M. Åbom, “Flow and Pressure Drop Calculation Using Two-Ports”, *Journal of Vibration and Acoustics*, Vol. 133, No. 4, 2011.

51. Verdière, K., R. Panneton, S. Elkoun, T. Dupont and P. Leclaire, “Transfer Matrix Method Applied to the Parallel Assembly of Sound Absorbing Materials”, *The Journal of the Acoustical Society of America*, Vol. 134, No. 6, pp. 4648-4658, 2013.

52. Verdière, K., R. Panneton, S. Elkoun, T. Dupont and P. Leclaire, “Comparison Between Parallel Transfer Matrix Method and Admittance Sum Method”, *The Journal of the Acoustical Society of America*, Vol. 136, No. 2, pp. 90-95, 2014.

APPENDIX A: COPYRIGHT PERMISSION FOR FIGURES

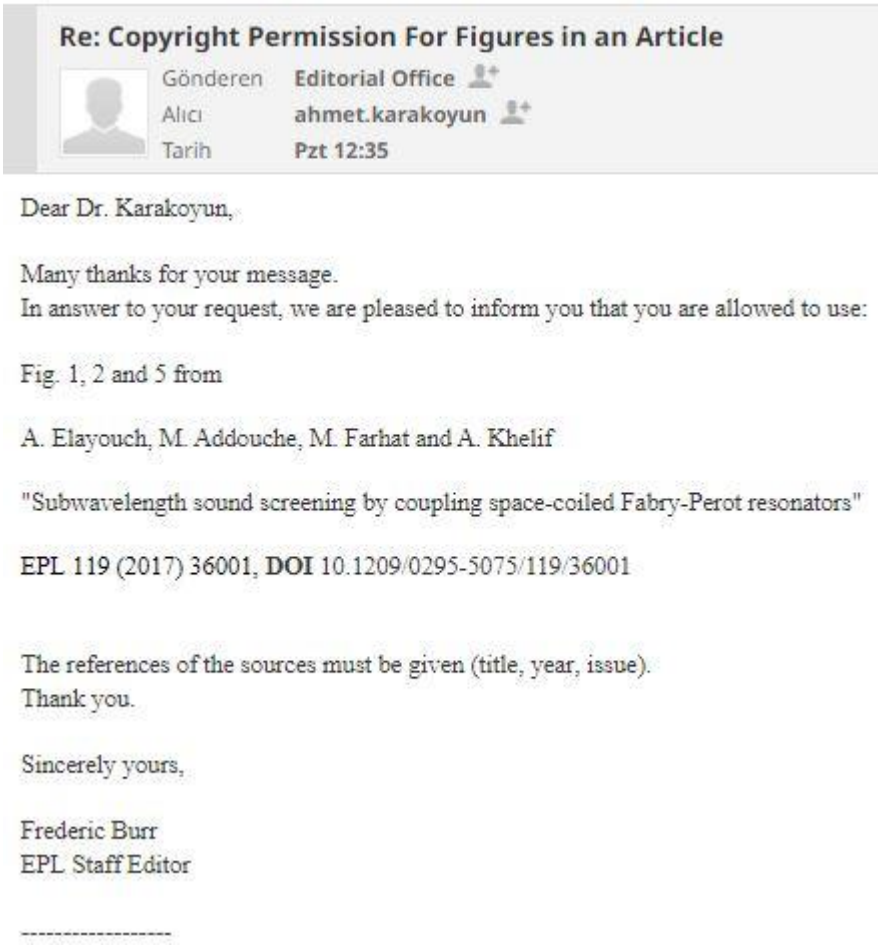

Re: Copyright Permission For Figures in an Article

Gönderen **Editorial Office**
Alıcı **ahmet.karakoyun**
Tarih **Pzt 12:35**

Dear Dr. Karakoyun,

Many thanks for your message.
In answer to your request, we are pleased to inform you that you are allowed to use:

Fig. 1, 2 and 5 from

A. Elayouch, M. Addouche, M. Farhat and A. Khelif

"Subwavelength sound screening by coupling space-coiled Fabry-Perot resonators"

EPL 119 (2017) 36001, **DOI** 10.1209/0295-5075/119/36001

The references of the sources must be given (title, year, issue).
Thank you.

Sincerely yours,

Frederic Burr
EPL Staff Editor

Figure A.1. Copyright permission of [11] for Figures 2.1, 2.2 and 2.3.